ANALYSIS AND APPLICATIONS OF CURRENT-SOURCE-MODE CONVERTERS IN LIGHT-EMITTING-DIODE LIGHTING SYSTEMS

ZHENG DONG

PhD

The Hong Kong Polytechnic University

2019

The Hong Kong Polytechnic University

Department of Electronic and Information Engineering

ANALYSIS AND APPLICATIONS OF CURRENT-SOURCE-MODE CONVERTERS IN LIGHT-EMITTING-DIODE LIGHTING SYSTEMS

Zheng DONG

A thesis submitted in partial fulfillment of

the requirements for the degree of

Doctor of Philosophy

November 2018

Certificate of Originality

I hereby declare that this thesis is my own work and that, to the best of my knowledge and belief, it reproduces no material previously published or written, nor material that has been accepted for the award of any other degree or diploma, except where due acknowledgment has been made in the text.

____________(Signed)

Zheng Dong (Name of student)

Abstract

Light-emitting-diodes (LEDs), which have been extensively applied in various lighting situations, are solid-state devices with specific v-i characteristics. The LED is becoming a promising new generation light source because of the advantages of environmental safety, long life expectancy and high efficiency. Based on an LED's v-i curve, the LED can be regarded as a non-ideal voltage source. Therefore, for LED drivers, the importance of consideration of the termination type and the corresponding choice of converter type should be fully reinforced. In this thesis, LED drivers are studied from the perspective of basic circuit theory. Current-source-mode (CSM) converters are derived from voltage-source-mode (VSM) converters based on the duality principle. This thesis aims to present a comprehensive comparison of the key performance areas in relation to LED lighting applications. A CSM single-inductor multiple-output (SIMO) converter with simple control strategy and the least number of inductors is constructed by using CSM converters for driving LEDs. In order to improve the efficiency of the CSM SIMO LED driver, the adaptive current bus technique is applied to the proposed CSM SIMO converter.

First, we study the basic requirement of the driving circuits and discuss the proper approach to driving LEDs in view of their characteristics. We compare voltage source driving and current source driving, and discuss their relative advantages and constraints. We specifically introduce the use of circuit duality principle for developing CSM drivers which are less known but are theoretically more versatile compared to their conventional VSM counterparts. The study highlights the effects of the choice of

driving circuits in terms of the number and size of circuit components used, duty cycle variation, sensitivity of control, nonlinearity and control complexity of LED drivers. We present a systematic and comparative exposition of the circuit theory of driving LEDs, with two examples supporting the high value and huge potential use of CSM converters in lighting systems.

SIMO LED drivers have the advantages of being compact, efficient and low cost. However, the voltage-to-current transfer function of each output of the SIMO converter is not independent, with significant cross regulation issues that necessitate the use of complex closed-loop control for achieving independent dimming function. Based on the duality principle, this thesis proposes a CSM SIMO dc-dc converter which is shown to be more suited for LED driving due to widened control range of the duty cycle and inherently inductor-less LED driving topology. The outputs of the CSM SIMO dc-dc converter are inherently independent, resulting in very simple control requirement involving only one closed-loop controller for providing the constant current feeder, and several simple open-loop controllers for independent dimmable driving of LEDs. Simultaneous voltage step-up and step-down of multiple outputs is an added feature that simplifies the input power source requirement especially for portable applications. The whole system is simple, reliable and low cost. Taking the CSM single-inductor dual-output (SIDO) dc-dc converter as an example, we illustrate the circuit operation and establish a small-signal model for facilitating the design of the feedback control. A direct duty-cycle dimming method is described.

Finally, an attempt is made to improve the efficiency of the CSM SIMO LED driver. This LED driver has many advantages, however, the low efficiency is a serious constraint for the widespread use of the CSM SIMO dc-dc converter. Another limiting factor is that the low-frequency pulse-width modulation (PWM) dimming method can not be extended to three or more outputs in this CSM SIMO dc-dc converter. We apply the adaptive current bus technique to the CSM SIMO dc-dc converter for improving the efficiency. The reason for the increase in efficiency is explained in terms of the energy flow path and the power consumption of devices. The problem of using low-frequency PWM dimming method is analyzed and solved. Regarding the voltage stress of switches, we compare the traditional series-input-connected structure with the CSM SIMO dc-dc converter, and conclude that the CSM SIMO dc-dc converter is more suited for high-step-down applications without the use of transformers.

Publications

Journal papers

- **Z. Dong**, C. K. Tse, and S. Y. Hui, "Current-source-mode single-inductor multiple-output LED driver with single closed-loop control achieving independent dimming function," *IEEE Journal of Emerging and Selected Topics in Power Electronics*, vol. 6, no. 3, pp. 1198–1209, Sept. 2018.

- **Z. Dong**, C. K. Tse, and S. Y. Hui, "Circuit theoretic considerations of LED driving: voltage-source versus current-source driving," *IEEE Transactions on Power Electronics*, 2018. (Early Access, DOI: 10.1109/TPEL.2018.2861914)

- X. L. Li, **Z. Dong**, and C. K. Tse, "Series-Connected Current-Source-Mode Multiple-Output Converters with High Step-Down Ratio and Simple Control," *IEEE Transactions on Power Electronics*, 2018. (Early Access, DOI: 10.1109/TPEL.2019.2892376)

- **Z. Dong**, X. L. Li, and C. K. Tse, "Improved-efficiency quasi-two-stage current-source-mode single-inductor multiple-output LED driver," *IEEE Transactions on Industry Applications*, 2018. (Submitted)

Conference papers

- **Z. Dong**, C. K. Tse, and S. Y. Hui, "Basic circuit theoretic considerations of LED driving: Voltage-source versus current-source driving," in *Proc. IEEE Annual Southern Power Electronics Conference*, Auckland, New Zealand, 2016, pp. 1–6.

- **Z. Dong**, C. K. Tse, and S. Y. Hui, "Single-inductor multiple-output current-source converter with improved cross regulation and simple control strategy," in *Proc. International Power Electronics Conference*, Niigata, Japan, 2018.

- X. L. Li, **Z. Dong**, and C. K. Tse, "Analysis of basic structure of interconnected converters for single-input multi-output applications," in *Proc. IEEE International Power Electronics and Application Conference and Exposition, (PEAC)*, Shenzhen, China, November 2018.

Acknowledgments

It is my pleasure and honor to pursue my Ph.D. degree at the Hong Kong Polytechnic University. I would like to express my gratefulness to a number of people.

First of all, I wish to thank Prof. Michael Tse for his continuous support, patient guidance and valuable advice. Prof. Tse is an active and open-minded mentor who has inspired me greatly, especially when I encountered difficulties in my work. He has always encouraged me to think deeply and freely during the course of this project. As the leader of Nonlinear Circuits and Systems Group, he has organized seminars and regular discussion sessions on complex systems, networks, control and applications, which have greatly broadened my horizon. Without his help, I could not have accomplished this Ph.D. study.

I am also very grateful to Prof. Ron Hui, the project coordinator of the RGC theme-based research project. With his coordination, I can view power electronics from different angles. The communication between the two teams at the University of Hong Kong and the Hong Kong Polytechnic University has greatly enhanced the research outcome and demonstrated the importance of collaboration.

I wish to thank all my colleagues in the Nonlinear Circuits and Systems Group. We have a lot of common topics to talk about as well as experience to share.

Last but not least, I would like to thank my wife for her love and ten years of companionship. She gave up her job in Chengdu for supporting my study, which has always been the biggest motivation for me to move forward. Sincere gratitude goes to my parents. Their love, care, and support make me stronger.

Contents

List of Figures

List of Tables

Chapter 1

Introduction

1.1 Background

In the development of electric lighting in the past one hundred years, the electric lighting industry has gone through three major stages [2–4]. The representative lighting devices of the three stages are incandescent lamps, fluorescent lamps and high intensity discharge (HID) lamps. It is now widely accepted that light-emitting-diodes (LEDs) are the new generation of high-power lighting sources [5–9].

With the advent of electricity generation, the carbon arc lamp, invented by Humphry Davy in 1870 in UK, was the first electric lighting device, but its use was restricted only for street and large building lightings. Light in the carbon arc lamp was produced by a wire filament after the wire filament was heated electrically. However, the arc lamp was not suitable for practical applications due to high cost and short lifespan. This limitation was lifted by Edison who discovered a new material out of more than 6,000 fiber materials. The new material was the Japanese bamboo silk which was durable and could produce light for more than 1,000 hours. In 1879, the high-resistance incandescent lamp, which was capable of continuously producing light for 40 hours, was invented. Thus, Edison invented the first lamp for a wide range of practical uses. The practical incandescent lamp invented by Edison kicked off the prevalent use of electricity in daily life.

The electric lighting devices continued to be improved after the invention of the fluorescent lamp. In 1939, the fluorescent lamp was invented and extensively used, and became another important lighting source. In 1959, the halogen lamp, which consists of halogen gas and a tungsten filament, injected new vitality into thermal radiation light source. The combination of the halogen gas and the tungsten filament can produce a halogen cycle chemical reaction, redepositing evaporated tungsten to the filament. The halogen lamp is small, and is superior to the incandescent lamp in terms of luminous efficacy and lifespan. In recent years, the production of halogen lamps have matured, achieving excellent stability and high shake-resistance. The halogen lamp can be directly used in power grids with the input voltage being 220 V or 110 V. Fluorescent lamps have high luminous efficacy, and are integrated with electronic ballasts, replacing traditional incandescent lamps in many applications. The power factor of the fluorescent lamp with electronic ballast can achieve 0.98, and the total harmonic distortion is less than 10%. The lifespan can be extended to 10,000 hours.

HID lamps, as the third generation of lighting sources, are suitable for large area and outdoor lighting. The working pressure inside the HID lamp normally exceeds 10 times atmospheric pressure. The HID lamp, which has a short and high-brightness discharge tube covered by glass or quartz, can be divided into three categories: high pressure mercury lamp, high pressure sodium lamp and metal halide lamp. The high pressure mercury lamp is the simplest HID lamp, and is mainly used in indoor lighting of industrial and mining premises. The high pressure sodium lamp needs to use a ceramic arc tube, in order to withstand the erosion of high temperature steam of sodium, thereby increasing the lifespan up to 24,000 hours. The metal halide lamp is the most complicated HID lamp, producing light by an electric arc through a gaseous mixture of vaporized mercury and metal halides. It is widely used in occasions requiring high luminous efficacy and high quality white light.

In the past 50 years, LEDs, which are solid-state lighting sources, have made major breakthroughs. An LED can operate at a low DC voltage. The conversion efficiency of light is very high, and the luminous surface is small. Thus, the color effect of LEDs far exceeds that of incandescent lamps. The lifespan can be increased to 100,000 hours. With the breakthrough in the performance of blue LEDs, white LEDs have come practically available. Many companies are bringing various LED products to the market. The 21st Century has become an era of solid-state lighting sources, and combining with green energy, LEDs become an environmentally friendly lighting source.

At present, lighting power consumption accounts for about 19% of the world's total energy consumption [10]. In the US, about 273 billion kWh is consumed by residential and commercial lighting systems in 2017. The rising consumption of energy and the surge in lighting power consumption will bring increasingly grave challenges in ecological environmental protection. Hydro energy for the production of electricity has various advantages such as being pollution free and renewable in nature. However, if the hydropower facilities are built without restriction, the natural environment would be seriously affected. The coal-fired power plants will aggravate the existing energy crisis, although thermal power technology is very mature. Therefore, we should enhance the use of renewable energy, and accelerate the development of various power generation technologies, for instance, solar energy, wind energy and nuclear energy. On the other hand, we need to accelerate the research, application and development of energy-efficient lighting sources. However, traditional lighting sources, such as incandescent lamps, fluorescent lamps, metal halide lamps, etc., consume a lot of energy and are inefficient, squandering large amounts of electric energy.

The traditional lighting sources have the disadvantage of low efficiency. Replacing traditional lightings by LEDs and other alternative forms of lighting sources has rapidly become a global trend. The LED, in particular, has become a promising new generation lighting source because of the advantages of environmental safety, long life expectancy and high efficiency [11].

With the gradual increase in the luminous efficacy of LEDs, the performance of

LED drivers has become a key limiting factor for the application of LEDs. Many designers attempt to improve the performance of LED drivers in many ways. An LED driver is a dc-dc converter that converts a voltage source to a specific current source for driving LEDs. In general, the input of an LED driver includes low DC voltage, high DC voltage, low-frequency AC voltage, high-frequency AC voltage. The output of the LED driver is a constant current source. It is obviously that properly designed LED drivers can significantly improve the efficiency and achieve energy saving of the whole system. The lifespan of the LED lighting system depends to a large extent on the quality of the LED driver. The theoretical lifespan of an LED can reach 100,000 hours. Thus, a reliable and durable LED driver can ensure long lifespan of the overall system.

1.2 Motivation

Traditional power converters, e.g., buck and boost converters [12–18], are designed for input voltage sources that are assumed in most everyday applications. Basically, for a traditional dc-dc converter, here called *voltage-source-mode* (VSM) converter, the input voltage is fixed, and the two complimentary switches and the inductor form the basic cell. The inductor is the high-frequency storage component. The capacitor behind the basic cell serves a filtering function. Through the use of *circuit duality* principle [19, 20], a family of current-source-mode (CSM) converters can be obtained from the common VSM converters.

Specifically, for the CSM converter, the input current is fixed, and the two complimentary switches and a capacitor form the basic cell. The capacitor is the high-frequency storage component. The inductor behind the basic cell serves only a filtering function.

In general, the input of a dc-dc converter should comply with the source type, and the output of a dc-dc converter can be controlled to deliver voltage or current. Thus,

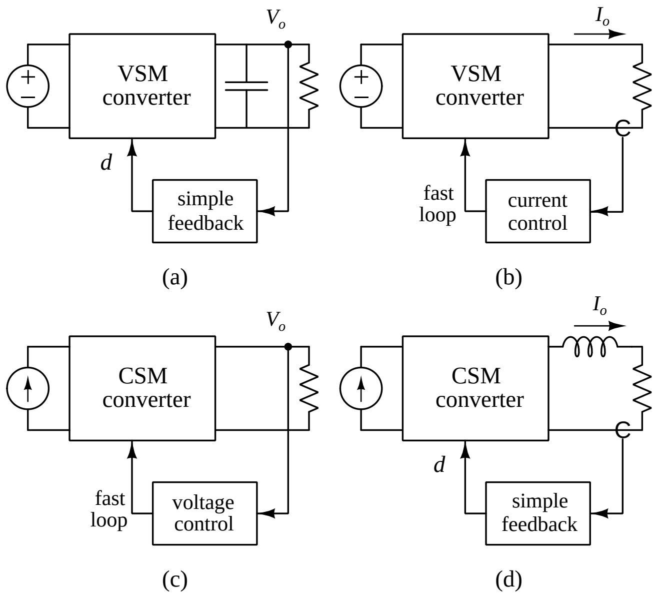

Figure 1.1: Four configurations for producing regulated output voltage or current. (a) Voltage to voltage conversion using VSM converter (traditional dc-dc converter with simple voltage feedback control); (b) voltage to current conversion using VSM converter (traditional dc-dc converter with current-programmed control); (c) current to voltage conversion using CSM converter; (d) current to current conversion using CSM converter.

there are four possible configurations using VSM and CSM converters for producing regulated voltage or current, as shown in Fig. 1.1. Since the voltage of each individual LED is different, the methods depicted in Figs. 1.1 (a) and (c) are not suitable for driving LEDs. In the traditional case of Fig. 1.1 (a), the output voltage is controlled through the duty cycle, i.e.,

$$V_o = F_v(D)V_{in} \tag{1.1}$$

where D is the duty cycle and $F_v(.)$ is the function defining the input-to-output voltage transfer ratio. According to equation (1.1), the output current in Fig. 1.1(b) can be obtained as

$$I_o = \frac{F_v(D)V_{in}}{R_o} \text{ or } \frac{F_v(D)V_{in} - V_{LED}}{r_{out}} \tag{1.2}$$

where R_o is the load impedance, r_{out} is the resistance connecting the converter output and the LED, and V_{LED} is the voltage across the LED. In theory, when we use a VSM converter to drive LEDs, the output current is determined by both the voltage transfer ratio and the load characteristic. However, the output current of the CSM converter in Fig. 1.1(d) can be obtained by controlling the duty cycle given a fixed input current, i.e.,

$$I_{\text{o}} = F_c(D)I_{\text{in}} \tag{1.3}$$

where D is again the duty cycle and $F_c(.)$ is the function defining the input-to-output current transfer ratio. The duty cycle in CSM version can control the output current directly. The load characteristic does not affect the current delivered by the CSM converter.

Through the above analysis, CSM converters are theoretically more versatile to drive LEDs. However, they are less known and seldom applied to LED drivers. In this thesis, based on specific LED v-i characteristics, the comparison between VSM converters and CSM converters are presented in terms of the number and size of circuit components used, duty cycle variation, sensitivity of control, nonlinearity and control complexity of LED drivers.

In many applications, multiple-output LED driving with independent dimming function is necessary [21–24]. The various output power levels are usually generated from a single power source. The single-inductor multiple-output (SIMO) dc-dc converter provides a low-cost solution as it uses only one inductor to generate multiple outputs. However, the existing SIMO dc-dc converter has certain drawbacks including the need for multiple closed-loop controls, the inevitable cross-regulation effects, the need of numerous current sensors, and so on. Thus, the SIMO converter constructed by CSM converters connecting in series becomes a possible solution to problems mentioned above.

Given the huge power consumption in lighting applications, high efficiency is an important design consideration for SIMO LED drivers. Although the CSM SIMO converter has obvious practical merits for current driving, the efficiency is lower than conventional VSM-based SIMO converters, the reason being that the conventional SIMO converter is a one-stage design whereas the CSM SIMO converter has two stages of power processing, including a VSM buck converter and a CSM buck converter. Therefore, improving efficiency of CSM SIMO converter becomes a key problem.

1.3 Thesis Organization

This thesis is organized as follows.

Chapter 2 provides a literature review. Discussions of LED's advantages, LED's characteristics, connection circuits, dimming methods and some basic LED drivers including SIMO LED drivers are presented.

Chapter 3 studies the driving circuit requirement for LED loads and examines the circuit transformation of power conversion circuits via the duality principle. This chapter investigates VSM and CSM drivers in terms of the main circuit components, the range of duty cycle variation, the sensitivity of the output current to the change of duty cycle, the nonlinearity of the control function and the control complexity. Two multiple-output converters are derived based on CSM converters which are suitable candidates for driving LEDs. The exact circuit configuration depends on the specific choice of the converter circuits. We emphasize that proper application of circuit concepts would form the basis of design of effective driving circuits for LED applications.

Chapter 4 constructs a CSM SIMO converter based on the circuit duality principle and the inherently inductorless CSM buck converter. The outputs of the CSM SIMO converter are independent, resulting in very simple control strategy. One closed-loop controller and several simple open-loop controllers can achieve independent dimming function. Both the high-frequency and the low-frequency PWM dimming methods can be applied to the CSM SIDO converter.

Chapter 5 proposes a quasi-two-stage CSM SIMO LED driver with an adaptive current bus for efficiency enhancement. The proposed structure can achieve high-step-down ratio without using transformers. The voltage stress in each constituent converter, unlike in the conventional configuration, depends only on its input voltage and output voltage, with no mutual influence. We explain the improvement in efficiency from the point of view of energy flow and power losses. Moreover, the low-frequency PWM dimming method is extended to three or more outputs.

The thesis concludes in Chapter 6, where major findings of the project are summarized and some thoughts on future works are presented.

Chapter 2

Literature Review

In this chapter, we first review some fundamental concepts that are highly relevant to designing proper LED drivers, including LED's v-i characteristics, connection circuits and dimming methods. On the other hand, the traditional LED drivers and SIMO LED drivers will be discussed and some strategies on improving the efficiency will be presented. Based on the analysis, an alternative solution to design LED drivers will be proposed.

2.1 Properties of LEDs

An LED is an incredibly useful device with specific v-i characteristics, and therefore, it is essential to master the advantages and characteristics of an LED. In this section, the merits of using LEDs are discussed, and the relationship between LED's forward voltage and the current flowing through the LED is reviewed. The LED's model is established to simplify analysis and design calculations.

2.1.1 Advantages of LEDs

As a new generation of lighting sources, LEDs have the following advantages [25–28] over traditional lighting sources:

(1) A LED has a low terminal voltage. Generally, the terminal voltage of an LED is low, which makes them suitable for use in outdoor lighting applications that require high-level safety. If an LED works in a wide range of operating temperature, the performance of the LED does not suffer performance degradation.

(2) The luminous efficacy is high. Generally, the rated power of an LED is low. The luminous efficacy is one parameter for describing the amount of light emitted per unit of power consumed by the bulb. Under the same lighting effect, the power consumption of LEDs is about one-eighth of that of the incandescent lamp. Therefore, in most LED lighting retrofit projects, the overall efficiency can be improved significantly.

(3) A LED has a long life expectancy. Compared with traditional lighting sources, LEDs have a long lifespan, which is the most significant advantage. The operating hours can reach 100,000 hours or more, being 10 times as long as most fluorescent lamps. Meanwhile, LEDs can work stably in special environments with no parts being easily damaged because of the structural features of LEDs.

(4) The actual LED is extremely small, which makes LEDs particularly well suited for applications requiring a large number of LEDs. For instance, LEDs are incredibly adaptable to a wide spectrum from traffic signals to residential and commercial applications.

(5) The response speed for LEDs is high. LEDs can turn on or off quickly without warm-up period, and frequent switching causes no degradation in LEDs. Thus high-frequency PWM dimming methods (as will be explained later) can be applied to drive LEDs.

(6) Unlike fluorescent or mercury vapor lamps, LEDs impose no harm to the environment. The mercury contained in mercury vapor lamps is an intractable material which needs to be handled specially at the end of the product's useful lifespan. However, none of these considerations are necessary with LEDs, making LEDs more environmentally friendly.

(7) LEDs possess better dimming capability than traditional lighting devices. For

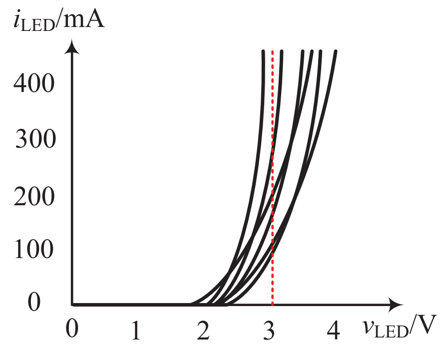

Figure 2.1: LED's v-i curves for different LEDs.

instance, when metal halides work at a lower power level, the efficiency is low and the dimming function may fail. However, LEDs have the capacity to operate at any percentage of their rated power by using LED drivers with the efficiency maintained high even when the power is reduced.

2.1.2 Characteristics of LEDs

One function of LED drivers is to provide the required voltage and current. To have a better grasp of LED drivers, we should study the LED's electrical characteristics [29, 30].

Fig. 2.1 shows the v-i curves for different LEDs, even among the same batch of LEDs. The x-axis and y-axis are the forward voltage across an LED and the corresponding current flowing through the LED, respectively. Based on Fig. 2.1, different LEDs could have different currents for the same voltage across the LEDs. The luminous flux is primarily determined by LED's current. Therefore, if an LED is driven by a constant voltage, the luminous flux cannot be controlled accurately, indicated in Fig. 2.1 by dotted lines. Moreover, the voltage of an LED basically varies within a rather narrow range as the LED's current changes. In other words, small changes of the LED's voltage can result in large changes of the LED's current.

Fig. 2.2 shows a typical LED's v-i curve which indicates that we can regulate LED's voltage, thereby regulating LED's current. When the forward voltage is smaller than a

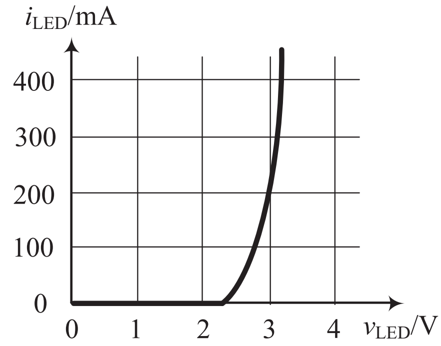

Figure 2.2: Typical LED's *v*-*i* characteristic.

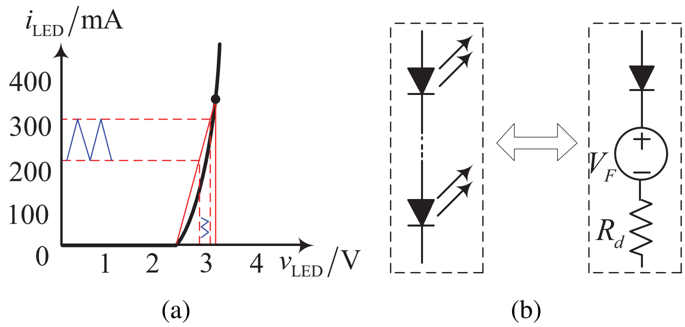

Figure 2.3: Ripple analysis from linearized model. (a) LED's voltage ripple vs. current ripple; (b) LED's simplified model.

specific threshold voltage, the current is usually quite small with no luminance. When the forward voltage is larger than a specific threshold voltage, the LED's current is changing in an approximately linear manner with the LED's voltage. The specific threshold voltage is called cut-in voltage V_F. However, when the forward voltage is larger than the cut-in voltage, a small change in LED's voltage will cause a large change in the LED's current. Thus, constant voltage source is not suited for driving LEDs [26]. Since the luminance of the LED is basically proportional to the LED's current, we can regulate the LED's current to regulate the luminance [31].

2.1.3 Model of an LED

In reality, an LED is a non-ideal voltage source having a characteristic *v*-*i* relationship, as typically shown in Fig. 2.3(a). When the forward voltage is higher than its cut-in

Table 2.1: Advantages of Different Companies.

	Technical strength	Flagship product	Package technology
Cree	High power chip	Xlamp	GaN and SiC substrates
Osram	Fluorescent material and vehicle lighting technology	Topled and Golden Dragon	SiC substrate
Philips	High power LED lighting die	Luxeon Reble	Si substrate
Nichia	Phosphor technology	High Flux	Sapphire substrate

voltage V_F, the LED's current is changing in an approximately linear manner with the LED's voltage. Therefore, an LED can be modeled as a series connection of an ideal diode, a voltage source V_F and a resistor, as shown in Fig. 2.3(b), with the forward voltage higher than V_F. The ratio of $\Delta v_o/\Delta i_o$ for a specific LED can be empirically found, e.g.,

$$\frac{\Delta v_o}{\Delta i_o} = R_d = \frac{3.15 - 2.27 \text{ V}}{350 \text{ mA}} = 2.5 \ \Omega. \tag{2.1}$$

2.1.4 Recent Progress in Enhancement of LEDs

In 1962, Holonyack [32] invented the first LED of visible red light by using gallium arsenide phosphide on gallium arsenide substrate. In 1972, Craford [33] further improved the brightness of the red LED, and created the first yellow LED at Monsanto by using gallium arsenide phosphide. In 1992, Nakamura [34, 35] at the Nichia Corporation led the development of the first bright blue LED by using GaN (gallium nitride). Since the blue LED can be produced commercially, the invention of the blue LED became the most critical milestone.

The world's major lighting giants, namely, Cree, Osram, Philips and Nichia, have launched large-scale commercial plans to commit to research and development of white LEDs. During the past two decades, each company has its own technical strengths, as shown in Table 2.1, and has contributed to the popularization of LEDs for general lighting applications.

According to the observation made in [36], the amount of light generated by one LED lamp package has increased by a factor of 20 to 30 per decade, and the luminous flux generated by one LED lamp costing a certain price (measured in lm/USD) has increased by a factor of 10 per decade. Based on the data collected in [5], for a typical 0.5 W LED (but ranging from 0.25 W to 1.0 W), the performance-to-price ratio as expressed in lumen per USD ranges from 500 to 1500 lm/USD, which means that midrange power white LEDs emitting 100 lm would cost about 10 cent. In 2016, for a retrofit LED light bulb emitting 500 lm (equivalent to a 40 W incandescent lamp), the cost of the associated LEDs was about 50 cent. In 2013, IHS Inc., a leading global marketing research company for information and analysis, reported that LED brightness had been steadily improved (i.e., high system luminous efficacy exceeding 150 lm/W) [37, 38], and the use of new materials allowed them to move into new applications for achieving energy saving.

Based on [5], the power range of the LED drivers can be broadly divided into three groups: low power (<25 W), medium power (25 W to 100 W) and high power (>100 W). The low power group suits ornament and interior lighting applications where the required luminous output is low. The medium power group suits general indoor lighting applications (including meeting room light, showroom light and flat light) where the required luminous output is relatively high. The high power group suits outdoor applications (including street lighting and floodlight) where the required luminous output is very high.

2.2 Connection Circuits and Dimming Methods

In applications where high brightness and high reliability are desired, it is necessary to use numerous LEDs. There are three ways for connecting LEDs, namely, series connection, parallel connection and hybrid connection [39–47]. In this section, the

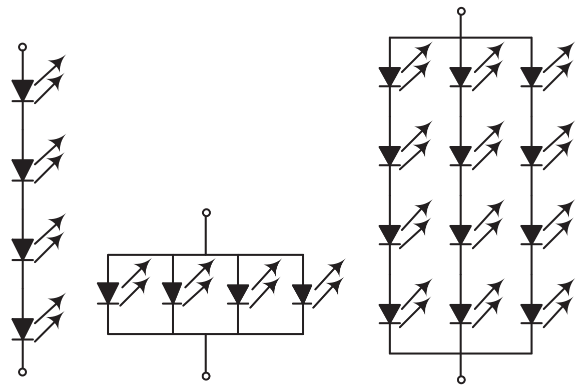

Figure 2.4: Connection circuits. (a) Series; (b) parallel; (c) hybrid.

advantages and disadvantages of various types of connection are analyzed, and their respective applications are discussed. Two basic dimming methods for LEDs, namely, PWM dimming and analog dimming are presented.

2.2.1 Connection Circuits

Series connection, which is shown in Fig. 2.4(a), can guarantee that the current flowing through each LED is identical. In view of the considerably wider range of linear relationship between the current and the luminance of the LED, the performance of luminance uniformity is good. The disadvantage is that failure of one LED will cause the whole LED string to fail. Also, with the increase of the number of LEDs, the terminal voltage of the LED string may exceed the safety limit. Furthermore, independent dimming function cannot be achieved for the individual LED lights.

The advantage of parallel connection is that a low terminal voltage can drive numerous LEDs, as shown in Fig. 2.4(b). The disadvantage is that the total current will increase with the increase of the number of LEDs. Another disadvantage is that the current flowing through each LED is different because of the difference in each LED's rated voltage, resulting in mismatch in the brightness of each LED. When any one of the LEDs is disconnected, the current flowing through the remaining LEDs will increase, which may damage the whole circuit.

As mentioned above, the problem of series-connected LEDs is the high terminal voltage when the number of LEDs is large. The problem of parallel connection is the large current when the number of LEDs is large. Therefore, hybrid connection, which combines the two styles of connection, solves the problems well. The terminal voltage and the total current can be reduced simultaneously. The whole circuit is relatively simple with high efficiency. The hybrid connection is suitable for driving a large number of LEDs, as shown in Fig. 2.4(c).

2.2.2 Dimming Methods

There are two basic control or dimming methods for LEDs, namely, PWM dimming and analog dimming [48], as shown in Fig. 2.5. Each of the methods has its own advantages and shortcomings. The PWM method is realized by switching on and off an LED string repeatedly while the LED's average current is maintained. The frequency of the LED string's switch is set from a few hundred hertz (cycles per second) to a few thousand hertz to avoid flickering and stroboscopic phenomena [49]. However, in some applications, such as machine vision and industrial inspection, high-speed cameras and sensors may respond much faster than the human eyes, thus the switching frequency of the LED strings should be raised to a few tens of kilohertz or higher, which is harder to implement. This issue, however, does not exist if we use an analog method. Additionally, PWM driving of LED backlights of display panels may easily lead to eye fatigue. Thus, some practical designs have resorted to analog driving, and some standard controller ICs are available for this purpose, such as LD5857 by Leadtrend Technology. The analog method is done by regulating the value of the forward current that flows into the LED. In view of the considerably wider range of linear relationship between the current and the luminance of the LED, an analog dimming method is applied to VSM and CSM converters for comparison in Chapter 3.

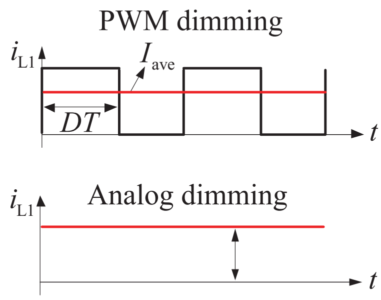

Figure 2.5: Two dimming methods.

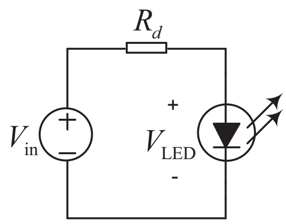

Figure 2.6: Resistor regulator.

2.3 LED Drivers

LED drivers commonly employ resistor regulators, linear regulators and switching dc-dc regulators [31, 50–52]. Details of the three drivers are provided below.

2.3.1 Resistor Regulator

The schematic diagram of the resistor regulator is shown in Fig. 2.6. The expected forward voltage can be obtained according to the LED's *v*-*i* curve. A resistor is connected in series with a voltage source and an LED. The current regulation process is achieved by controlling the voltage across the current limiting resistor, i.e.,

$$R_d = \frac{V_{\text{in}} - V_{\text{LED}}}{I_{\text{LED}}}. \tag{2.2}$$

where V_{in} is the input voltage, I_{LED} is the current following through an LED, and V_{LED} is the forward voltage drop of an LED.

This regulator is the simplest way to drive LEDs, only requiring a current limiting

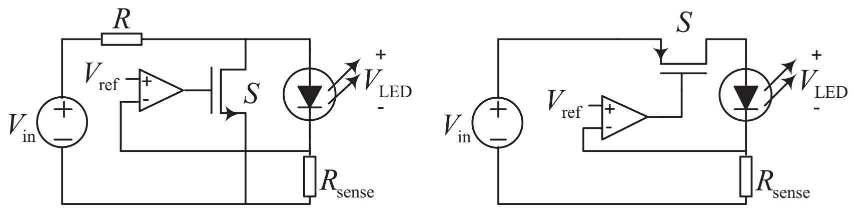

Figure 2.7: Linear regulator. (a) Parallel linear regulator; (b) series linear regulator.

resistor to regulate the LED's current. But it also has some disadvantages. One disadvantage is that small changes in the input voltage can cause large changes in the LED's current, leading to large changes in the luminous flux. Another obvious disadvantage is that the current limiting resistor consumes a great deal of power, making the whole system inefficient.

2.3.2 Linear Regulator

Compared with resistor regulator, the linear regulator can greatly improve the precision of the LED's current. The power switch working in the linear region can be equivalent to a dynamic resistance. The negative feedback network maintains the LED's current at a constant value by adjusting the equivalent resistance of the power switch. However, because the power switch operates in the linear region, lot of power is consumed and the efficiency of the system is low. The power switch can be connected in parallel or in series, as shown in Fig. 2.7.

When the power switch is connected in parallel, the switch and the LEDs can be regarded as a current divider, as shown in Fig. 2.7(a). A current limiting resistor is necessary to limit the current. As the input voltage increases, the current flowing through the LEDs increases. The increase of the feedback voltage causes the decrease of the dynamic resistance of the power switch, further causing the increase of the current flowing through the power switch. Since the total current flowing through the current limiting resistor will increase, the voltage across the current limiting resistor will in-

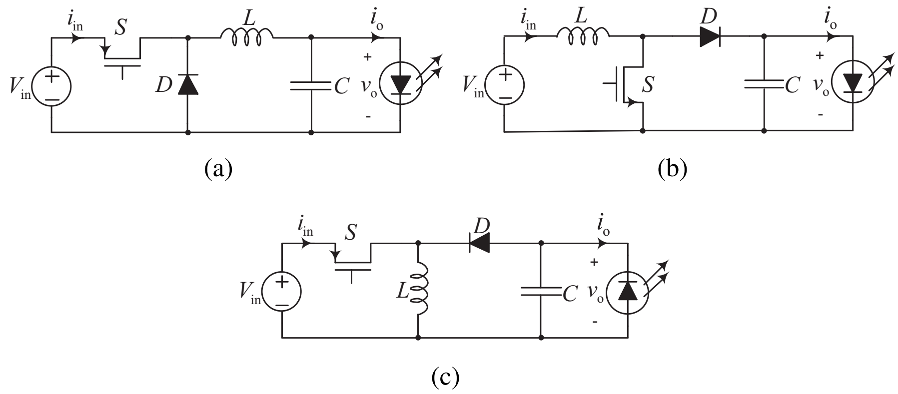

Figure 2.8: Three basic LED drivers. (a) Buck; (b) boost; (c) buck-boost.

crease and the voltage across the LEDs will decrease. The current flowing through the LEDs remains constant because of the negative feedback network. The current limiting resistor decreases the efficiency of the driver. It is difficult to keep the LED's current constant when the input voltage varies in a wide range.

When the power switch is connected in series, the switch and the LEDs can be regarded as a voltage divider, as shown in Fig. 2.7(b). The current limiting resistor is no longer needed. As the input voltage increases, the dynamic resistance of power switch increases, leading to the increase of the voltage across the power switch. The current flowing through the LEDs remains constant. Compared with the parallel linear regulator, the series linear regulator can remove the current limiting resistor, which can greatly improve the efficiency of the LED driver. However, because the input voltage should be higher than the LEDs' voltage combining with the saturation voltage of the power switch, the range of the input voltage is limited.

2.3.3 Switching DC-DC Regulator

The switching converter can regulate the output voltage by regulating the duty cycle. Theoretically, the power loss of the switch can be reduced to zero. The switching converter, which is an efficient power conversion device, can easily regulate LED's current. The traditional feedback signal of the VSM converter derives from the output voltage. The VSM converters can be used for driving LEDs by deriving the feedback signal from the output current. Three basic LED drivers, namely, buck, boost and buck-boost converters, are shown in Fig. 2.8.

The basic working principle of the buck converter [53–56] is briefly described here. When the switch is ON, the power supply charges the inductor and the load simultaneously. When the switch is OFF, the energy stored in the inductor charges the load. The switch works periodically. The output voltage can be regulated by controlling the duty cycle. The buck converter is a step-down dc-dc converter.

The basic working principle of the boost converter [57–60] is briefly described here. When the switch is ON, the power supply charges the inductor. When the switch is OFF, the power supply and the energy stored in the inductor charge the load. The switch works periodically. The output voltage can be regulated by controlling the duty cycle. The boost converter is a step-up dc-dc converter.

The basic working principle of the buck-boost [61–64] converter is briefly described here. When the switch is ON, the power supply charges the inductor. When the switch is OFF, the energy stored in the inductor charges the load. The switch works periodically. The output voltage can be regulated by controlling the duty cycle. The buck-boost converter can achieve voltage step-up or step-down function.

2.4 SIMO LED Drivers

In many applications, multiple-output LED driving with independent dimming functions is necessary, such as color-temperature control, multiple dimming control and lighting in power-saving mode [21–24]. The various output power levels are usually generated from a single power source.

The most direct and effective way to achieve independent dimming functions is to use a parallel structure, as shown in Fig. 2.9(a). The parallel-connected converters are completely independent, and the cross-regulation effects can be eliminated. However,

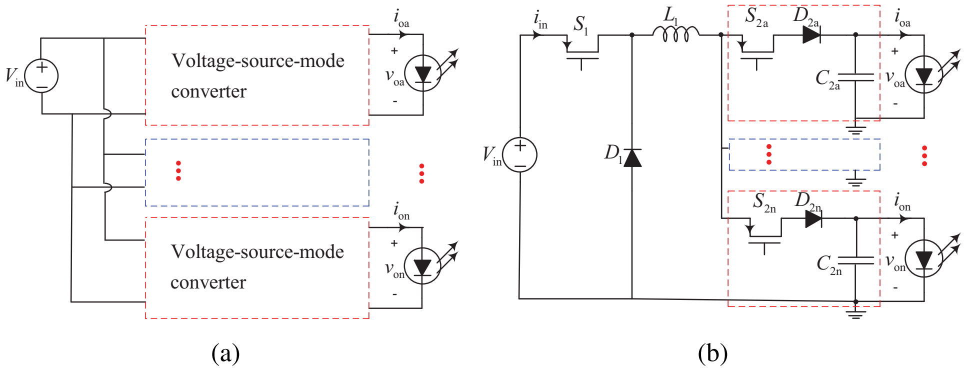

Figure 2.9: Conventional multiple-output topologies. (a) Parallel-connected dc-dc converters; (b) conventional SIMO dc-dc converter.

this parallel structure requires extra sets of components, increasing the cost and complexity of the system. Compared to the parallel-connected dc-dc converters, the SIMO dc-dc converter [65–69] provides a low-cost solution as it uses only one inductor to generate multiple outputs. Fig. 2.9(b) shows an existing SIMO dc-dc converter. The function of diodes D_{2a} to D_{2n} is to prevent the reverse current.

Obviously, the existing SIMO dc-dc converter has certain drawbacks including the need for multiple closed-loop controls and the inevitable cross-regulation effects [70–76]. Previous works have analyzed the steady-state voltage gain and the cross-regulation problem of the SIMO dc-dc converter [77,78], and some solutions have been proposed, including the coordination of multiple control loops under three different operation modes, namely, discontinuous conduction mode (DCM), pseudo-continuous conduction mode (PCCM) and continuous conduction mode (CCM), to achieve independent dimming functions and alleviate cross-regulation effects.

Under DCM operation, the pulse-train (PT) and time-multiplexing (TM) control techniques have been employed [70, 78]. In this case, the SIMO dc-dc converter with n outputs divides up the main switching cycle into n sub-intervals. Each sub-interval supplies power to an output. Since the inductor current decreases to zero before each sub-interval ends, the PT and TM control techniques can achieve independent dimming function and suppress cross regulation. However, there are three main drawbacks.

First, the SIMO dc-dc converter can only work under light load condition incurring large current ripple, high switching noise and high switching device dissipation. Second, when we set the main switching frequency, other switching frequencies are $1/n$ of the main switching frequency. This arrangement is not desirable, especially when the number of outputs increases. Third, the control strategies are complex and the number of current sensors required is large.

Under PCCM operation, an extra switch connected in parallel with the inductor is needed to improve the power levels and suppress cross-regulation effects [72, 73]. In this mode, each switching cycle contains a freewheeling interval for improving load capability. The extra switch thus imposes a higher cost to the design, and the switching loss could be increased because of the non-zero inductor current.

Under CCM operation, moreover, in order to achieve independent dimming functions and reduce the cross-regulation effects, various control techniques have been proposed. A digital control method for the SIMO dc-dc converter has been considered [74], involving separate control of common-mode and differential-mode output voltages. However, with the differential-mode loop gain kept constant under load change, the cross-regulation effects cannot be eliminated. Another approach is to apply multiple-loop control [75], which uses an outer loop to regulate the inductor current using an average current mode control and an inner loop to regulate each output. However, the effects of cross regulation are still significant because of the different bandwidths in the control loops. Furthermore, a predictive digital current mode control strategy has been proposed [79], which exploits the computational capability to calculate the duty cycle of the next switching cycle. The predictive control allows the SIMO dc-dc converter to reduce cross-regulation effects. An alternative digital control strategy was also reported [80], which uses a feedback network containing a multiple-variable controller based on shaping a family of open-loop multiple-input multiple-output transfer function matrices. This method can achieve independent dimming functions and minimize the cross-regulation effects. However, these digital control strategies are rather complex. The circuit cost and computational burden are expectedly high.

All the strategies mentioned above are based on the VSM converters. Through the use of *circuit duality* principle [19, 20], a family of CSM converters can be obtained from the common VSM converters. The differences between VSM and CSM converters are presented below.

The first difference is that for a VSM converter, the input voltage is assumed to be fixed, and the two complementary switches and the inductor form the basic cell. For a CSM converter, the input current is fixed, the two complementary switches and the capacitor form the basic cell. The second difference is that the inductor's function in a VSM converter is totally different from the inductor's function in a CSM converter. The inductor in a VSM converter is a high-frequency switching storage component while the inductor in a CSM converter is a filter component. The third difference is that VSM converters deliver voltage to the output. If we use openloop control for VSM converters, the duty cycle will change the output voltage which is not suitable for LED dimming. However, CSM converters deliver current to the output. Openloop control is adequate for CSM converters, as the duty cycle will change the output current directly. The fourth difference is that the value of the switching storage *inductor* in a VSM boost converter must be chosen to guarantee operation in the intended mode. In the CSM buck converter, the value of the switching storage *capacitor* must be chosen to guarantee operation in the intended mode.

Despite their long history of existence [81], CSM converters are still relatively less analyzed or applied for driving LEDs. The main reason for this omission is that voltage sources are a more common form of power sources and can be connected to the input terminals of a VSM converter directly. It has sometimes been misunderstood that the CSM converters are simply VSM converters with an additional storage upon superficial inspection of the circuits. Such misconception has created confusion and prevented proper understanding of the characteristics of CSM converters. Furthermore, resistive loads are also a commonly assumed form of loads and more widely included in analysis. A comparatively smaller amount of literature has thus been devoted to discuss the application of CSM converters and the dual operation of driving LEDs [66, 82–86].

In [81], the duality principle enables the attainment of CSM converters based on VSM converters. Both the CSM isolated and CSM non-isolated versions are derived in this work [81]. At that stage, however, LED lighting was largely unknown. The author predicted that the CSM circuits would help to complete a supplementary portion in the large area of the problems associated with power electronics circuits.

If transformer isolation is desired, flexibility exists in combining the two stages through appropriate switching arrangement and transformer design. An example of a dual power supply with power factor correction and current load driving can be found in [87], which represents an early attempt in applying duality principle for deriving alternative current-based topologies. It should be noted that although the design described in [87] did not explicitly address the LED driving applications at the time it was published, it should now become apparent that such a design is highly relevant to the driving of LED lighting systems.

Qin *et al.* [83] proposed an LED driver without electrolytic capacitor by using CSM converters and duality principle. The output can be regarded as a current source controlled by duty cycle, which is suited for driving LEDs. The problem in this paper is that the inductor is designed to attenuate harmonics at double of the line frequency, requiring the use of a large inductance. The cost of the circuit is high and the power density is low.

Galkin *et al.* [84] presented a comparative study of applying VSM and CSM converters for driving LEDs. In [86], we present a complete exposition of the circuit theoretic analysis of LED driving methods and the basic topological requirements of practical LED drivers that are fed from standard voltage sources.

In [88], the current source generator, which is constructed by using half-bridge converter, connects with a CSM buck converter to form a CSM transformer isolated converter. The size and cost of the LED driver are increased because of the relatively complicated current source generator. Therefore, it is not a desirable design for the current source generator.

Given the huge power consumption in lighting applications, high efficiency is an important design consideration for SIMO LED drivers. Recently, Lee *et al.* [43] proposed a quasi-hysteretic finite-state-machine-based control strategy using an FPGA (Field Programmable Gate Array) hardware for driving multiple-string LEDs. This control strategy has no compensation loop and is simple to implement. The drawback, however, is that the converter cannot operate in CCM. Furthermore, Wai and Liaw [89] presented a bidirectional single-input multiple-output converter with high efficiency. However, since their proposed converter contains one coupled inductor and one auxiliary inductor, the volume and cost of the system are inevitably increased. Another price to pay for a higher efficiency is that this topology adopts four power switches, leading to increased cost and complexity of the controller.

In some multiple-output applications, the input voltage is much higher than the output voltage. A high voltage step-down ratio is thus desirable. Also, since the input is a high voltage, the use of high-voltage components is necessary. Switching losses are thus increased. In order to overcome these limitations, a series-input-connected structure for driving LEDs has been proposed [1]. Due to the series connection at the input terminal, the input voltages of the connected converters become lower, leading to low voltage stress of the components. The use of low-voltage components and low on-resistance switches can increase the efficiency. However, the drawback is that if one converter fails, other converters would have to share the input voltage, leading to increased voltage stress in each converter. A duty cycle exchanging control can be applied to the input-series-output-series connected dc-dc converter [90] to reduce the voltage stress of switches. This scheme is, however, only applicable to two-converter configurations.

In this thesis, we introduce an inductorless CSM converter and a series structure of connecting multiple CSM converters based on duality principle. This converter and the connection configuration are effectively the dual versions of the usual dc-dc converter and the parallel configuration shown in Fig. 2.9(a).

2.5 Summary

This chapter provides a literature review on some electrical characteristics of LEDs, connection circuits, dimming methods and traditional LED drivers. For most practical purposes, the input of an LED driver is required to connect to a voltage source, leading to obvious constraints for CSM converters. In order to fully exploit the advantages of CSM converters for SIMO conversion applications, CSM converters and voltage-to-current converter are combined to form a two-stage converter. The voltage-to-current converter is in practice a common dc-dc converter controlled to deliver constant output current. According to the analysis on the circuit requirement for converting power from a voltage input termination to an LED output termination, the CSM SIMO converter is proposed. Some strategies for improving the efficiency of SIMO LED drivers are studied. Therefore, our focus in this dissertation is on presenting a systematic and comparative exposition of the circuit theory of driving LEDs, designing CSM SIMO LED drivers and improving the efficiency of the system.

Chapter 3

VSM and CSM LED Drivers

3.1 Introduction

In the previous chapter, we reviewed some basic characteristics of LEDs, connection circuits, dimming methods and LED drivers. In this chapter, we will study the circuit duality principle and examine the circuit transformation of power conversion circuits via the duality principle. The comparison between VSM LED drivers and CSM LED drivers will be investigated in terms of the main circuit components, the range of duty cycle variation, the sensitivity of the output current to the change of duty cycle, the nonlinearity of the control function and the control complexity. Two multiple-output converters are derived based on CSM converters which are suitable candidates for driving LEDs. The exact circuit configuration depends on the specific choice of the converter circuits. We emphasize that proper application of circuit concepts would form the basis of design of effective driving circuits for LED applications. Some practical configurations of 10-W LED driving circuits are presented in this chapter for the purpose of illustration.

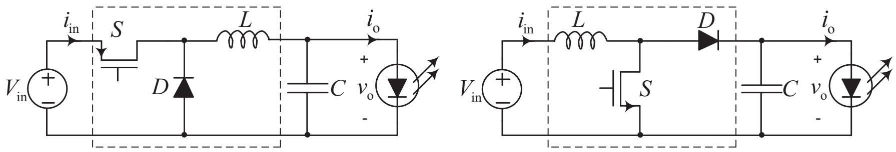

Figure 3.1: Basic converters (referred to as VSM converters in this thesis). (a) VSM buck converter; (b) VSM boost converter.

3.2 Circuit Duality Principle

The conventional buck and boost converters, here referred to as VSM buck and boost converters, are shown in Fig. 3.1. The input termination is fed by a voltage source, which is normally a constant DC voltage. The converters deliver voltage to an LED load, and the duty cycle controls the input-to-output voltage ratio. Thus, the output can be regarded as a controllable voltage source. For a VSM converter, under CCM operation, the well-known steady-state voltage gain, M, is

$$M = \frac{V_o}{V_{in}} = \begin{cases} D & \text{for VSM buck converter} \\ \dfrac{1}{1-D} & \text{for VSM boost converter} \end{cases} \tag{3.1}$$

where D is the steady-state duty cycle, V_{in} and V_o are the input and output voltages.

The duality transformation of a VSM converter to a CSM converter follows the following standard procedure [19]:

1. A dual graph is obtained, as illustrated in Fig. 3.2.

2. Voltage sources are replaced by current sources, and vice versa. Capacitors are replaced by inductors, and vice versa. Resistors (R) are replaced by conductors ($G = 1/R$).

3. An "on" switch is replaced by an "off" switch, and vice versa. Hence, duty cycle D becomes $(1 - D)$.

The current-source-mode counterparts of the buck and boost converters are shown in

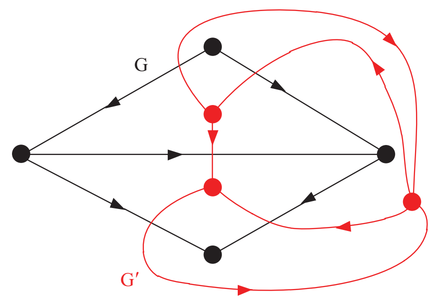

Figure 3.2: Graph G and its dual G'.

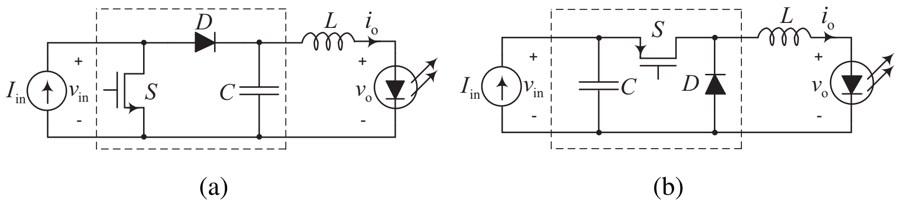

Figure 3.3: Dual or CSM converters. (a) CSM buck converter; (b) CSM boost converter. Common misconception may result from superficial circuit inspection, e.g., the CSM boost converter "looks" like a buck converter preceded by a capacitor. The switching storage here is the capacitor C and its value must comply with the respective operating mode, whereas the "small" inductor only serves to smooth the output current and is not part of the converter circuit.

Fig. 3.3. The input termination is fed by a current source. The converters deliver current to an LED load. The duty cycle controls the current ratio of the input and output. Thus, the output can be regarded as a controllable current source.

The basic working principle of the CSM buck converter is briefly described here. When the switch is ON, the input current source is short and the capacitor charges the load. When the switch is OFF, the input current charges both the capacitor and the load. The input current is injected into the basic cell, and the capacitor delivers energy to the load. The capacitor follows the amp-second balance.

The basic working principle of the CSM boost converter is briefly described here. When the switch is ON, the input current source and the capacitor charge the load. When the switch is OFF, the input current source charges the capacitor. The inductor charges the load. The input current is injected into the basic cell, and the capacitor delivers energy to the load. The capacitor follows the amp-second balance.

For a CSM converter under CCM operation, the steady-state current gain, M', is directly obtained by replacing D with $1 - D$ in the corresponding VSM equation, i.e.,

$$M' = \frac{I_o}{I_{\text{in}}} = \begin{cases} 1 - D & \text{CSM buck converter} \\ \dfrac{1}{D} & \text{CSM boost converter} \end{cases} \tag{3.2}$$

where I_{in} and I_o are input and output currents. We should point out that *the CSM converter has often been misinterpreted as a VSM converter plus a storage component (capacitor or inductor).* For instance, from a superficial inspection of the circuit of Fig. 3.3(a), one may be mistaken to consider the CSM buck converter as a VSM boost converter if we replace the current source by a voltage source connected in series with an inductor. This viewpoint is obviously incorrect. The VSM boost converter and the CSM buck converter are totally different. First, the value of the switching storage capacitor in the CSM buck converter, like its inductor counterpart in the VSM boost converter, must be chosen to guarantee operation in the intended mode. In fact, the CSM buck converter, as shown in the dashed block, generates current to the load consisting a smoothing inductor and an LED. Second, the current source constructed by a voltage source behind an inductor is an alterable current source. Thus, when the power changes, the input current would change accordingly while the input voltage would be constant. However, for the CSM buck converter, the input current is constant and unaffected by the power output. The range of duty cycle variation in the CSM buck converter is thus wide, as will be explained in Section 3.3.2. Third, the CSM buck converter inherently delivers current directly to the output, and this property dramatically simplifies the control circuit, as will be explained in Section 3.3.5.

There are two variables of an LED, i.e., the forward voltage and the operating current. According to (3.1), for a VSM converter, we can adjust the duty cycle to control the output voltage which is connected to the forward voltage of the LED. The operating current, which determines the luminance, changes with the forward voltage.

Table 3.1: Parameters of Test Circuits

	VSM buck converter	CSM buck converter	VSM boost converter	CSM boost converter
V_{in}	48 V	—	24 V	—
I_{in}	—	500 mA	—	100 mA
T	20 μs	20 μs	20 μs	20 μs
L	2000 μH	2000 μH	2000 μH	2000 μH
C	47 μF	47 μF	47 μF	47 μF

Moreover, according to (3.2), for a CSM converter, we can theoretically adjust the duty cycle to control the operating current of the LED, leading to direct luminance control.

3.3 Comparison of VSM and CSM Drivers

Here, we compare the VSM and CSM drivers in terms of number and size of the main circuit components, the range of duty cycle variation, the sensitivity of the output current to change of the duty cycle, and the extent of nonlinearity. The load is composed of a string of n white LEDs stacked in series. All converters are designed to operate in continuous CCM. (In the case of CSM converters, the CCM operation corresponds to continuous capacitor voltage mode (CCVM).) For effective illustration, we present alongside the following analysis a set of measured data from experimental circuits. The circuit parameters of the prototypes are listed in Table 3.1. Each LED is rated at 1 W and 350 mA. All converters employ the same set of components: MOSFET, diode, inductor and capacitor. In the test circuits, we set $n = 10$.

3.3.1 Number and Size of Circuit Components

In order to compare the number and size of the main circuit components of the VSM and CSM converters, we analyze the output ripple amplitude, which affects the color drift characteristic and lifetime of LEDs. In the case of the VSM buck converter, the

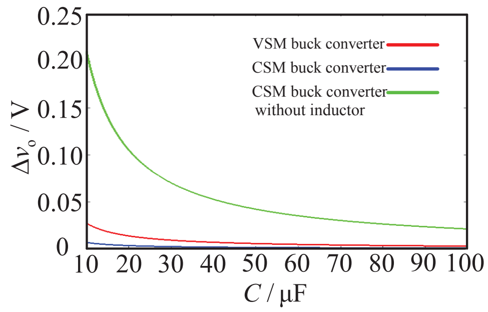

Figure 3.4: Relationship between ripple and capacitance value of VSM and CSM buck converters

current ripple of the inductor can be obtained as

$$\Delta i_L = \frac{V_{\text{in}} - n\,(V_F + I_o R_d)}{L} DT \tag{3.3}$$

where I_o is the steady-state average output (load) current, V_F and R_d are as defined in Fig. 2.3. The output voltage ripple, which corresponds to the current ripple in (3.3), can be calculated as

$$\Delta v_o = \frac{\{V_{\text{in}} - n\,(V_F + I_o R_d)\}\,DT^2}{8LC} \tag{3.4}$$

where C is the output capacitor which is included for ripple reduction and is not regarded as part of the switching converter.

In the case of the CSM buck converter, the current ripple of the inductor, which is also the output current ripple, can be calculated as

$$\Delta i_o = \frac{(I_{\text{in}} - I_o)\,(1 - D)\,T^2}{8LC} \tag{3.5}$$

where I_o is the steady-state average output current. According to (2.1) and (3.5), the equivalent voltage ripple of the CSM buck converter is

$$\Delta v_o = \frac{nR_d\,(I_{\text{in}} - I_o)\,(1 - D)\,T^2}{8LC}. \tag{3.6}$$

where L is the output inductor (similar to the output capacitor in the VSM case) which

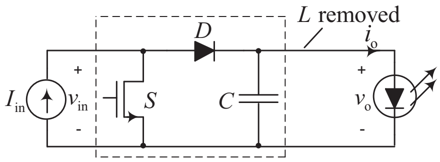

Figure 3.5: CSM buck converter with output inductor removed

plays no role in switching storage and is not part of the converter.

Furthermore, in the case of the CSM buck converter, if inductor L is removed, the new output voltage ripple of the CSM buck converter can still meet the usual requirement as long as the capacitance value is chosen appropriately. The output voltage ripple of the CSM buck converter without the output inductor is

$$\Delta v_o = \frac{I_{\text{in}} - I_o}{C}(1 - D)T. \tag{3.7}$$

Taking $I_o = 350$ mA as an example, according to equations (3.4), (3.6) and (3.7), the voltage ripples of the LEDs for different drivers are plotted in Fig. 3.4, from which we see that the voltage (or current) ripple magnitude of the LED driven by the CSM buck converter is smaller than that driven by the VSM buck converter having the same L and C values (same size). Furthermore, the output voltage (or current) ripple of the CSM buck converter without the inductor increases slightly. However, with a slightly larger capacitance, the ripple can be dramatically reduced to meet the requirement. Without the inductor, the size, weight and cost of the circuit can be significantly reduced, as shown in Fig. 3.5.

In the case of the traditional VSM boost converter, the output voltage ripple is

$$\Delta v_o = \frac{I_o DT}{C} \tag{3.8}$$

where I_o is the steady-state average output (load) current, and the current ripple in an

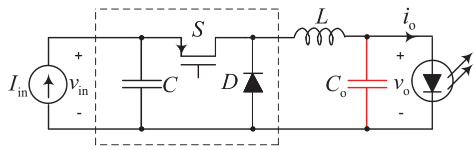

Figure 3.6: CSM boost converter with additional output capacitor.

LED load driven by the VSM boost converter is

$$\Delta i_o = \frac{I_o DT}{nR_d C}. \tag{3.9}$$

In the case of the CSM boost converter, the current ripple of the inductor is also the output current ripple, which can be found as

$$\Delta i_o = \Delta i_L = \frac{n(V_F + I_o R_d)}{L}(1 - D)T. \tag{3.10}$$

Since the LED's current is the inductor's current, the current ripple amplitude in the CSM boost driving converter is larger than that in the VSM boost converter. It should be noted that for the CSM boost converter, in order to reduce the output current ripple, a capacitor should be connected to the output terminal, as shown in Fig. 3.6. This smoothing or filtering arrangement may be necessary for practical purposes but bears no theoretical mandate as far as the current output of the CSM boost converter is concerned. In fact, the average output current magnitude of the CSM boost converter is unaffected.

The current ripple of the LED driver using a CSM boost converter connected with an additional capacitor is given by

$$\Delta i_o = \frac{(V_F + I_o R_d)(1 - D)T^2}{8nR_d L C_o}. \tag{3.11}$$

Taking $I_o = 350$ mA as an example, according to (3.9), (3.10) and (3.11), the current ripples of the LEDs using different drivers are plotted in Fig. 3.7. Here, we see that

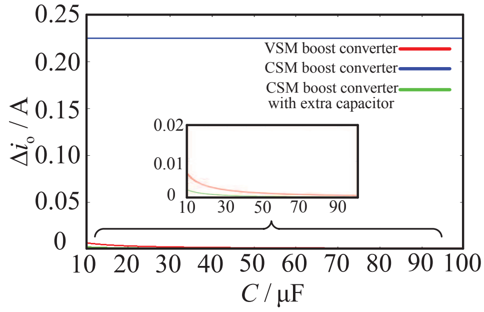

Figure 3.7: Relationship between ripple and the capacitance value of VSM and CSM boost converters

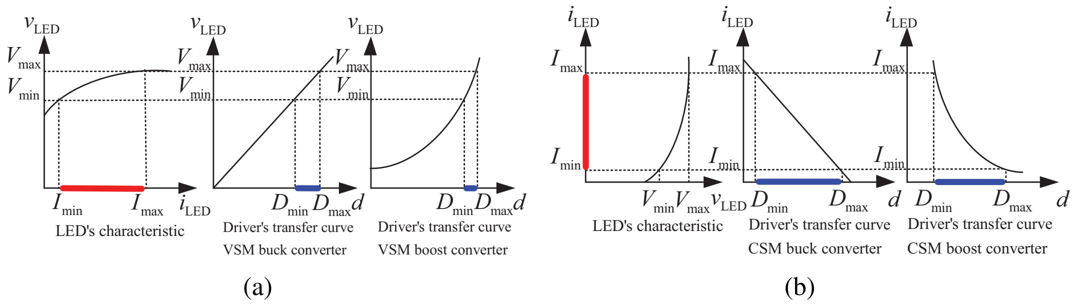

Figure 3.8: Current control under VSM and CSM driving. (a) Variations of LED current and voltage under VSM driving; (b) variations of LED current and voltage under CSM driving.

the current ripple amplitude of the CSM boost converter is much larger than in the other drivers. After inserting an extra capacitor at the output, the current ripple can be reduced significantly. However, the size, weight and cost of the circuit will be inevitably increased.

3.3.2 Range of Duty Cycle Variation

For the VSM converters, the input voltage is the constant voltage source. Based on (3.1), we can derive the driver's transfer characteristics for VSM buck and VSM boost converters. Combining the converter's transfer characteristic and the LED's *v*-*i* characteristic, we obtain an overall transfer characteristic as shown in Fig. 3.8(a). For the CSM converters, however, the input current is constant. Based on (3.2) and the LED's *v*-*i* characteristic, we obtain the overall transfer characteristic as shown in Fig. 3.8(b).

Table 3.2: Theoretical Duty Cycle Range (I_o = 150–350 mA)

	VSM buck	CSM buck	VSM boost	CSM boost
D_{max}	0.656	0.700	0.238	0.667
D_{min}	0.552	0.300	0.094	0.286
D_{span}	0.104	0.400	0.144	0.381

From Fig. 3.8(a), it is obvious that, for VSM driving, the output current can be changed by adjusting the output voltage, which can be adjusted or controlled via the duty cycle over a rather narrow range, making the control rather sensitive. (Here, we do not discuss the case where the output voltage of the VSM converter is connected to the LED load via a small resistor, where current adjustment is undesirably sensitive.) For CSM driving, however, as shown in Fig. 3.8(b), the output current can be changed by adjusting the duty cycle directly. Thus, the corresponding change in the duty cycle is much greater, and the current control can be achieved with the duty cycle varying over a wide range.

Suppose the range of duty cycle is the value of duty cycle from D_{min} to D_{max}, i.e.,

$$D_{\text{span}} = D_{\text{max}} - D_{\text{min}}. \tag{3.12}$$

Based on the simplified model of Fig. 2.3, the theoretical duty cycle ranges of these converters are shown in Table 3.2. In general, CSM converters have a wider range of duty cycle variation than VSM converters over the same range of current variation. Thus, CSM converters are more desirable for applications requiring higher output current resolution. In single-output applications, the advantage of the wide range of duty cycle is not easy to recognize. However, in multiple-output applications, the wide range of duty cycle will bring many benefits.

3.3.3 Sensitivity

We define *sensitivity* as the absolute ratio of the variation of the steady-state output current (ΔI_o) to the corresponding variation of the steady-state duty cycle (ΔD). Thus, *sensitivity* is a function of D and can be written as

$$S = |f(D)| = \left|\frac{dI_o}{dD}\right| \approx \left|\frac{\Delta I_o}{\Delta D}\right|. \tag{3.13}$$

Based on the simplified model of LED, and using (3.1), (3.2) and (2.1), the relationship between I_o and D for VSM and CSM converters is

$$I_o = \begin{cases} \dfrac{V_{\text{in}}D}{nR_d} - \dfrac{V_F}{R_d} & \text{VSM buck converter} \\ I_{\text{in}}(1-D) & \text{CSM buck converter} \\ \dfrac{V_{\text{in}}}{nR_d(1-D)} - \dfrac{V_F}{R_d} & \text{VSM boost converter} \\ \dfrac{I_{\text{in}}}{D} & \text{CSM boost converter} \end{cases} \tag{3.14}$$

According to (3.13) and (3.14), the expression of *sensitivity* can be given as

$$S = \begin{cases} \dfrac{V_{\text{in}}}{nR_d} & \text{VSM buck converter} \\ I_{\text{in}} & \text{CSM buck converter} \\ \dfrac{V_{\text{in}}}{nR_d(1-D)^2} & \text{VSM boost converter} \\ \dfrac{I_{\text{in}}}{D^2} & \text{CSM boost converter} \end{cases} \tag{3.15}$$

The maximal/minimal value of the *sensitivity* is the worst/best value of S, i.e.,

$$\begin{cases} S_{\max} = \left|\dfrac{(\Delta I_o)_{\max}}{\Delta D}\right| \\ S_{\min} = \left|\dfrac{(\Delta I_o)_{\min}}{\Delta D}\right| \end{cases} \tag{3.16}$$

where $(\Delta I_o)_{\max}$ and $(\Delta I_o)_{\min}$ are the maximal and minimal ΔI_o corresponding to the variation of duty cycle ΔD. In practice, a smaller S is more desirable because of

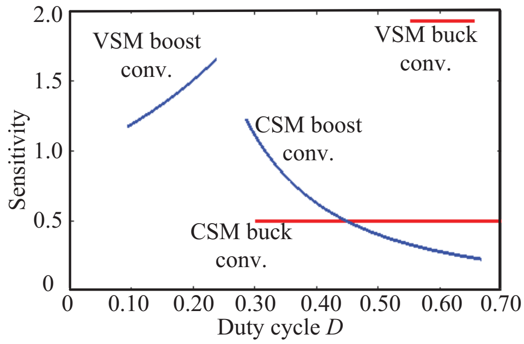

Figure 3.9: Sensitivity S versus duty cycle D.

Table 3.3: Theoretical Sensitivity (I_o = 150–350 mA)

	VSM buck	CSM buck	VSM boost	CSM boost
S_{max}	1.92	0.50	1.65	1.22
S_{min}	1.92	0.50	1.17	0.22

the smaller ΔI_o caused by the same variation of D. Table 3.3 and Fig. 3.9 show the variation in S. According to Fig. 3.9, CSM converters have lower *sensitivity* than VSM converters for the whole range of duty cycle.

3.3.4 Nonlinearity

According to equation (3.14), we can plot the duty-cycle-to-output transfer characteristic of the drivers, as shown in Fig. 3.10. In order to evaluate the linearity of the transfer characteristic, we adopt a measure, known as *nonlinearity* N [91], which is defined as

$$N = \frac{\Delta W}{W} \tag{3.17}$$

where W is the root-mean-square of the transfer characteristic $I_o = f(D)$ in equation (3.14), ΔW is the root-mean-square of the difference between the transfer characteristic

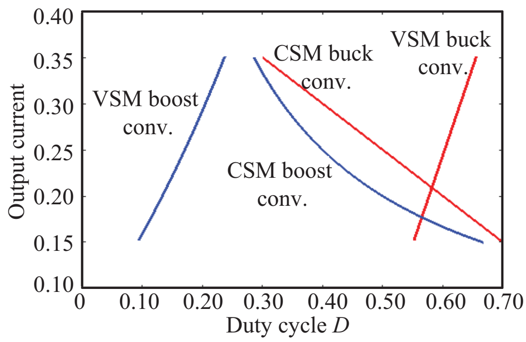

Figure 3.10: Output current I_o versus duty cycle D.

Table 3.4: Theoretical Nonlinearity (I_o = 150–350 mA)

	VSM buck	CSM buck	VSM boost	CSM boost
W	0.2583	0.2566	0.2528	0.2291
ΔW	0	0	0.0044	0.0303
N	0	0	0.0174	0.1323

of (3.14) and the line $I_o = f_L(D)$ that connects the border points. Specifically we have

$$\begin{cases} W &= \sqrt{\dfrac{\int_{D_{\min}}^{D_{\max}} f^2(D)dD}{D_{\max} - D_{\min}}} \\ \Delta W &= \sqrt{\dfrac{\int_{D_{\min}}^{D_{\max}} [f(D) - f_L(D)]^2 \, dD}{D_{\max} - D_{\min}}} \end{cases} \tag{3.18}$$

Theoretical values of nonlinearity N are calculated and given in Table 3.4, based on the simplified model of LED shown in Fig. 2.3.

The nonlinearity can affect the stability of the control system. In general, a smaller N is more desirable. According to Fig. 3.10 and Table 3.4, the VSM and CSM buck converters have smaller values of N than the VSM and CSM boost converters.

3.3.5 Control Complexity

For VSM converters, we apply the conventional current-mode control which programmes the inductor current (peak or average) directly via a fast inner current loop. The resulting variation of the duty cycle is, however, very small due to the output volt-

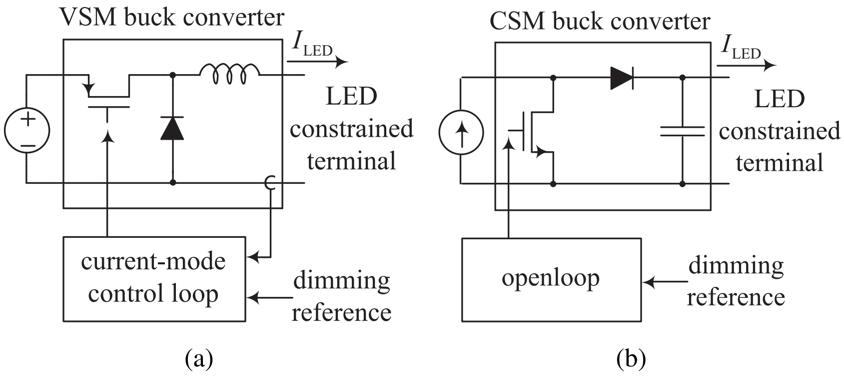

Figure 3.11: Control for VSM and CSM driving, showing (a) the need for inner current loop; (b) simple openloop control.

age being more or less fixed according to the LED's *v-i* curve. For CSM converters, if the load and input current do not change, the duty cycle can directly set the output current in an openloop configuration, and in the case of varying load, the output current can be regulated via a simple control that adjusts the duty cycle in a closed-loop manner. However, the current-mode control in VSM converters requires current sensing and a fast loop under the command of a current reference for achieving dimming control. The openloop option in CSM converters may reduce complexity, whose validity is of course subject to the provision of an input current source. As mentioned previously, in CSM converters, replacing the closed-loop control with an openloop control can be achieved by virtue of the wide control range, sensitivity and nonlinearity. Furthermore, the output current of a CSM converter can be directly controlled by the duty cycle regardless of the difference in each LED's rated voltage. Compared to the conventional use of a VSM converter in delivering current (a dc-dc converter under current-mode control), the CSM converter requires a much simpler and direct control, as shown in Fig. 3.11. In multiple-output LED driver applications, the openloop control strategy can greatly reduce the complexity and cost of the controller (as will be explained later). Thus, we only need one closed-loop controller to construct the constant current generator, and use several openloop controllers for the CSM LED drivers.

A dimming reference can be produced by an analog dimmer circuit. For the VSM buck converter, we can regulate the analog dimmer to regulate the reference signal, thereby regulating the output current. For the CSM buck converter, we control the analog dimmer to adjust the duty cycle in order to regulate the output current.

Remarks: It should be noted that despite the inherent features of CSM converters that facilitate current driving, the need for a feeding current source will still require a VSM converter for connection to an input voltage source. Thus, under the current constraint of voltage source input, the advantages of CSM converters become apparent in multiple-output applications.

3.4 Implementations of Multiple-Output CSM converters

In power electronics, we usually derive design solutions from the point of view of voltage terminations involving VSM converters. For LED driving, CSM converters have relative advantages, as studied in the previous section. In some recent applications [92, 93], CSM driving has been discussed on the basis of some existing ballast circuits which feed current directly and can be connected to the CSM converters discussed in this thesis. In cascade connection, we can in fact distribute power by controlling current in the downstream drivers although we customarily do so by controlling voltage. When the specific loads are LEDs, we show that the use of current driving in power distribution would not incur additional loss and cost, despite the need for an additional voltage-to-current converter. Moreover, the practical merit of using CSM converters for driving LEDs would become more apparent in applications requiring separately dimmed multiple outputs. In the following, we illustrate the convenient use of CSM converters in multiple-output applications.

The traditional voltage-based structure of a multiple-output converter is shown in

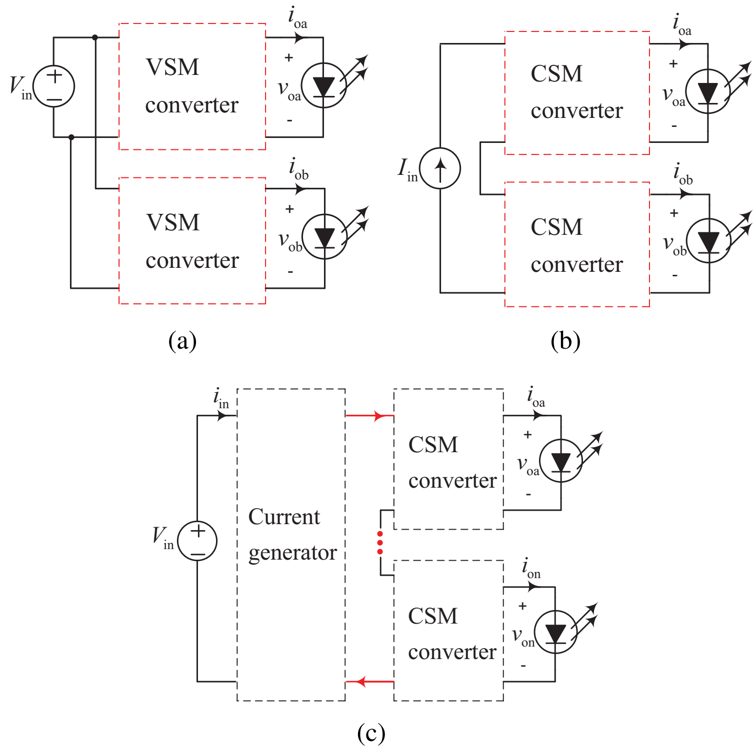

Figure 3.12: Multiple-output converters. (a) Parallel structure with input being voltage source; (b) series structure with input being current source; (c) series structure with input being voltage source.

Fig. 3.12(a). In a dual fashion, the current-based structure of a multiple-output converter is shown in Fig. 3.12(b). However, in practical situations, voltage source is the common form. If CSM converters are to be used to improve controllability of individual output currents, a current generator is needed. The general form of a multiple-output driver is shown in Fig. 3.12(c), which consists of a current generator and a number of series connected CSM converters delivering controllable currents to a set of LED loads.

3.4.1 Control Strategy

The exact circuit configuration depends on the specific choice of the converter circuits. The current generator consists of one switch, one diode and one inductor. A buck-type converter is used for this purpose in this thesis. Fig. 3.13 shows the control diagram

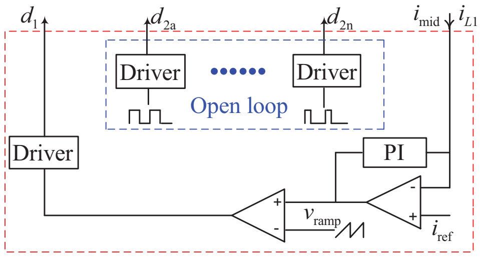

Figure 3.13: Typical control strategy.

of the multiple-output converters in Fig. 3.12(c) under CCM operation. The current generator employs a standard PI controller to regulate the current that feeds the CSM converters. Current i_{L1} is the inductor current of the current generator. Signal d_1 is used to drive switch S_1. Moreover, as explained in Section 3.3.2, CSM converters have a wide controllable range of current using direct duty cycle control, enabling a much higher brightness resolution to be implemented. The signals, d_{2a} to d_{2n}, as shown in Fig. 3.13 drive switches in the corresponding CSM converters.

It is useful at this point to compare a prior control strategy described in ref. [94], which combines average current mode control and charge control. This design, however, necessitates the use of $n - 1$ current sensors (where n is the number of outputs) to achieve independent dimming function. As shown in Fig. 3.13, our CSM multiple-output converter only needs one current sensor to generate the constant current. The individual outputs are controlled by the corresponding duty cycles. Independent dimming functions can be achieved easily without using current sensors. Another difference is that the inductor current in ref. [94] is the sum of all output currents. Thus, the inductor current will increase significantly as the number of outputs increases, whereas the control strategy shown in Fig. 3.13 works well as long as the inductor current is higher than the largest output current. The power level will automatically be adjusted by varying the voltages at the inputs of the CSM converters.

The rapid change of the output voltage of the current source generator may present a design challenge for the controller. In practice, however, the variation frequency of this voltage is at the switching frequency range which is well above the crossover

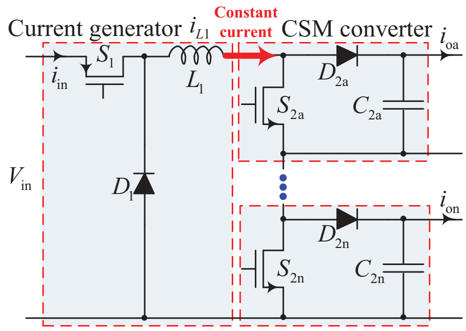

Figure 3.14: CSM SIMO converter

frequency of the feedback compensation circuits, as will be explained in Section 4.4. Thus, despite the variation of the output voltage of the current source generator, as reflected by the waveform of the inductor's current, the control design remains simple as long as the crossover frequency is set sufficiently low, for instance, at about 1/10 of the switching frequency.

3.4.2 Single-Inductor Multiple-Output LED Driver

When buck-type CSM converters are used as the downstream CSM converters, as shown in Fig. 3.14, the output smoothing inductor is unnecessary and can be removed, as explained previously in Section 3.3.1, resulting in minimum number of inductors used. This converter only uses one inductor achieving design simplicity, small volume and low cost. In order to demonstrate the design advantages, we compare the CSM SIMO converter under CCM operation with the SIMO converter previously studied in [70, 78] under DCM operation, the SIMO converter studied in [80] under CCM operation and the series-connected SIMO converter studied in [95].

In terms of control strategy, the CSM SIMO converter uses one closed-loop controller and several simple openloop controllers based on the analysis in Section 3.4.1. The whole control circuit is very simple. However, the SIMO converters studied in [70, 78] under DCM operation adopts time-multiplexing or pulse-train control method which is a relatively complex method. The SIMO converter studied in [80] under CCM operation adopts a multivariable digital control method which is a more complex control method and could increase the cost and complexity of the controller. The SIMO converter reported in [95] is essentially a combination of two boost converters sharing an inductor, necessitating the use of multiple closed-loop controllers for achieving independent dimming functions. In terms of the controller cost, our CSM SIMO converter has the lowest cost while other converters need more expensive controllers to achieve independent dimming. In terms of the main circuit cost, each of the SIMO converters reported in [70, 78, 80] and in Fig. 3.14 has one inductor, $n + 1$ switches, $n + 1$ diodes and n capacitors. The SIMO converter reported in [95] has one inductor, n switches, n diodes and no capacitor. In terms of the current sensors, because each individual output needs one current sensor, those converters reported in [70, 78, 80, 95] require n current sensors, one for each driver. The number of chip pins and the cost of chip packaging normally increase with the increase of the number of LED strings. However, the CSM SIMO converter requires only one current sensor for the front-end current generator. This configuration is advantageous to circuit integration, and the cost of chip packing can be decreased. In terms of mutual interference or cross regulation of the outputs, the CSM SIMO converter and the converter reported in [70, 78] under DCM operation do not present any issue on mutual interference of the outputs, whereas the converter in [80] under CCM operation requires a complex digital controller to minimize mutual interference. The converter studied in [95] is a combination of two boost converters sharing one inductor. This shared inductor is a switching storage, and hence this converter is essentially a VSM SIMO converter. The outputs are coupled to the same inductor. Again, minimizing the mutual interference requires a complex controller. A summary of the comparison between the various SIMO converters is given in Table 3.5.

Table 3.5: Comparison between The CSM SIMO Converter and Existing SIMO Converters. Number of Outputs = n.

	CSM SIMO converter (Fig. 3.14)	SIMO converter [70, 78] in DCM	SIMO converter [80] in CCM	SIMO converter [95]
Control strategy	Openloop (simple)	TM* or PT** control (medium)	Multivariable digital control (hard)	Complicated digital control (hard)
Controller cost	Low	Medium	High	High
Number of switches	n+1	n+1	n+1	n
Number of diodes	n+1	n+1	n+1	n
Number of capacitors	n	n	n	0
Number of inductors	1	1	1	1
Number of current sensors	1	n	n	n
Cross regulation	Excellent	Excellent	Good	Good

*TM control is time-multiplexing control; **PT control is pulse-train control.

3.4.3 High-Voltage-Step-Down LED Driver

The first current generator stage is a VSM buck converter which steps down the voltage level. In addition, the capacitors, C_{2a} to C_{2n}, serve as a voltage divider to divide the voltage. The subsequent multiple CSM boost converters further step down the output voltage. Thus, this converter is suitable for high-voltage-step-down voltage ratio applications without using transformers.

Based on volt-second balance of the buck converter (current generator stage) and amp-second balance of the CSM converters (LED drivers), the voltage ratio of the CSM high-voltage-step-down converter is given by

$$V_{oa} = V_{\text{in}} D_1 D_{2a} - D_{2a}(\frac{V_{ob}}{D_{2b}} + ... + \frac{V_{on}}{D_{2n}}). \tag{3.19}$$

According to equation (3.19), the input voltage V_{in} is primarily stepped down by two duty cycle values, D_1 and D_{2a}, which is further reduced by subtracting a positive

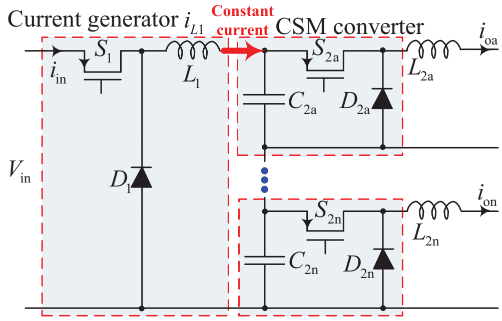

Figure 3.15: High-voltage-step-down converter

value. When S_1 is OFF and D_1 is ON, the voltage stress of switch S_1 is always equal to V_{in}. When S_{2a} is OFF and D_{2a} is ON, the voltage stress of switch S_{2a} is always equal to V_{C2a} which can be expressed as

$$V_{C2a} = \frac{P_{oa}}{I_{L1}} \tag{3.20}$$

where P_{oa} is the power level of the corresponding channel and I_{L1} is the steady-state current of inductor L_1.

Based on the analysis above, the voltage stress of switch S_1 at the high-voltage side is V_{in} which is always a high voltage. The voltage stresses of switches S_{2a} to S_{2n} at the low-voltage side are V_{C2a} to V_{C2n} which are always low voltages. This structure enables the use of low-voltage CSM boost cells and components. The voltage stress V_{C2a} can be designed to a reasonable value according to the output power level and the inductor current level. Compared with the converter studied in ref. [1], the disadvantage of the converter presented in Fig. 3.15 is that the use of high-voltage components in the current generator stage is mandatory. However, this sacrifice comes with a few merits. First, the cost of the power circuit is reduced, and the control circuit (openloop control) achieves design simplicity and low cost. Second, only one current sensor is needed in multiple-output applications. Third, the voltage stress is fixed for switches S_{2a} to S_{2n}. The change of power level in one LED string or the change of the number of outputs will not affect the voltage stresses in other CSM drivers. In order to

Table 3.6: Comparison of The High-Voltage-Step-Down Converter (Fig. 3.15) and A Prior Circuit [1]. Number of Outputs = n.

	Converter in Fig. 3.15	Converter in [1]
Control complexity	Easy	Hard
Controller cost	Low	High
Number of switches with high voltage stress	1	0
Number of switches with low voltage stress	n	$4n$
Number of diodes	n+1	0
Number of capacitors	n	n
Number of inductors	n+1	n
Number of sensors	1	n
Voltage stresses of switches	Fixed	Increased with the decrease of n

demonstrate the design advantages, we compare the structure given in Fig. 3.15 with a previously reported circuit [1], as summarized in Table 3.6.

3.5 Experimental Demonstrations

In this section, we compare the VSM and CSM converters experimentally for LED driving applications, with the aim of verifying the analytical results presented earlier. Parameters and components of our laboratory prototypes are given in Table 3.1.

Experimental waveforms showing the range of duty cycle are shown in Fig. 3.16, including the measured maximal and minimum duty cycle, $D_{\max}$ and $D_{\min}$. The measured results are consistent with theoretical results. The errors in VSM converters are due to the device characteristic of the LED load, i.e., v-i characteristic, since the VSM converter regulates the current indirectly through the LED's v-i curve. However, the CSM converter regulates the current directly via the duty cycle. From the measured results, CSM converters control the output current with a wider range of duty cycle compared to VSM converters. The results are given in Table 3.7.

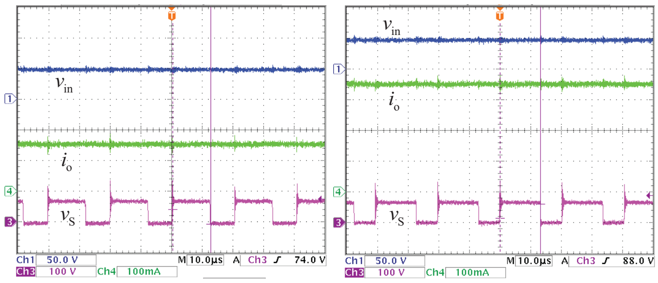

(a)

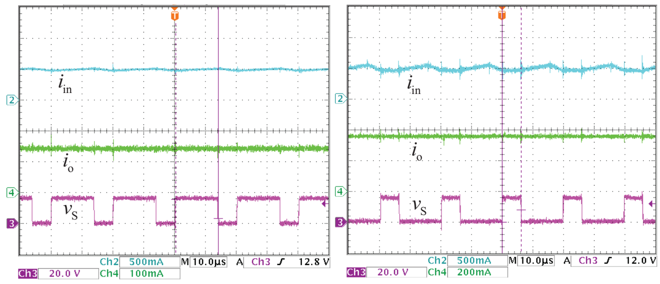

(b)

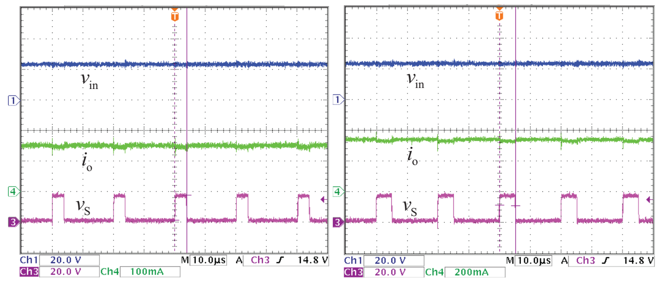

(c)

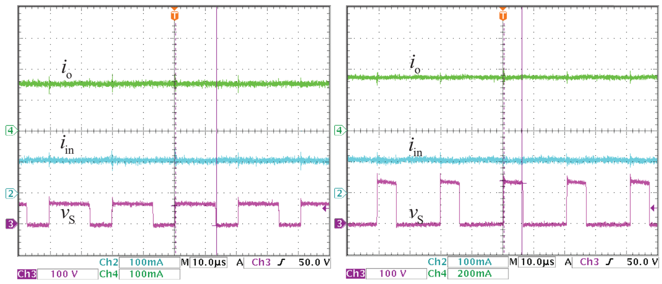

(d)

Figure 3.16: Practical range of duty cycle. (a) VSM buck converter I_o = 150–350 mA; (b) CSM buck converter I_o = 150–350 mA; (c) VSM boost converter I_o = 150–350 mA; (d) CSM boost converter I_o = 150–350 mA.

Another point worth noting is that the current ripple in Fig. 3.16(b) is the ripple of the CSM buck converter without the smoothing inductor. We see that the current ripple has the same order of magnitude as the ripple in Fig. 3.16(a), thus validating the

Table 3.7: Measured Duty Cycle (I_o = 150–350 mA)

	VSM buck converter	CSM buck converter	VSM boost converter	CSM boost converter
D_{max}	0.660	0.695	0.254	0.660
D_{min}	0.610	0.310	0.184	0.290
D_{span}	0.050	0.385	0.070	0.370

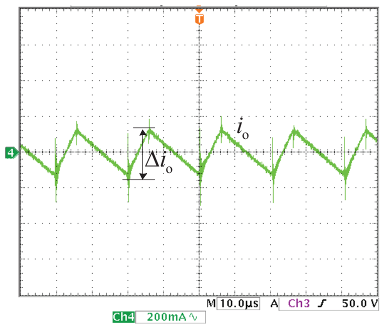

Figure 3.17: Current ripple of the CSM boost converter without an extra capacitor.

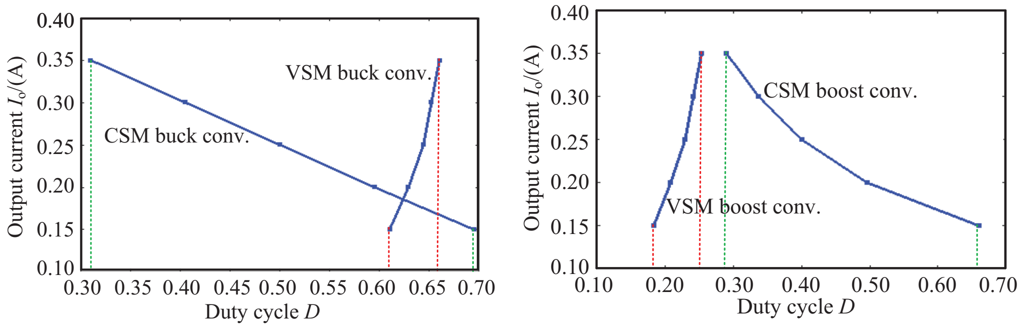

(a) (b)

Figure 3.18: Measured output current versus duty cycle. (a) VSM and CSM buck converters; (b) VSM and CSM boost converters.

Table 3.8: Measured Parameters

	VSM buck converter	CSM buck converter	VSM boost converter	CSM boost converter
S_{max}	6.25	0.53	4.17	1.06
S_{min}	2.63	0.50	2.00	0.30
W	0.0125	0.0963	0.0175	0.0925
ΔW	0.0010	0.0004	0.0012	0.0096
N	0.0800	0.0042	0.0686	0.1038

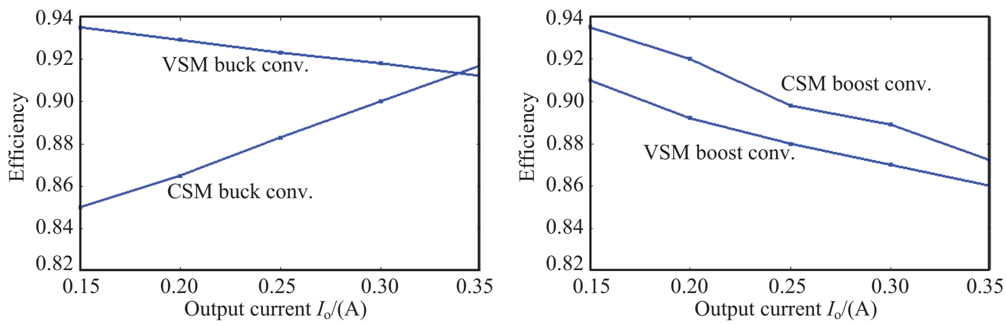

(a) (b)

Figure 3.19: Comparison of efficiency. (a) VSM and CSM buck converters; (b) VSM and CSM boost converters.

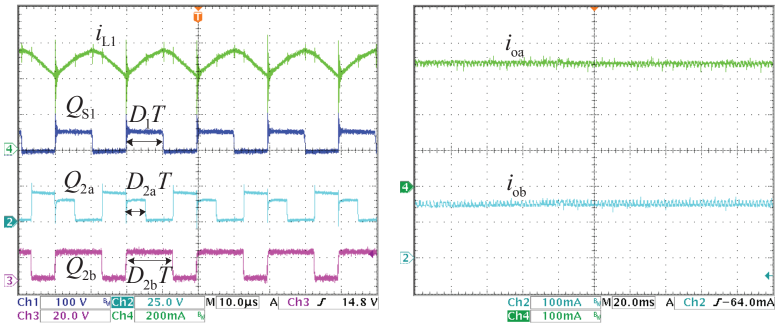

(a) (b)

Figure 3.20: Steady-state and transient response waveforms in the single-inductor two-output converters. (a) Drive signals and i_{L1}; (b) two output currents.

analysis presented in Section 3.3. The current ripple shown in Fig. 3.16(d) is the ripple of the CSM boost converter with an extra capacitor. In some applications, the extra capacitor is necessary to reduce the output current ripple. Without the extra capacitor, the current ripple amplitude becomes significant, as shown in Fig. 3.17.

The measured output current versus the duty cycle is shown in Fig. 3.18, from which we obtain the values of S and N, as tabulated in Table 3.8. From the measured parameters, the CSM converters have smaller values of S than VSM converters. Notable error in S can be found in VSM converters due to the device characteristic of the LED load. The CSM buck converter has a smaller value of N than the VSM buck converter. However, the CSM boost converter has a larger value of N than the VSM boost converter.

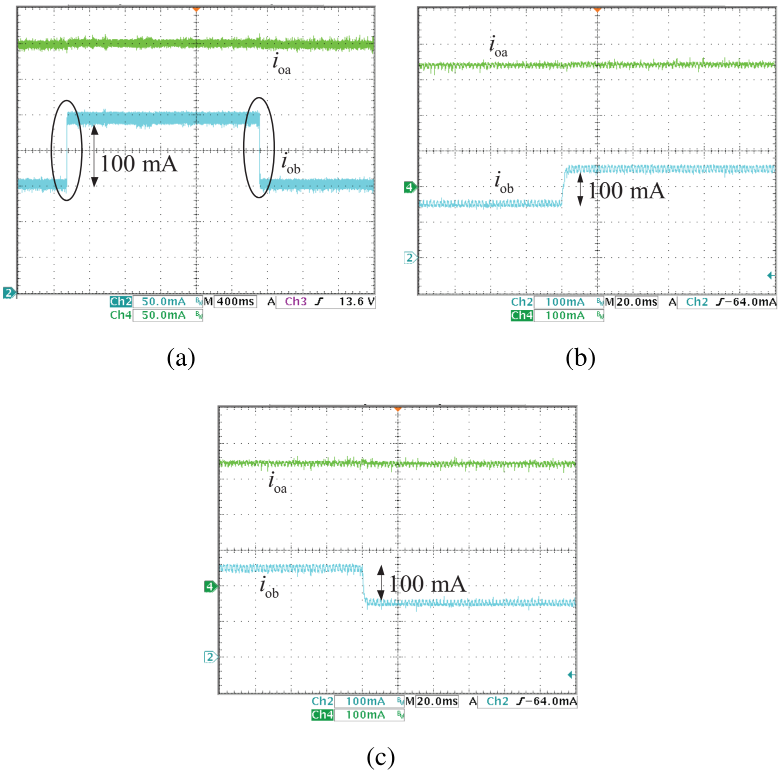

Figure 3.21: Transient response showing independence of outputs of the CSM SIMO converter. (a) Transient response of a 100 mA step applied to one output; (b) 150 mA to 250 mA; (c) 250 mA to 150 mA. In both cases, the other current output is unaffected.

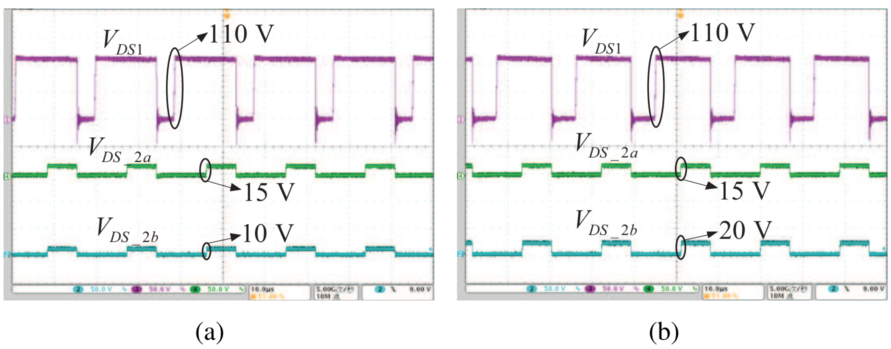

Figure 3.22: Steady-state waveforms in the CSM high-voltage-step-down converter. (a) One string with 3 LEDs, the other string with 2 LEDs; (b) one string with 3 LEDs, the other string with 4 LEDs.

The efficiencies, for comparison purposes, are plotted in Fig. 3.19. Compared with the VSM buck converter, the CSM buck converter has a lower efficiency because the MOSFET switch always carries the input current which is higher than the output current. Compared with the VSM boost converter, the CSM boost converter has a higher efficiency.

We take the single-inductor two-output converter as an example for demonstration. The experimental waveforms are shown in Fig. 3.20. There are two LED strings. Four LEDs stacked in series form one string with an output current of 350 mA. Six LEDs stacked in series form another string, with an output current of 150 mA. The three switches are operated at the same frequency of 50 kHz. Fig. 3.20(a) presents the details of the drive signals and current i_{L1}. In one period, we identify four sub-intervals. In the first sub-interval, S_1, S_{2a} and S_{2b} are ON, and the inductor's current ramps up. During the second sub-interval, S_1 and S_{2b} are ON while S_{2a} is OFF, and the inductor's current continues to ramp up. During the third sub-interval, S_1 and S_{2a} are OFF while S_{2b} is ON, and the inductor's current ramps down. In the last sub-interval, S_1, S_{2a} and S_{2b} are OFF, and the inductor's current continues to go down. Fig. 3.20(b) presents the steady-state waveforms of the two output currents. Since the average current of i_{L1} is constant, we need only to regulate the duty cycle of CSM buck converter to achieve independent dimming function.

Fig. 3.21 presents the transient response waveforms when a 100 mA step current is applied in I_{ob}. The output current I_{ob} steps between 150 mA and 250 mA. The waveform of the other output current, I_{oa}, is shown in Fig. 3.21(a), and in detail in Figs. 3.21(b) and 3.21(c). To change the output current i_{ob} from 150 mA to 250 mA, we need only to change the reference value of current i_{ob}, and hence duty cycle d_{2b}. During the whole process, current i_{oa} has remained unaffected. It is clearly shown that the SIMO converter can achieve independent dimming function.

Fig. 3.22 shows the voltage stresses of switches in the CSM high-voltage-step-down converter. There are two LED strings. The input voltage is 110 V which is the high-side voltage. Current I_{L1} is controlled to stay at 100 mA. In Fig. 3.22(a), three LEDs stacked in series form one string with an output current of 160 mA, and two LEDs stacked in series form another string with an output current of 160 mA. According to Fig. 3.22(a), the voltage stress of switch S_1 is 110 V. The voltage stresses of switches S_{2a} and S_{2b} are 15 V and 10 V, respectively, which are much lower than the input voltage. The experimental results are in agreement with the analysis. Fig. 3.22(b) shows the voltage stresses of switches in the high-voltage-step-down converter with the only difference being that the number of LEDs in one string is changed from 2 to 4. The voltage stresses of switches S_1 and S_{2a} remain unchanged, but the voltage stress of switch S_{2b} is 20 V which is the voltage of capacitor C_{2b}. Comparison between the waveforms in Figs. 3.22(a) and 3.22(b) shows that the voltage stress only depends on parameters of the corresponding channel with no influence of other LED channels. This structure allows the use of low-voltage CSM cells. However, in [1], the voltage stresses of switches increased with the decrease of the number of LED strings. Experimental results are fully consistent with our analysis.

3.6 Summary

In this chapter, we examine the driving circuit requirement for LED loads. Our starting point is the LED characteristic and basic circuit theory. We highlight the importance of consideration of the termination type and the corresponding choice of converter type. Specifically we introduce the mostly unknown current-source-mode converters which can be derived via the application of duality principle and compare these converters with the conventional and mostly known voltage-source-mode converters. We focus on comparison of the key performance areas in relation to LED lighting applications. Since current-source-mode drivers inherently contain no inductors, they can be conveniently used in constructing multiple-output driving converters employing a minimum number of inductors. The single-inductor-multiple-output current-source-mode converter performs better, with lowered cost, compared with the traditional configurations based on voltage-source-mode converters. In high-voltage-step-down applications, the current-source-mode converter offers fixed low voltage stress, and is well suited for high-voltage-step-down applications. Finally, we emphasize that proper application of circuit concepts would form the basis of design of effective driving circuits for LED applications.

Chapter 4

Current-Source-Mode Single-Inductor Multiple-Output LED Driver

4.1 Introduction

The previous chapter reviews the circuit duality principle and presents the comparison between VSM converters and CSM converters. The CSM converters, being inherently inductorless, are found to be highly suited for driving LEDs. In this chapter, we introduce an inductorless CSM buck converter and a series structure of connecting multiple CSM converters, as shown in Fig. 4.1(a). This converter and the connection configuration are effectively the dual versions of the usual dc-dc converter and the parallel configuration shown in Fig. 2.9(a). One inductor is needed to construct a constant current for feeding the CSM converters that drive the LEDs. It should be noted that the CSM converters *inherently contain no inductor*, while performing the intended power processing function. The CSM SIMO dc-dc converter derived from Fig. 4.1(a) is presented in Fig. 4.1(b). This converter makes full use of the properties of the CSM converter to achieve independent dimming function and guarantee good cross-regulation performance, while significantly simplifying the control circuit.

Taking the CSM single-inductor dual-output (SIDO) converter as an example, in

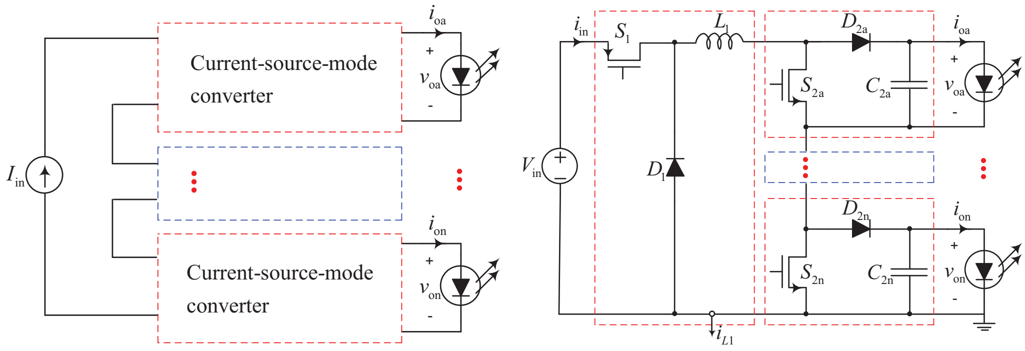

(a) (b)

Figure 4.1: Alternative topologies. (a) Series-connected dc-dc converters; (b) CSM SIMO dc-dc converter. Each CSM converter consists of a set of switching capacitor arrangement S_{2k}, D_{2k} and C_{2k}, similar to the conventional switching inductor arrangement in the dc-dc converter. Capacitor C_{2k} with appropriate value is a switching storage (not a smoothing output capacitor) drawing current from L_1 and injecting current to the output by action of switch S_{2k}.

this chapter, we will describe the operation of the proposed CSM SIDO dc-dc converter. The relationship between the input voltage and the two output voltages will be investigated. The CSM SIDO dc-dc converter allows multiple voltage output levels. The control strategy, the small-signal model and feedback configuration are presented in detail. The independent dimming function and the principle of eliminating cross-regulation effects are discussed. Both the high-frequency and the low-frequency PWM dimming methods can be applied to the CSM SIDO dc-dc converter. Practical configurations and experimental results of the CSM SIDO dc-dc converter are presented. Finally, we conclude this chapter.

4.2 VSM Buck Converter and CSM Buck Converter

Duality is a well established circuit theoretic concept that enables circuits to be transformed with invariant properties while interchanging current and voltage [19]. Applying duality transformation, the VSM buck converter shown in Fig. 3.1(a) becomes the CSM buck converter, shown in Fig. 3.3(a). While the VSM buck converter is supposedly fed by a voltage source, the CSM buck converter is fed by a current source [86].

Table 4.1: Parameters of Test Circuits

	VSM buck converter	CSM buck converter
V_{in}	48 V	—
I_{in}	—	500 mA
T	20 μs	20 μs
L	2000 μH	2000 μH
C	10-100 μF	10-100 μF

The output voltage of the VSM buck converter is controllable via the duty cycle, and the basic cell consists of a switch, a diode and an inductor which serves as a high-frequency switching power storage. The output capacitor simply serves a filtering function for voltage delivery. In the dual case, the CSM buck converter consists of a switch, a diode and a switching storage capacitor. The output inductor serves a filtering function delivering current to the load. The voltage gain of the VSM buck converter and the current gain of the CSM buck converter are determined as equation (3.1) and equation (3.2), respectively.

The practical LED is replaced by an ideal diode, a voltage source V_F and a resistor in series, as shown in Fig. 2.3. Theoretical calculations can be performed based on the simplified LED model. The circuit parameters of the VSM buck converter and the CSM buck converter are listed in Table 4.1.

Fig. 3.4 shows the comparison of the voltage ripples in the VSM buck converter and the CSM buck converter. If the inductor is removed from the CSM buck converter. the output voltage ripple of the CSM buck converter is expectedly higher than that of the VSM buck converter. However, with a larger capacitance value, the output voltage ripple can be reduced significantly. Thus, the CSM buck converter can maintain a low output ripple even in the absence of the output filtering inductor. The cost and volume of the circuit can be lowered. This characteristic provides a basis for deriving the SIMO converter.

For the VSM buck and CSM buck converters, the regulation range can be visualized

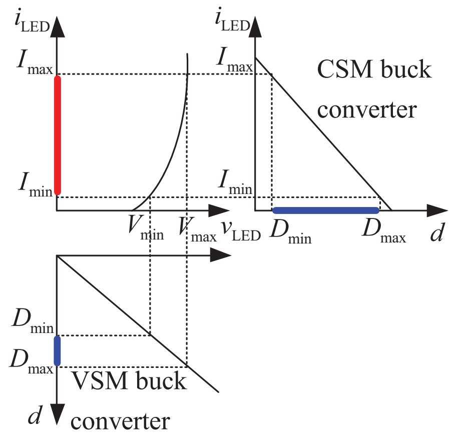

Figure 4.2: Voltage, current and duty cycle ranges for VSM and CSM buck converter driving LED.

in Fig. 4.2. Based on (3.1) and (3.2), we can plot the drivers' transfer curves. The VSM buck converter adjusts the duty cycle to change the output voltage, and hence to change the output current. Because of this inherent *v*-*i* characteristic, the variation of the duty cycle is small for a wide range of current. This makes direct control of output current infeasible, and feedback control of output current is usually required. However, in the CSM buck converter case, the duty cycle has an inherent wide varying range corresponding to a range of output current. Direct (openloop) control of duty cycle can be used for dimming control. As we will see later, the use of a series structure can decouple all individual dimming controls for multiple-output driving applications, resulting in almost perfect cross regulation performance. This property provides a basis for the implementation of simplest yet effective control for multiple-output converter.

4.3 Single-Inductor Dual-Output DC-DC Converter Using Current-Source-Mode Converters

In this section, we will describe in detail the CSM single-inductor dual-output (SIDO) converter for LED driving applications for illustration of the beneficial properties offered by CSM configuration in multiple-output LED driving. The circuit is shown in

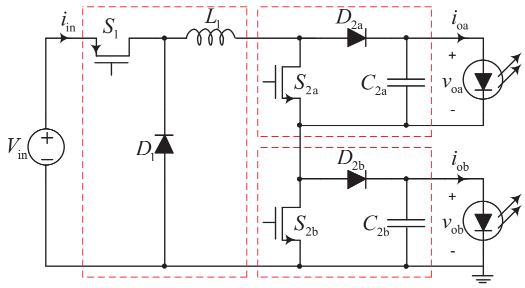

Figure 4.3: Single-inductor dual-output configuration using CSM switching converters.

Fig. 4.3. Here, the current through L_1 is kept constant and is used to feed the two CSM buck converters. From the analysis in Section 3.3.1, the inductor of the CSM buck converter can be removed. This property is desirable for modular design. The CSM buck modules can be connected in series to drive individual LED strings. Thus, only one inductor is needed in this design, achieving fully independent dimming of two LED strings.

4.3.1 Operation

The CSM SIDO dc-dc converter contains three switches, namely, S_1, S_{2a}, and S_{2b}. Every switch may operate in either ON or OFF state. Thus, there are eight possible operating modes. Denoting ON state by 1 and OFF state by 0, we represent the eight possible modes as 111, 110, 101, 100, 011, 010, 001 and 000, as shown in Fig. 4.4.

Mode 1: S_1, S_{2a} and S_{2b} are ON. In this mode, V_{in} charges up the inductor and i_{L1} ramps up. The capacitors are discharged to the corresponding loads. Mode 2: S_1 and S_{2a} are ON while S_{2b} is OFF. If $V_{in} > V_{ob}$, then $(V_{in} - V_{ob})$ charges up the inductor and i_{L1} ramps up. Otherwise, $(V_{in} - V_{ob})$ discharges the inductor and i_{L1} ramps down. At the same time, capacitor C_{2a} is discharged to the load. Mode 3: S_1 and S_{2b} are ON while S_{2a} is OFF. This mode is similar to Mode 2. If $V_{in} > V_{oa}$, then $(V_{in} - V_{oa})$ charges up the inductor and i_{L1} ramps up. If not, $(V_{in} - V_{oa})$ discharges the inductor and i_{L1} ramps down. Capacitor C_{2b} is discharged to the load. Mode 4: S_1 is ON while

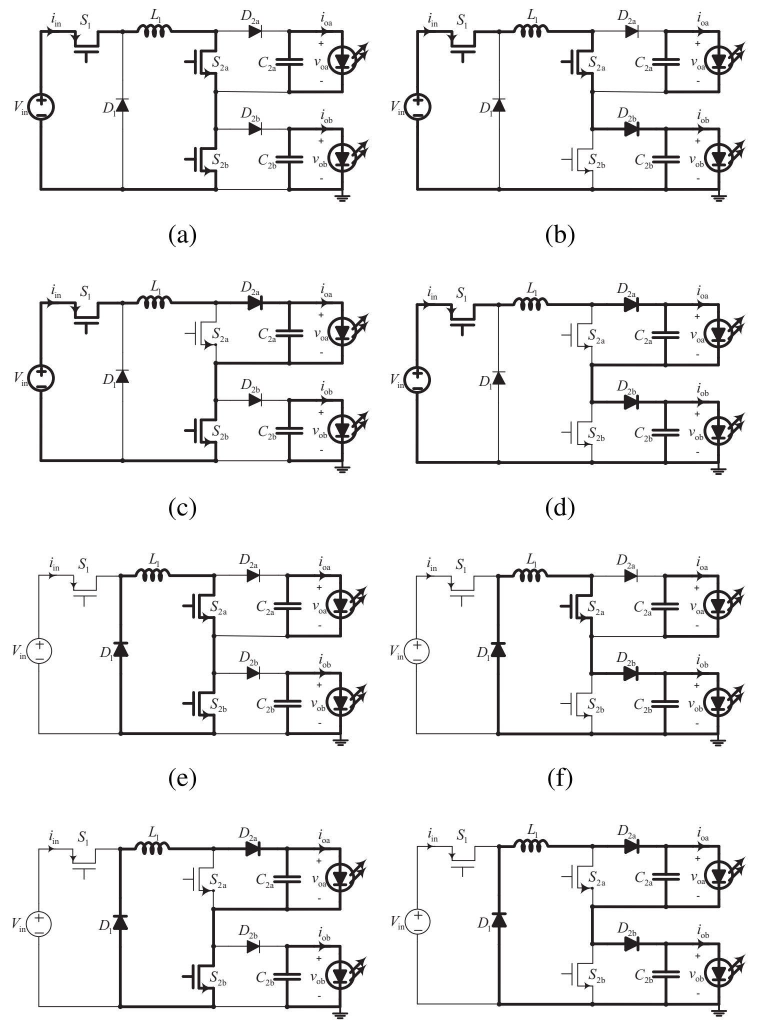

Figure 4.4: Operating modes. (a) S_1, $S_{2\text{a}}$, and $S_{2\text{b}}$ are ON; (b) S_1 and $S_{2\text{a}}$ are ON and $S_{2\text{b}}$ is OFF; (c) S_1 and $S_{2\text{b}}$ are ON and $S_{2\text{a}}$ is OFF; (d) S_1 is ON and $S_{2\text{a}}$ and $S_{2\text{b}}$ are OFF; (e) S_1 is OFF and $S_{2\text{a}}$ and $S_{2\text{b}}$ are ON; (f) S_1 and $S_{2\text{b}}$ are OFF and $S_{2\text{a}}$ is ON; (g) S_1 and $S_{2\text{a}}$ are OFF and $S_{2\text{b}}$ is ON; (h) S_1, $S_{2\text{a}}$, and $S_{2\text{b}}$ are OFF.

S_{2a} and S_{2b} are OFF. If $V_{\text{in}} > V_{oa} + V_{ob}$, then $(V_{\text{in}} - V_{oa} - V_{ob})$ charges up the inductor and i_{L1} ramps up. If $V_{\text{in}} < V_{oa} + V_{ob}$, then $(V_{\text{in}} - V_{oa} - V_{ob})$ discharges the inductor and i_{L1} ramps down. Mode 5: S_1 is OFF while S_{2a} and S_{2b} are ON. In this mode, the inductor current is in a freewheeling mode. The capacitors continue to be discharged to the corresponding loads. Mode 6: S_1 and S_{2b} are OFF while S_{2a} is ON. Voltage V_{ob} discharges the inductor and i_{L1} ramps down. Capacitor C_{2a} is discharged to the load. Mode 7: S_1 and S_{2a} are OFF while S_{2b} is ON. Voltage V_{oa} discharges the inductor and

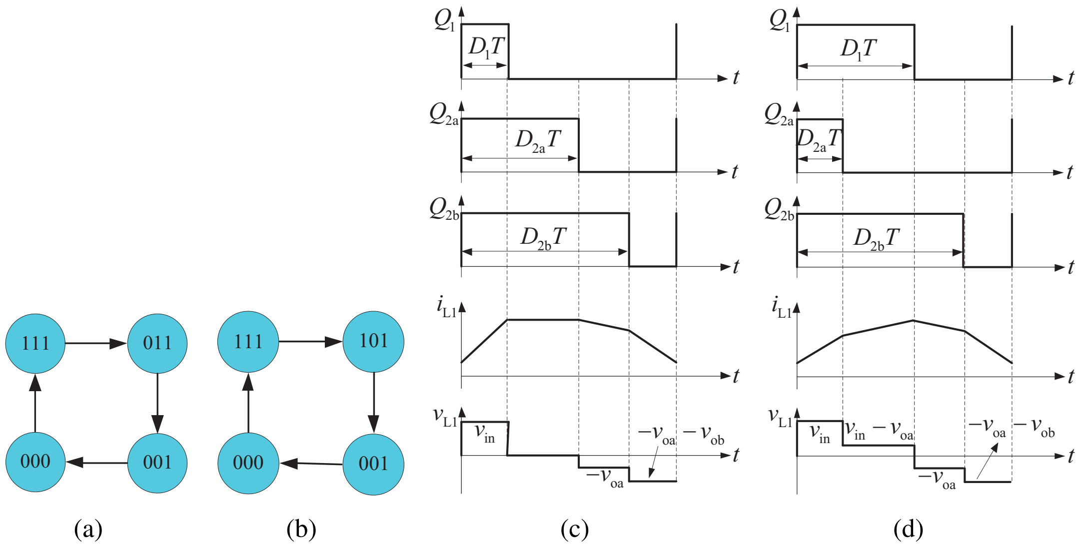

Figure 4.5: Mode flow graphs and theoretical waveforms. (a) Flow graph 1; (b) flow graph 2; (c) key waveform set 1; (d) key waveform set 2.

i_{L1} ramps down. Capacitor C_{2b} is discharged to the load. Mode 8: S_1, S_{2a} and S_{2b} are OFF. Voltage $(V_{oa} + V_{ob})$ discharges the inductor and i_{L1} ramps down.

A possible control scheme is to make the three switches operate at the same frequency and employ an analog dimming method. The three switches turn on at the same time. Due to the varying input voltage, output load and inductor current, the voltage and current across the inductor could be different. A number of combinations are possible. We will describe two cases in detail. In the first case, the mode flow graph is shown in Fig. 4.5(a). There are four subintervals. Current i_{L1} initially ramps up, remains constant, and eventually ramps down at different rates, as shown in Fig. 4.5(c). In the second case, the mode flow graph is shown in Fig. 4.5(b). Again four subintervals are identified. Current i_{L1} initially ramps up to the peak value at different rates, and eventually ramps down to the initial value at different rates, as shown in Fig. 4.5(d). Like the parallel-connected VSM converters sharing the same input constant voltage, the series-connected CSM converters share the same input constant current, resulting in good performance on the cross-regulation effect.

4.3.2 Mixed Voltage Conversion

Suppose I_{L1} is the steady-state inductor current, I_{oa} and I_{ob} are the steady-state output currents. For the SIDO dc-dc converter, as the input power is equal to the output power, we have

$$V_{\text{in}} D_1 I_{L1} = V_{oa} I_{oa} + V_{ob} I_{ob}. \tag{4.1}$$

The input voltage is

$$V_{\text{in}} = \frac{V_{oa} I_{oa}}{D_1 I_{L1}} + \frac{V_{ob} I_{ob}}{D_1 I_{L1}} \tag{4.2}$$

Since $V_{ob} = 0$ is assumed, I_{ob} is also zero, and the input voltage is

$$V_{\text{in}} = \frac{V_{oa} I_{oa}}{D_1 I_{L1}} \tag{4.3}$$

Thus, the duty cycle of switch S_1 is

$$D_1 = \frac{V_{oa} I_{oa}}{V_{\text{in}} I_{L1}}. \tag{4.4}$$

Since $D_1 < 1$, equation (4.4) becomes

$$\frac{V_{oa}}{V_{\text{in}}} < \frac{I_{L1}}{I_{oa}}. \tag{4.5}$$

Also, since $I_{L1} > I_{oa}$, the output voltage can be higher or lower than the input voltage. This property is desirable for many applications. For instance, in hand-held battery-powered electronic devices [22], the use of this CSM SIDO dc-dc converter only needs one battery, instead of more batteries in series, to achieve voltage step-down and step-up functions of multiple outputs simultaneously.

4.4 Control Design

As explained in the foregoing section, when the input is a voltage source, the parallel-connected structure shown in Fig. 2.9(a) is the most effective multiple-output structure to achieve independent dimming function and alleviate the cross-regulation effects because the parallel VSM converters are completely independent. In a dual fashion, the series-connected structure shown in Fig. 4.1(a) is the most effective way to achieve independent dimming function and alleviate the cross-regulation effects when the input is a current source. In LED driving applications, the use of CSM driving has inherent advantages as explained earlier. However, in reality, a voltage source is the most common form of available power source. Thus, a converter feeding a constant current for the CSM driving converters is needed. This configuration requires only one inductor in total.

4.4.1 Control Strategy

First, a single closed-loop control is needed for the current source that feeds the multiple CSM drivers. In this SIMO converter, each CSM driver needs one direct open-loop control for independent dimming control, as illustrated in Section 3.3.5. Specifically, direct duty cycle control in the CSM converter has wide control range and good sensitivity. The constant current supply in this CSM SIMO dc-dc converter can ensure that the output current is purely controlled by the corresponding duty cycle, thus ensuring independent dimming function and superb cross-regulation performance. The entire control circuit involves only one closed-loop controller and several open-loop controllers, as shown in Fig. 3.13. The system implements a low-cost, stable, and simple control strategy to achieve all needed functions with zero cross-regulation effect.

4.4.2 Small-signal Model

The CSM SIDO dc-dc converter contains one inductor and two capacitors, resulting in a third-order system. Thanks to the open-loop control of CSM drivers, the control design is greatly simplified. For the CSM buck converter shown in Fig. 3.3(a), the capacitor voltage and output (inductor) current are the state variables. We may establish the small-signal model of the CSM buck converter by applying state-space averaging to the ON-time and the OFF-time state equations, which are given as

$$\begin{bmatrix} \frac{di_o}{dt} \\ \frac{dv_C}{dt} \end{bmatrix} = \begin{cases} \begin{bmatrix} \frac{-R_d}{L_o} & \frac{1}{L_o} \\ \frac{-1}{C} & 0 \end{bmatrix} \begin{bmatrix} i_o \\ v_C \end{bmatrix} + \begin{bmatrix} \frac{-V_F}{L_o} \\ 0 \end{bmatrix} & \text{for ON time} \\ \begin{bmatrix} \frac{-R_d}{L} & \frac{1}{L_o} \\ \frac{-1}{C} & 0 \end{bmatrix} \begin{bmatrix} i_o \\ v_C \end{bmatrix} + \begin{bmatrix} \frac{-V_F}{L_o} \\ 0 \end{bmatrix} + \begin{bmatrix} 0 \\ \frac{1}{C} \end{bmatrix} i_{\text{in}} & \text{for OFF time} \end{cases} \tag{4.6}$$

where i_{in} is the input current to the CSM buck converter and L_o is the output inductor of the CSM buck converter included here for completeness sake, as defined in Fig. 3.3(a). Upon application of averaging and small-signal linearization, we get

$$\begin{bmatrix} \frac{d\tilde{i}_o}{dt} \\ \frac{d\tilde{v}_C}{dt} \end{bmatrix} = \begin{bmatrix} \frac{-R_d}{L_o} & \frac{1}{L_o} \\ \frac{-1}{C} & 0 \end{bmatrix} \begin{bmatrix} \tilde{i}_o \\ \tilde{v}_C \end{bmatrix} + \begin{bmatrix} 0 \\ \frac{1-D}{C} \end{bmatrix} \tilde{i}_{\text{in}} + \begin{bmatrix} 0 \\ \frac{-I_{\text{in}}}{C} \end{bmatrix} \tilde{d} \tag{4.7}$$

where $\tilde{i}_o$, $\tilde{v}_C$, $\tilde{d}$ and $\tilde{i}_{\text{in}}$ are the respective small-signal variables for the CSM buck converter; and D denotes the steady-state duty cycle value. Moreover, to facilitate calculation of the input impedance, we also define the input voltage of this CSM buck converter as v'_{in} which should not be confused with the input voltage V_{in} of the entire SIDO converter. The small-signal expression for v'_{in} can be readily found as

$$\tilde{v}'_{\text{in}} = (1 - D)\tilde{v}_C - V_C\tilde{d} \tag{4.8}$$

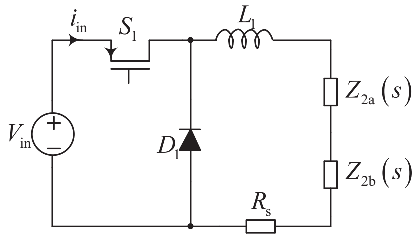

Figure 4.6: Equivalent circuit model of SIMO converter using CSM drivers.

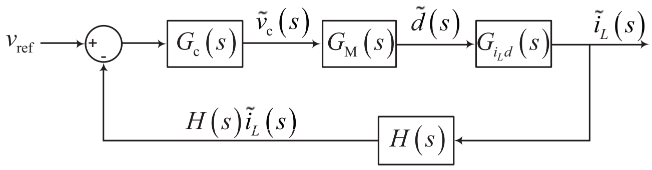

Figure 4.7: The small-signal ac equivalent diagram.

where uppercase denotes steady-state values, as usual. It should be noted that for the purpose of driving LEDs, the inductor of the CSM buck converter (L_o) can be removed, as explained earlier in Section 3.3.1. The input impedance of the CSM buck converter in the s-domain can be found as

$$Z(s) = \left.\frac{\tilde{V}'_{in}(s)}{\tilde{I}_{in}(s)}\right|_{D(s)=0} = \frac{(1-D)^2(sL+R_d)}{s^2LC + sR_dC + 1} = \frac{(1-D)^2R_d}{sR_dC+1}. \tag{4.9}$$

The circuit in Fig. 4.3 can be simplified to the circuit shown in Fig. 4.6, where $Z_{2a}(s)$ and $Z_{2b}(s)$ are the input impedances of the two CSM converters, and can be obtained from equation (4.9).

Furthermore, assuming that the two output CSM drivers work under the same condition, the control-to-output-current transfer function for the circuit of Fig. 4.6 can be obtained as

$$G_{i_{Ld}(s)} = \left.\frac{I_{L1}(s)}{D(s)}\right|_{V'_{in}(s)=0} = \frac{V_{in}}{sL_1 + \frac{(1-D_{2a})^2R_d}{1+sR_dC_{2a}} + \frac{(1-D_{2b})^2R_d}{1+sR_dC_{2b}}}. \tag{4.10}$$

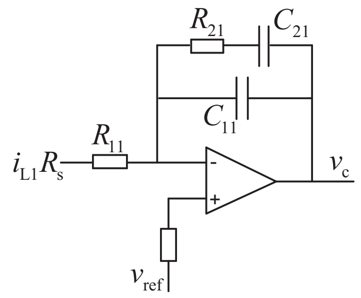

Figure 4.8: Type II compensation network.

4.4.3 Loop Gain Analysis and Compensation

The aim of the compensation network is to ensure good dynamic performance and stability of the system. For the SIDO converter, the inductor current is controlled using the small-signal block diagram shown in Fig. 4.7, where $H(s)$ is the transfer function of the current sampling, $G_c(s)$ is the transfer function of the current compensation network, V_m is the peak-to-peak value of the ramp signal of the pulse-width modulator, and $G_{i_L d}(s)$ is the control-to-output-current transfer function given in (4.10). Also, $H(s)$ is equal to the sampling resistor R_s and $G_M(s)$ is equal to $1/V_m$. The loop gain can be readily obtained as

$$T(s) = H(s) \cdot G_c(s) \cdot G_{i_L d}(s)/V_m \tag{4.11}$$

In this work, a Type II compensation network is employed, as shown in Fig. 4.8. The transfer function of the compensation network is

$$G_c(s) = \frac{V_c(s)}{I_{L1}(s)R_s} = -\frac{K\left(1+\dfrac{s}{\omega_z}\right)}{s\left(1+\dfrac{s}{\omega_p}\right)} \tag{4.12}$$

where

$$K = \frac{1}{R_{11}\left(C_{11}+C_{21}\right)} \approx \frac{1}{R_{11}C_{21}},$$

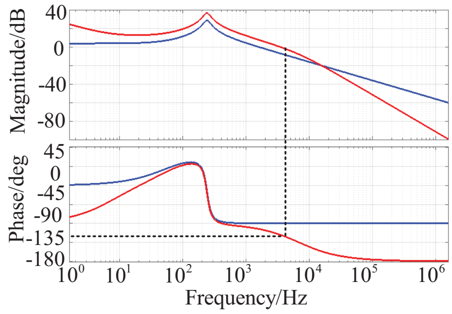

Figure 4.9: Frequency response of loop gain. Blue: openloop. Red: closed-loop.

$$\begin{aligned}
\omega_z &= \frac{1}{R_{21}C_{21}}, \\
\omega_p &= \frac{C_{11}+C_{21}}{R_{21}C_{11}C_{21}} \approx \frac{1}{R_{21}C_{11}}, \text{ and} \\
\omega_z &< \omega_p.
\end{aligned}$$

The transfer function has a DC gain K, an integrating pole, a zero at w_z, and a pole at w_p.

The circuit shown in Fig. 4.6 is a first-order circuit. The openloop frequency response is shown in Fig. 4.9 as blue curves. The input voltage and the output impedance are not always fixed, resulting in variation of the inductor current. The compensation network in the closed-loop system is designed to achieve good dynamic performance and a fixed inductor current. The closed-loop frequency response is shown in Fig. 4.9 as red curves. The crossover frequency f_g is 3.1 kHz, and the phase margin is 63°. The system has the desired crossover frequency and phase margin.

4.4.4 PWM Dimming

The PWM dimming method is a commonly used dimming method. For the CSM SIDO dc-dc converter, the bus current i_{L1} is kept constant. Switches S_{2a} and S_{2b} turn on and off the LED string repeatedly to regulate the LED's current, thereby regulating the luminance.

We set the three switches at the same frequency of 50 kHz. The capacitance value

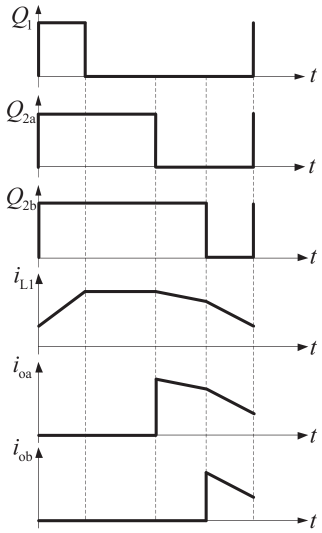

Figure 4.10: Waveforms of high-frequency PWM dimming. All switches operate at same high frequency.

is 10 nF for C_{2a} and C_{2b}. The average currents $i_{\mathrm{oa-av}}$ and $i_{\mathrm{ob-av}}$ are inversely proportional to duty cycles d_{2a} and d_{2b}, respectively. The three switches are controlled independently. The two output currents can be adjusted arbitrarily by controlling d_{2a} and d_{2b}. Taking this specific case shown in Fig. 4.10 as an example, current of output a, denoted as i_{oa}, is equal to zero when S_{2a} is ON, and is equal to i_{L1} when S_{2a} is OFF. A similar situation is observed for output b. The theoretical waveforms of the high-frequency PWM dimming method are shown in Fig. 4.10. The operating modes are basically the same as in Fig. 4.4. The only difference is that when S_{2a} or S_{2b} is OFF, the corresponding output current becomes zero.

In the specific application of cool-warm color-temperature mixing system, the ratio of cool light to warm light determines the output light color. For this application, we may operate switches S_{2a} and S_{2b} at 400 Hz, and switch S_1 at 50 kHz. The capacitance value is 220 μF for C_{2a} and C_{2b}. The bus current i_{L1} is kept constant via application of appropriate control circuit. Switch S_{2a} and switch S_{2b} are always switched in complementary fashion, i.e., one is ON while the other is OFF, and vice versa. Taking this specific case shown in Fig. 4.11(a) as an example, current of output a, i.e., i_{oa}, is zero when S_{2a} is ON, and is equal to the average current of i_{L1} when S_{2a} is OFF. A similar

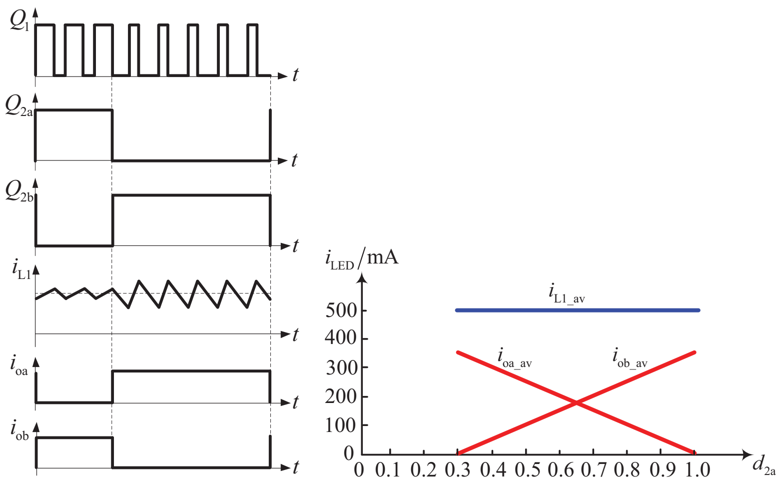

(a) (b)

Figure 4.11: Low-frequency PWM dimming. (a) Key waveforms; (b) the color-temperature regulation.

situation is observed in output b. When S_1 is ON, the operation shuffles between the mode shown in Fig. 4.4(b) and that in Fig. 4.4(c). In this case, when switch S_{2a} or S_{2b} is ON, the corresponding output current becomes zero. Moreover, when S_1 is OFF, the operation shuffles between the mode shown in Fig. 4.4(e) and that in Fig. 4.4(f), and in this case, when switch S_{2a} or S_{2b} is ON, the corresponding output current becomes zero. Fig. 4.11(b) shows the relationship between the color temperature and the duty cycle d_{2a}. The ratio of cool light to warm light can be regulated by controlling either d_{2a} or d_{2b}.

4.5 Experimental Results

In order to verify the feasibility of the CSM SIDO dc-dc converter, a laboratory prototype was constructed. The values of prototype's components are shown in Table 4.2.

The measured waveforms for the two operating cases, corresponding to the two switching sequences of Fig. 4.5, are shown in Fig. 4.12. For the operation corresponding to the sequence shown in Fig. 4.12(a), V_{in} is equal to 50 V. The load in output a

Table 4.2: Parameters of CSM SIDO DC-DC Converter

Circuit Parameters	Value
Rated input voltage	48 V
Rated inductor current	500 mA
Main inductor L_1	1000 μH
Capacitor C_{2a}	10 nF / 220 μF
Capacitor C_{2b}	10 nF / 220 μF
Output currents i_{oa} and i_{ob}	0 - 350 mA
Switch frequency of S_1	50 kHz
Switch frequency of S_{2a}	50 kHz / 400 Hz
Switch frequency of S_{2b}	50 kHz / 400 Hz
Capacitor C_{11}	4.7 nF
Capacitor C_{21}	4.7 μF
Resistor R_{11}	2 kΩ
Resistor R_{21}	5 kΩ
MOSFETs S_1, S_{2a} and S_{2b}	IRF540NPBF
Diodes D_1, D_{2a} and D_{2b}	MUR1560

consists of a string of 2 white LEDs stacked in series, and the current flowing through the LEDs is 350 mA. The load in output b consists of a string of 3 white LEDs stacked in series, and the current flowing through the LEDs is 150 mA. One switching cycle is divided into four subintervals. During the first subinterval, S_1, S_{2a} and S_{2b} are ON, and the inductor current ramps up. During the second subinterval, S_1 is OFF while S_{2a} and S_{2b} are ON, and the circuit is in the freewheeling mode. In the third subinterval, S_1 and S_{2a} are OFF while S_{2b} is ON, and the inductor current ramps down. During the last subinterval, S_1, S_{2a} and S_{2b} are OFF, and the inductor current continuously ramps down.

For the operation corresponding to the sequence shown in Fig. 4.12(b), V_{in} is equal to 32 V. The load in output a is composed of a string of 4 white LEDs stacked in series, and the current flowing through the LEDs is 350 mA. The load in output b is formed by a string of 6 white LEDs stacked in series, and the current flowing through the LEDs is 150 mA. Again, one switching cycle has four subintervals. In the first subinterval, S_1, S_{2a} and S_{2b} are ON, and the inductor current ramps up. In the second

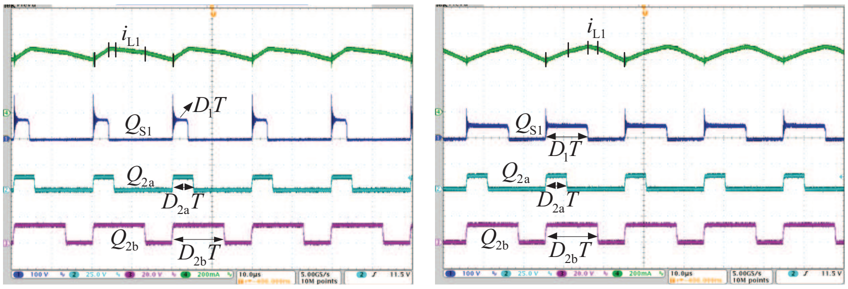

(a) (b)

Figure 4.12: Experimental waveforms of two operating cases. (a) Case 1; (b) case 2, corresponding to Fig. 4.5.

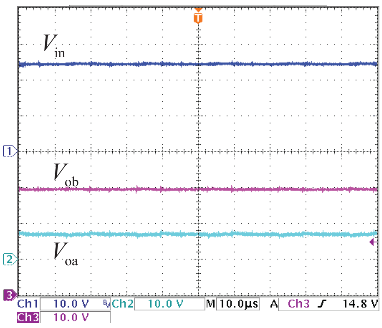

Figure 4.13: Relationship between input and output voltages, showing simultaneous step-up and step-down function. V_{in} = 24 V, V_{oa} = 6.6 V, and V_{ob} = 28 V.

subinterval, S_1 and S_{2b} are ON while S_{2a} is OFF, and the inductor current ramps up. In the third subinterval, S_1 and S_{2a} are OFF while S_{2b} is ON, and the inductor current ramps down. Finally in the last subinterval, S_1, S_{2a} and S_{2b} are OFF, and the inductor current continuously ramps down. The experimental results are in perfect agreement with the analysis.

Fig. 4.13 shows the input and output voltages, illustrating the simultaneous step-up and step-down functions. Here, V_{in} is equal to 24 V, V_{oa} is 6.6 V, and V_{ob} is 28 V. The load in output a consists of a string of 2 white LEDs stacked in series and the load in output b consists of a string of 10 white LEDs stacked in series. The range of the output voltage can thus be broadened with this configuration. In some applications, e.g., hand-held battery-powered applicances, this CSM SIDO dc-dc converter requires a single battery, instead of two batteries in series, to generate different voltage levels.

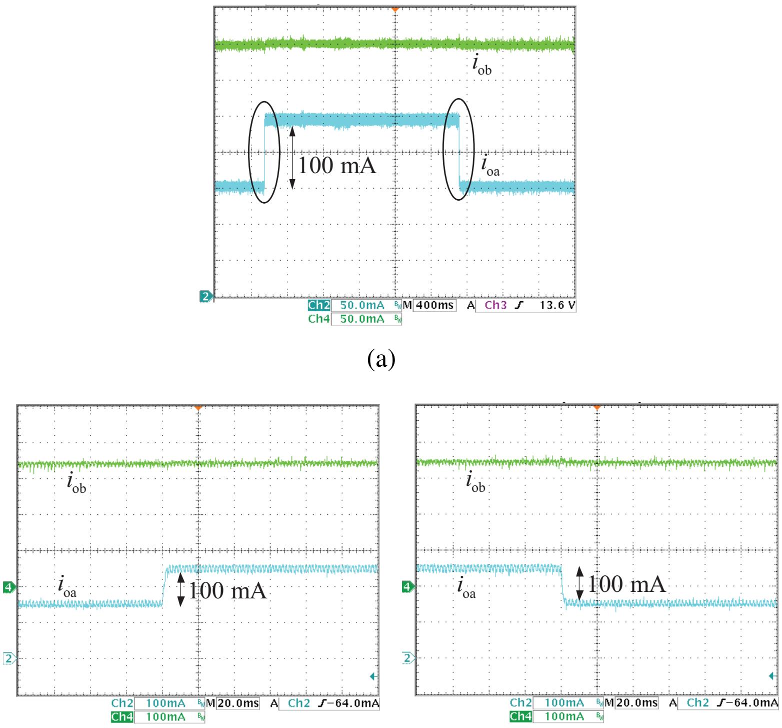

(a)

(b) (c)

Figure 4.14: Transient response showing independence of the two output currents or cross regulation. (a) Transient response of a 100 mA step applied to one output; (b) 150 mA to 250 mA; (c) 250 mA to 150 mA. In both cases, the other current output is unaffected.

Fig. 4.14 shows independent dimming and the transient response when a 100 mA step current is applied to output *a*. The load in output a consists of a string of 5 white LEDs stacked in series and the load in output b consists of a string of 5 white LEDs stacked in series. The output current I_{oa} steps between 150 mA and 250 mA. The waveform of the other output current, I_{ob}, is shown in Fig. 4.14(a), and in detail in Figs. 4.14(b) and 4.14(c). It is clearly shown that when current I_{oa} steps from the steady-state value 150 mA to 250 mA, current I_{ob} is unaffected and maintained constant. The independent dimming function is achieved with open-loop control in this CSM SIMO dc-dc converter. Furthermore, the cross-regulation effect is almost completely eliminated because of the constant current feeder. The decoupling performance of the CSM SIDO dc-dc converter is verified.

The experimental waveform of high-frequency PWM dimming method is shown

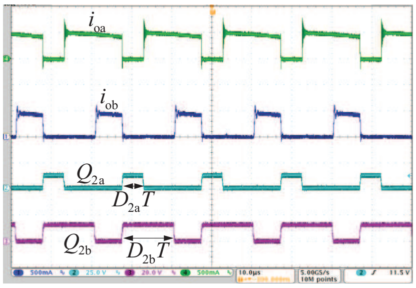

Figure 4.15: Experimental waveforms of high-frequency PWM dimming.

in Fig. 4.15. The load in output a consists of a string of 2 white LEDs stacked in series and the load in output b consists of a string of 2 white LEDs stacked in series. The value is 10 nF for C_{2a} and C_{2b}. When S_{2a} is ON, current i_{oa} is zero. When S_{2a} is OFF, current i_{oa} becomes 500 mA which is the value of i_{L1}. We may control duty cycle d_{2a} to set the average current $i_{oa-\mathrm{av}}$ arbitrarily, thus performing dimming conveniently. A likewise situation applies to the other output. For channel a, the average input current of the CSM buck converter is 500 mA and the average output current is 350 mA. Thus, duty cycle D_{2a} is 0.30. For channel b, the average input current of the CSM buck converter is 500 mA and the average output current is 150 mA. Thus, duty cycle D_{2a} is 0.70. The experimental results verify that the high-frequency PWM dimming method can be applied to the CSM SIDO dc-dc converter and the output currents can be set independently with an open-loop control.

Figs. 4.16(a) and 4.16(b) show color-temperature dimming performance of the CSM SIDO dc-dc converter using a low-frequency PWM dimming method. The load in output a consists of a string of 2 white LEDs stacked in series and the load in output b consists of a string of 2 white LEDs stacked in series. For switches S_{2a} and S_{2b}, the switching frequency is 400 Hz. For switch S_1, the switching frequency is 50 kHz. The value of C_{2a} and C_{2b} is 220 μF. Switches S_{2a} and S_{2b} are switched complementarily. When S_{2a} is ON and S_{2b} is OFF, current i_{ob} assumes the value of i_{L1} which is 500 mA. Likewise, when S_{2b} is ON and S_{2a} is OFF, current i_{oa} is 500 mA. For channel a, the average input current of the CSM buck converter is 500 mA and the average output

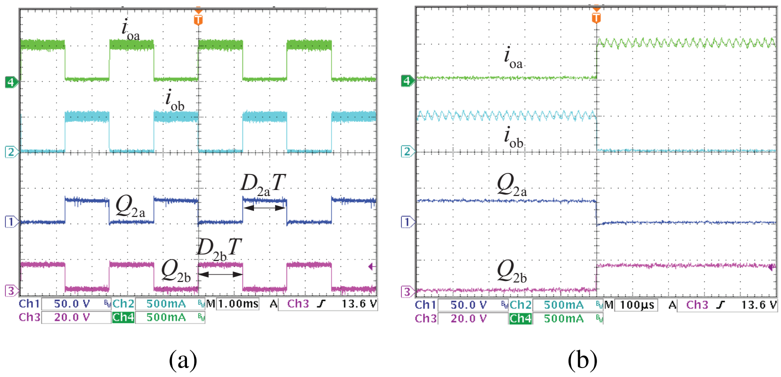

Figure 4.16: Experimental waveforms of low-frequency PWM dimming. (a) Color-temperature dimming performance; (b) enlarged view.

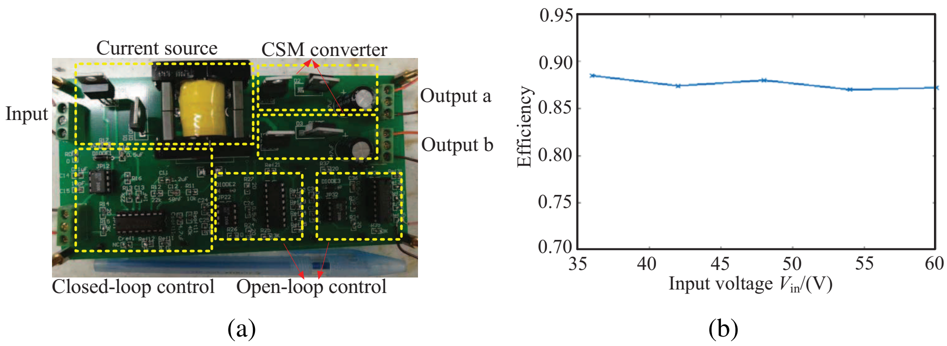

Figure 4.17: (a) Prototype and (b) measured efficiency of proposed CSM SIMO LED driver.

current is 250 mA. Thus, duty cycle D_{2a} is 0.50. For channel b, because switch S_{2a} and switch S_{2b} are always switched in a complementary fashion, duty cycle D_{2b} is 0.50 and the average output current of channel b is 250 mA. Controlling either d_{2a} or d_{2b} achieves the color temperature as desired.

Fig. 4.17(a) shows the prototype of the proposed CSM SIMO LED driver. Fig. 4.17(b) shows the measured efficiency, which is not optimized, within an input range of 48V ± 25%.

4.6 Summary

The dual versions of the traditional buck, buck-boost and boost dc-dc converters, referred to as current-source-mode converters, convert a current to another current (or voltage with special control) basically using high-frequency switching of a storage capacitor. However, rarely have these CSM converters been seriously studied and developed for practical use. In view of the driving requirement and characteristics of LEDs, the CSM converters are found to be highly suited for driving LEDs as well as other current delivery functions. The input voltage source, however, necessitates the use of a current generator stage for feeding the CSM converters. The inherent absence of inductors and ease of control for independent dimming make the design of multiple-output converters much simpler, as demonstrated in this chapter. In addition, the simultaneous voltage step-up and step-down functions for multiple-output applications present a very useful feature that simplifies input source requirement such as the use of battery type in many portable devices. Both the PWM dimming method and the analog dimming method are applied to the proposed converter. The design of the LED driver has been verified experimentally.

Chapter 5

Quasi-Two-Stage CSM SIMO LED Driver with Improved Efficiency

5.1 Introduction

High brightness is the basic requirement in lighting systems. A direct way to enhance the brightness is to connect more LEDs in series. However, the disadvantage is that failure of one LED will cause the whole LED string to fail. Also, with the increase of the number of LEDs, the terminal voltage of the LED string may exceed the safety limit. Furthermore, independent dimming function cannot be achieved for the individual LED lights. Therefore, a multiple-output converter is a better solution for independent regulation of the current flowing through each string. All the output currents are generated from a single power source, as shown in Fig. 2.9(a). However, this conventional structure has obvious disadvantages. The cost and size could increase because we need to use several VSM converters and each contains an inductor. The power density is inevitably reduced.

In order to increase power density, the SIMO converter has been proposed, as shown in Fig. 2.9(a). When the conventional SIMO converter works under DCM, the cross-regulation effect can be avoided [21, 96], but the power level is still limited. When the conventional SIMO converter works under CCM, complex control strategies [79, 80] are needed in order to eliminate the cross-regulation effect. Thus, although this conventional SIMO converter has only one inductor, the concerns mentioned above remain legitimate.

In the previous chapter, we investigated CSM SIMO LED driver, as shown in Fig. 4.1(b), in detail. A simple control strategy and the associated working principle have been illustrated. Here, it is worth noting that only one inductor is needed to construct a current source for feeding the CSM buck converters which inherently contain no inductor. The limiting factors of CSM SIMO LED driver, however, includes the relatively low efficiency and the restricted number of outputs under low-frequency PWM dimming control.

In this chapter, we propose a quasi-two-stage CSM SIMO LED driver with an adaptive current bus for efficiency enhancement. The control strategy is simple, and independent dimming function can be achieved easily. Also, the proposed structure can achieve high-step-down ratio without using transformers. The voltage stress in each constituent converter, unlike in the conventional configuration, depends only on its input voltage and output voltage, with no mutual influence.

5.2 Operation of CSM SIMO Converter with Adaptive Current Bus Technique

From the output terminal perspective, the output current is a controlled variable because LED's current is proportional to the luminance of the LED over a considerably wider range. From the input terminal perspective, a converter topology is normally designed with either voltage or current as the input. Thus, only two configurations in Fig. 1.1 are suited for driving LEDs. A VSM converter assumes a voltage source as its input because the input terminal is connected to a switching inductor. Likewise, a

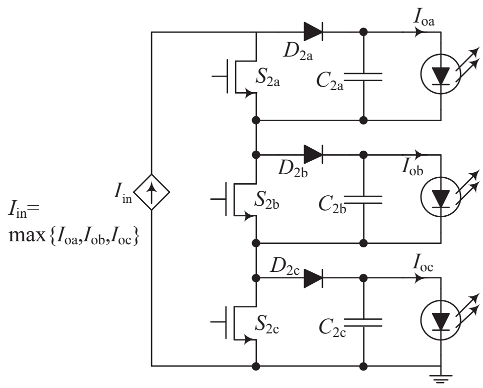

Figure 5.1: Adaptive current input arrangement.

CSM converter assumes a current source as its input because the input terminal is connected to a switching capacitor. When the load is an LED, in a VSM buck converter, the range of the duty cycle is very narrow, and both the voltage transfer ratio and the load characteristic can influence the process of regulating the output current. In a CSM converter, However, the duty cycle can directly control the output current. The CSM buck converter contains no inductor, has a better control-to-output sensitivity and requires simpler control circuits when used for delivering regulated current, as studied previously [86, 97].

In this chapter, we propose an adaptive current bus technique for coordinating the outputs of the CSM SIMO converter. Fig. 5.1 shows the conceptual arrangement of a single-input three-output dc-dc converter, where the input current I_{in} is always equal to the largest output current. A buck converter is employed to construct this adaptive current bus. We take the single-input three-output CSM converter as an example to illustrate the operation, as shown in Fig. 5.2.

Suppose current I_{oa} is the largest among the three output currents. The closed-loop controller in the first stage will regulate the inductor current at I_{oa}. Switch S_{2a} is always OFF, and diode D_{2a} is always ON, making $I_{oa} = I_{\text{in}}$.

<ins>Mode 1</ins>: S_1, S_{2b} and S_{2c} are ON. In this mode, $(V_{\text{in}} - V_{oa})$ charges up the inductor and i_{L1} ramps up. Capacitors C_{2b} and C_{2c} are discharged to the corresponding loads.

<ins>Mode 2</ins>: S_1 and S_{2b} are ON while S_{2c} is OFF. Voltage $(V_{\text{in}} - V_{oa} - V_{oc})$ charges or

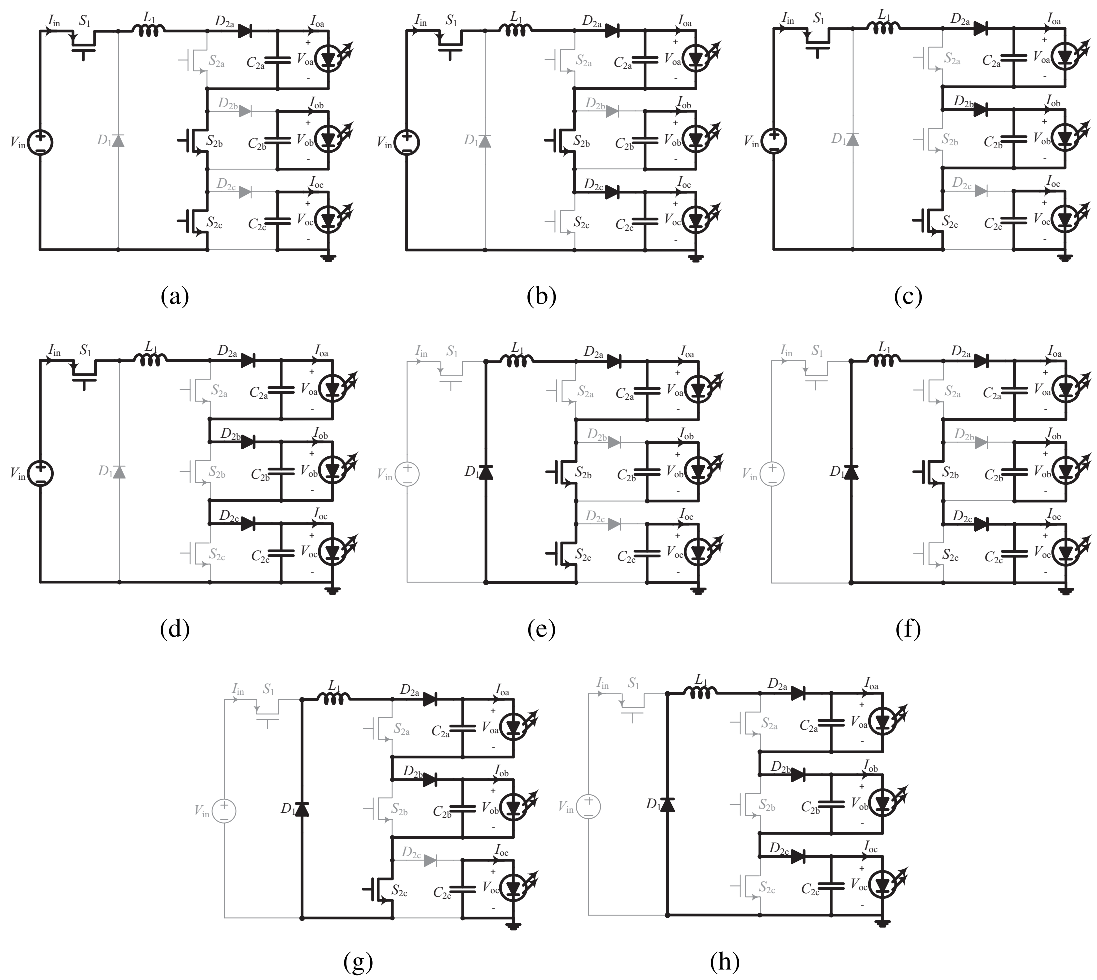

Figure 5.2: Operating modes with S_{2a} being always OFF. (a) S_1, S_{2b}, and S_{2c} are ON; (b) S_1 and S_{2b} are ON and S_{2c} is OFF; (c) S_1 and S_{2c} are ON and S_{2b} is OFF; (d) S_1 is ON and S_{2b} and S_{2c} are OFF; (e) S_1 is OFF and S_{2b} and S_{2c} are ON; (f) S_1 and S_{2c} are OFF and S_{2b} is ON; (g) S_1 and S_{2b} are OFF and S_{2c} is ON; (h) S_1, S_{2b}, and S_{2c} are OFF.

discharges the inductor, and i_{L1} ramps up or down. Capacitor C_{2b} is discharged to the load.

Mode 3: S_1 and S_{2c} are ON while S_{2b} is OFF. This mode is similar to Mode 2.

Mode 4: S_1 is ON while S_{2b} and S_{2c} are OFF. Voltage ($V_{\text{in}} - V_{oa} - V_{ob} - V_{oc}$) charges or discharges the inductor, and i_{L1} ramps up or down.

Mode 5: S_1 is OFF while S_{2b} and S_{2c} are ON. In this mode, V_{oa} discharges the inductor and i_{L1} ramps down. Capacitors C_{2b} and C_{2c} are discharged to the corresponding load.

Mode 6: S_1 and S_{2c} are OFF while S_{2b} is ON. Voltage (V_{oa} + V_{oc}) discharges the inductor, and i_{L1} ramps down. Capacitor C_{2b} is discharged to the load.

Mode 7: S_1 and S_{2b} are OFF while S_{2c} is ON. This mode is similar to Mode 6.

Mode 8: S_1, S_{2b} and S_{2c} are OFF. Voltage (V_{oa} + V_{ob} + V_{oc}) discharges the inductor, and i_{L1} ramps down.

5.3 Properties of the CSM SIMO Converter with Adaptive Current Bus

In this section, we focus on the CSM SIMO converter described in Section 5.2, and apply the adaptive current bus technique to achieve the required regulation function, high-step-down ratio, high efficiency and independent dimming function.

5.3.1 Working Principle of Control Circuit

The control scheme is conceptually shown in the schematic diagram of Fig. 5.3. The digital control compares the value of each reference current, and selects the highest output current as the reference current of the controller in first stage. Once the reference current is fixed, a closed-loop control is employed to control the first stage. The inductor current and the reference current are connected to the inverting and non-inverting ports of the error amplifier (EA), respectively. In this way, the inductor current is always equal to the highest output current. The switch in the highest-output-current converter will always be OFF, i.e., switch S_{2a} in Fig. 5.2. The output of the EA and a sawtooth waveform are compared to generate the driving signal. Thus, inductor current I_{L1} is always lower than the specified current limitation I_{ov}. The output of the comparator in the protection circuit is always at a high level. Hence, the output of the AND gate always follows the output signal of the PWM generator.

The second stage is open loop. The inductor current, which is also the input current of each CSM buck converter, is equal to the largest output current. The duty cycle can

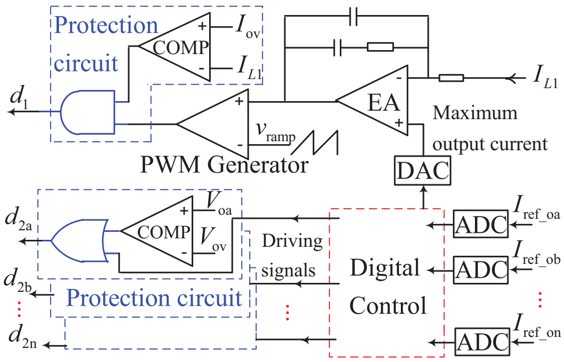

Figure 5.3: Control block diagram.

be calculated by the digital controller based on (1.3), giving the desired output current for each converter. Thus, each output voltage is lower than the specified voltage limit, the output of the comparator, which is also the primary input to the OR gate, is always at a low level. Hence, the output of the OR gate always follows the secondary input which is also the computed result generated by digital controller.

The blue dashed boxes contain the protection circuit. As mentioned above, when inductor current I_{L1} is lower than the specified current limit, the feedback network operates normally. However, in the event of a fault, inductor current I_{L1} goes higher than the specified current limit. The low level output of the comparator always sets the output of the AND gate to a low level. Therefore, switch S_1 is OFF. The system stops working. When the output voltage is lower than the specified voltage limit, the feedback network works normally. However, when an LED string is open, the current flowing through it is still controlled to be constant, causing the output capacitor voltage to increase. When the capacitor voltage reaches the specified voltage limit, the output of the comparator is always at a high level which sets the output of the OR gate to a high level. The switch in the corresponding CSM buck converter is ON. Compared with the traditional SIMO converter [70, 77, 78] (Fig. 2.9(b)) and the input-series-connected converter [1], the advantage of the proposed converter is that when the switch is in the ON state, the CSM buck converter is naturally protected. The corresponding converter will be shorted and other converters continue to work normally.

5.3.2 High Voltage Step-Down Ratio

The input-series-connected converter [1] can be applied to high voltage step-down applications. This circuit enables the use of low-profile components, permitting possible circuit integration. The power density can be increased and the cost can be reduced. However, there are some drawbacks of the input-series-connected converter. First, if any one of the converters is shorted, the other converters have to share the input voltage together. Thus, the drain-to-source breakdown voltage of switches should be higher in order to allow a higher voltage stress level in the event of converter failure. Second, the input-series-connected converter adopts a common duty cycle control approach. Although this approach is simple, it cannot realize independent dimming function. Also, the protection strategy is complicated which may increase the design complexity.

In the case of the proposed converter shown in Fig. 4.1(b), the switching frequencies are independent. Independent dimming function can be achieved readily, offering a great deal of flexibility in the dimming design. The CSM buck converter possesses a natural protective function as mentioned in Section 5.3.1. Regarding the voltage stress, referring to Fig. 4.1(b), when S_1 is OFF, D_1 will be ON. Thus, the voltage stress of switch S_1, namely V_{ds_1}, is equal to V_{in}. The voltage stress of switch S_1 is dependent on the input voltage only. The states of switches S_{2a} to S_{2n} do not affect the voltage stress of switch S_1. Suppose output current I_{oa} is the largest output current. Taking switch S_{2b} as an example, when S_{2b} is OFF and D_{2b} is ON, the voltage stress of switch S_{2b}, namely, V_{ds_2b}, is equal to V_{ob}. Other switches do not affect the voltage stress of switch S_{2b}. In the event of a CSM buck converter triggering a short-circuit protection, the voltage stress of switch S_{2b} still maintains V_{ob}. The same situation is observed in other CSM buck converters. The voltage stress of switches S_{2a} to S_{2n} is dependent on the corresponding output voltage only. Thus, we may select switches simply based on the rated input and output voltages. In high input voltage and low output voltage situations, we can employ low-profile components to all CSM buck converters. For

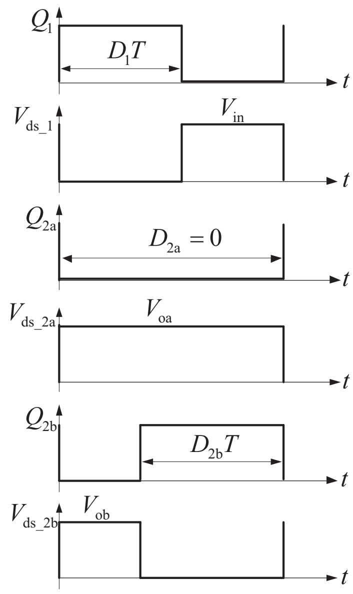

Figure 5.4: Theoretical voltage stress of each switch.

the proposed CSM SIMO converter, therefore, we need only one high-voltage-stress switch, namely, S_1. The theoretical waveforms of switches are shown in Fig. 5.4.

5.3.3 High-Efficiency Quasi-Two-Stage Power Processing

In this section, we analyze the efficiency of the CSM SIMO converter in terms of energy flow paths. Compared with the traditional SIMO converter, the CSM SIMO converter has a lower efficiency for two main reasons. First, the number of power processing stages is two. Specifically, energy is processed by a VSM buck converter and a CSM buck converter before reaching the load. Thus, the CSM SIMO is a two-stage converter. Second, the inductor current should be higher than each individual output current, leading to an increased circulating current in the circuit.

According to the working principle of the control strategy, the inductor current is equal to the largest output current. The switch in the highest-output-current string is always OFF. The equivalent circuit of the CSM SIMO converter is shown in Fig. 5.5(a). The red dotted box in Fig. 5.5(a) represents the input-to-load path that processes energy in one stage. The blue dotted box in Fig. 5.5(a) represents input-to-load path that

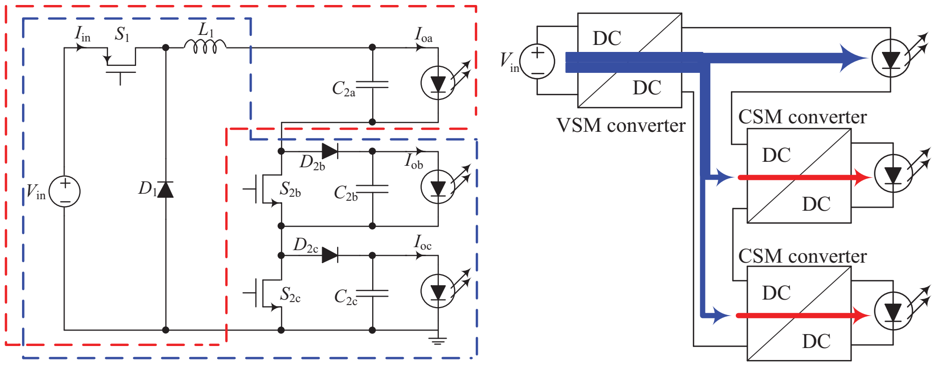

(a) (b)

Figure 5.5: Energy-flow-path analysis. (a) Equivalent circuit of the CSM SIMO converter; (b) energy flow path.

processes energy in two stages. The corresponding energy flow path is summarized in Fig. 5.5(b). The blue lines correspond to power flown in the first power stage. The red lines represent the power flown in the second power stage. When an adaptive current bus is applied to the CSM SIMO converter, part of the total power is processed by one stage and the rest by two stages. Thus, the converter is no longer a full two-stage converter and can be regarded as a quasi-two-stage converter having an obvious improvement in efficiency. Specifically, the input-to-load energy path for the converter with the largest output current is processed by one stage.

The inductor current in the first stage is always larger than any of the output currents. This leads to an increased circulating current. However, with the proposed adaptive current bus technique, the circulating current is minimal as the inductor current is set to the same level of the largest output current and not higher, thus further improving the efficiency of the CSM SIMO converter.

In the following, the efficiency of the CSM SIMO converter is analyzed. The power loss mechanism in a switch is illustrated in Fig. 5.6. Here, I_d is the current following through the switch when the switch is ON, and V_{ds} is the drain-source voltage when the switch is OFF. The on-state power loss P_{con} can be calculated as

$$P_{\text{con}} = {I_d}^2 R_{\text{on}} \frac{(t_3 - t_2)}{T} \tag{5.1}$$

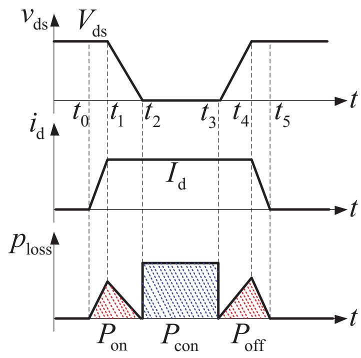

Figure 5.6: Power loss mechanism in a switch.

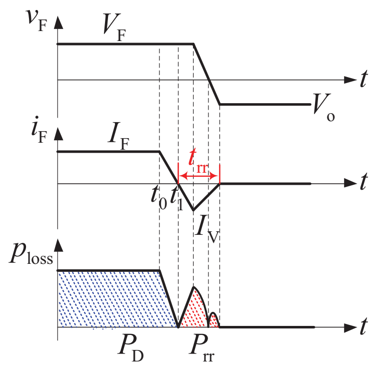

Figure 5.7: Power loss mechanism of a diode.

where R_{on} is the equivalent resistance when the switch is ON, and T is the switching cycle. The turn-on power loss P_{on} can be obtained as

$$P_{on} = \frac{1}{2}V_{ds}I_d\frac{(t_2 - t_0)}{T}. \tag{5.2}$$

The turn-off power loss P_{off} can be obtained as

$$P_{off} = \frac{1}{2}V_{ds}I_d\frac{(t_5 - t_3)}{T}. \tag{5.3}$$

Thus, the total power loss P_{loss} for a switch can be expressed as

$$P_{loss} = P_{con} + P_{on} + P_{off}. \tag{5.4}$$

For a diode, the power loss mechanism is illustrated in Fig. 5.7. Here, I_F is the current following through the diode when the diode is ON, and V_F is the forward voltage drop of the diode when the diode is ON. Also, I_V is the reverse valley current. The parameter t_{rr} is the reverse recovery time, and V_o is the reverse voltage. The on-state power loss P_D can be calculated as

$$P_D = \frac{1}{2} V_F I_F \frac{(t_0 + t_1)}{T}. \tag{5.5}$$

The reverse recovery power loss P_{rr} depends on V_F, V_o, I_V and t_{rr}, i.e.,

$$P_{\text{rr}} = f(V_F, V_o, I_V, t_{\text{rr}}). \tag{5.6}$$

Thus, the total power loss P_{loss} in a diode can be expressed as

$$P_{\text{loss}} = P_D + P_{\text{rr}}. \tag{5.7}$$

For switch S_1, the drain-source voltage is always equal to V_{in}. The inductor current under the adaptive current bus control is equal to the largest output current, which is always lower than the inductor current without the adaptive current bus [97]. As current I_{L1} is decreased, P_{on} and P_{off} are accordingly decreased based on equations (5.2) and (5.3). The power loss P_{con} in (5.1) can be expressed as

$$P_{\text{con}} = {I_d}^2 R_{\text{on}} \frac{(t_3 - t_2)}{T} = {I_{L1}}^2 R_{\text{on}} \frac{I_{\text{in}}}{I_{L1}} = \frac{P I_{L1} R_{\text{on}}}{V_{\text{in}}} \tag{5.8}$$

where P is the input power. Thus, the power loss P_{con} is also reduced. The total power loss in switch S_1 is reduced according to (5.4).

For each switch in each of the CSM buck converters, the drain-source voltage is always equal to the output voltage V_{ok}. As the bus current I_{L1} is lowered, P_{on} and P_{off} are accordingly reduced based on the same principle mentioned above. The power loss

P_{con} in (5.1) can be expressed as

$$P_{\text{con}} = {I_d}^2 R_{\text{on}} \frac{(t_3 - t_2)}{T} = {I_{L1}}^2 R_{\text{on}} \left(1 - \frac{I_{ok}}{I_{L1}}\right) = I_{L1} R_{\text{on}} (I_{L1} - I_{ok}). \tag{5.9}$$

Thus, the power loss P_{con} for each of the switches in the CSM buck converters is also reduced. The total power loss of switch in each CSM buck converter is reduced according to equation (5.4).

For diode D_1, the forward voltage drop V_F is constant. The power loss P_D can be expressed as

$$P_D = \frac{1}{2} V_F I_F \frac{(t_0 + t_1)}{T} = \frac{1}{2} V_F (I_{L1} - \frac{P}{V_{\text{in}}}). \tag{5.10}$$

As the bus current I_{L1} is reduced, P_D is accordingly reduced. Assuming that parameters I_V and t_{rr} are fixed, the reverse recovery power loss of diode D_1 remains the same. Thus, the total power loss of diode D_1 is reduced based on equation (5.7).

For diodes in the CSM buck converters, the forward voltage drop V_F is also constant. The power loss P_D can be expressed as

$$P_D = V_F I_{L1} \frac{I_{ok}}{I_{L1}} = V_F I_{ok}. \tag{5.11}$$

Although the bus current I_{L1} is smaller, P_D remains the same based on equation (5.11). Assuming that parameters I_V and t_{rr} are fixed, the reverse recovery power loss of the diodes in CSM buck converters remain constant when the inductor current changes. Thus, the total power loss of diodes remains constant.

For the sampling resistor, the power loss is

$$P_{\text{sen}} = {I_{L1}}^2 R_{\text{sen}} \tag{5.12}$$

where R_{sen} is the resistance of the sampling resistor. The power loss of the sampling resistor is also reduced as current I_{L1} decreases.

In summary, the use of the adaptive current bus reduces the overall power loss of the CSM SIMO converter.

5.3.4 Independent Dimming Function

As mentioned above, the inductor current is always equal to the largest output current. Therefore, regulating the inductor current will automatically regulate the largest output current. Other output currents can be regulated by controlling duty cycles of the corresponding CSM buck converters. The independent dimming function can be easily achieved. Since each output current can be regulated independently, any output current could be the largest current. A maximum current detection circuit can be used to identify the largest current output and set it as the new reference for the inductor current. The CSM SIMO converter works in the same way with a new inductor current value.

While the above dimming method works well under analog dimming, a situation might arise that deserves special attention if low-frequency PWM dimming was used. Taking the single-output LED driver of Fig. 5.8(a) as an example, although the two switches are independent, switch S_2 cannot work at a switching frequency lower than the switching frequency of S_1. If switch S_1 works at a high switching frequency and switch S_2 works at a low switching frequency, the ON time of S_2 is much longer than that of S_1. During the ON state of switch S_2, switch S_1 periodically turns on and off, causing the inductor current to move up, as illustrated in Fig. 5.8(b). As shown in the blue circle, when S_2 is ON, the inductor current goes up and stays constant in one duty cycle of switch S_1. There is no discharging process for the inductor. Thus, the inductor current will ramp up continuously, causing damage to the circuit.

Our proposed solution is as follows. We operate switch S_1 at a high switching frequency and switches S_{2a}, S_{2b} and S_{2c} at a low switching frequency, as shown in Fig. 5.9. Suppose I_{oa} is the largest output current. Then, switch S_{2a} is always OFF.

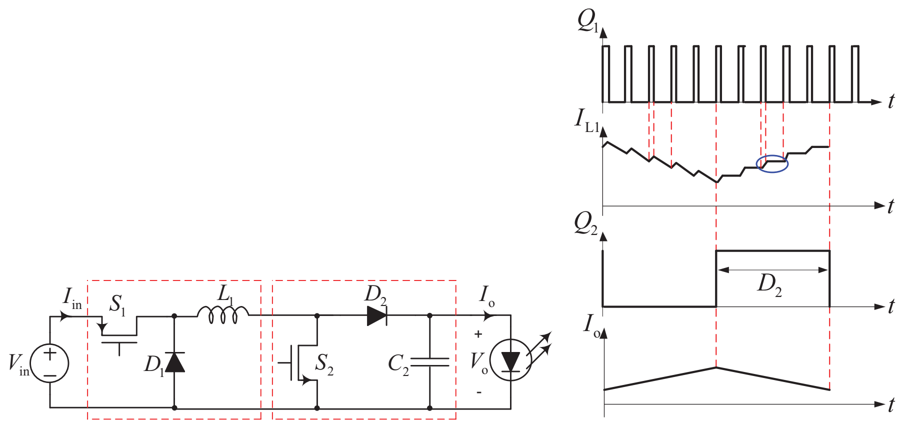

Figure 5.8: An undesirable situation under low-frequency PWM dimming. (a) CSM single-output LED driver; (b) theoretical waveforms.

The inductor current now directly powers the LED string having the highest current. As shown in the red circle in Fig. 5.9, when switches S_{2b} and S_{2c} are in the ON state simultaneously, there will be no short circuit phenomenon since the LED string having the largest current is always being powered. This largest output current can be regulated arbitrarily by regulating the inductor current, while other output currents can be regulated via adjusting their corresponding duty cycles. The independent dimming function can thus be achieved readily.

5.4 Experimental Demonstration

A CSM SIMO converter with the aforedescribed adaptive current bus has been constructed and tested. The values of components used are shown in Table 5.1.

Fig. 5.10 shows the steady-state waveforms of the CSM SIMO converter. Here, I_{oa} is the highest output current which is equal to 350 mA. Thus, the inductor current is controlled at 350 mA via feedback control of switch S_1. Switch S_{2a} is always OFF. Other output currents can be regulated freely by changing other duty cycles in the individual CSM buck converters. The inductor current and the driving signal of switch S_1 are shown in Fig. 5.10(a). The driving signals of switches S_{2a}, S_{2b} and S_{2c} are

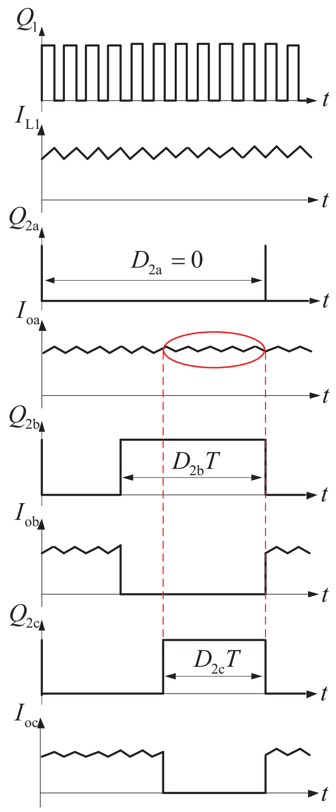

Figure 5.9: Theoretical waveforms of CSM SIMO LED driver with adaptive current bus under low-frequency PWM dimming.

shown in Fig. 5.10(b). The experimental results verify the working principle of the adaptive current bus technique.

The measured voltage stresses of the switches are shown in Fig. 5.11. In this case, I_{oa}, I_{ob} and I_{oc} are equal to 350 mA, 150 mA and 250 mA, respectively. When switch S_1 is OFF, the drain-source voltage of switch S_1 is equal to 48 V, which is the input voltage V_{in}. Since I_{oa} is the maximum current, switch S_{2a} is always OFF. The drain-source voltage of switch S_{2a} is always equal to V_{oa}. The measured voltage stress is about 6.6 V. For switches S_{2b} and S_{2c}, the measured voltage stresses are about 5.5 V and 6 V, respectively. The measured values are in perfect agreement with the theoretical values. In this paper, the input voltage is 48 V, and the output voltages are 5.5 V, 6 V and 6.6 V. The voltage stress in each CSM buck converter is influenced only by the corresponding output voltage. No mutual interactions are observed, which is

Table 5.1: Parameters of CSM SIDO Converter

Circuit Parameters	Value
Rated input voltage	48 V
Rated inductor current	350 mA
Main inductor L_1	2000 μH
Capacitors C_{2a} to C_{2n}	10 nF / 220 μF
Output currents I_{oa} to I_{on}	0 - 350 mA
Number of LEDs in one string	2
Number of LED string	3
Switch frequency of S_1	50 kHz
Switch frequency of S_{2a} to S_{2n}	50 kHz / 1 kHz

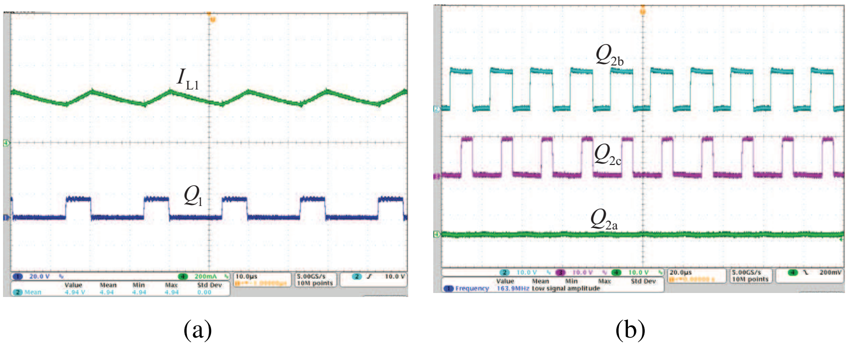

Figure 5.10: Steady state waveforms. (a) Inductor current (highest output current); (b) other driving signals.

desirable for component selection. From the experimental results, apart from the high-rating switch used for S_1, other switches in the CSM buck converters may employ low-rating devices, reducing the cost of the system.

Experimental waveforms showing the transient response are presented in Fig. 5.12. Initially, I_{oa}, I_{ob} and I_{oc} are set at 150 mA, 250 mA and 350 mA, respectively. The largest output current is thus I_{oc}. The inductor current is equal to I_{oc}, and switch S_{2c} is always OFF. The inductor current in this paper is smaller than in the case without the adaptive current bus [97]. Also, I_{oa} and I_{ob} are set via adjusting d_{2a} and d_{2b}, respectively. When I_{oc} steps from 350 mA to 150 mA, I_{ob} takes over as the largest output current. The inductor current becomes I_{ob}, and switch S_{2b} is always OFF. Then, I_{oa} and I_{oc} are set by adjusting d_{2a} and d_{2c}, respectively. The driving signals, the inductor

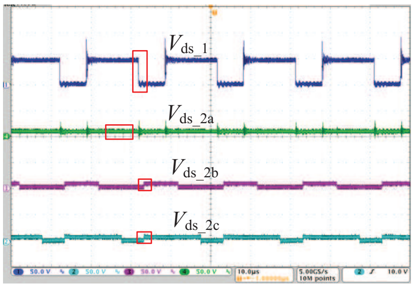

Figure 5.11: Measured voltage stresses of switches.

current and the the transient response are presented in Fig. 5.12(a). When I_{oc} steps from 150 mA back to 350 mA, I_{oc} resumes as the largest output current. The process is shown in Fig. 5.12(b). The details of the transient response shown in Figs. 5.12(a) and 5.12(b) are given in Figs. 5.12(c) and 5.12(d), respectively. The experimental results are consistent with the theoretical analysis.

Fig. 5.13 shows the low-frequency independent dimming function. Here, I_{oa} is the largest output current which is equal to the inductor current, as shown in Fig. 5.13(a). The frequency is 1000 Hz for switches S_{2b} and S_{2c}, and is 50 kHz for switch S_1. When switches S_{2b} and S_{2c} are in the ON state simultaneously, there is no short circuit phenomenon because the LEDs in converter A is always connected to the circuit. In an earlier work [97], low-frequency PWM dimming method can only be applied to two-output dc-dc converters, and the independent dimming function cannot be achieved because of the use of master-slave control strategy. In this paper, however, such restriction is lifted by the application of adaptive current bus technique. The low-frequency PWM dimming method can be extended to three or more outputs in CSM SIMO converter. Each output can achieve dimming independently.

The measured efficiency is shown in Fig. 5.14. The red and blue curves represent the efficiency of the CSM SIMO converter with and without [97] adaptive current bus, respectively. It is clearly shown that the adaptive current bus technique can improve the efficiency of the CSM SIMO converter significantly.

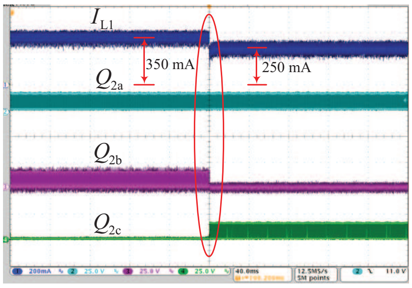

(a)

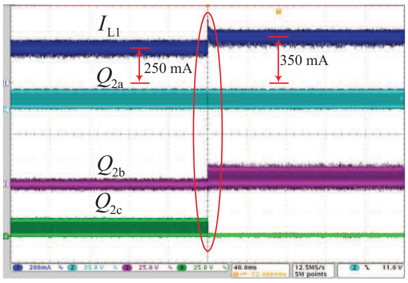

(b)

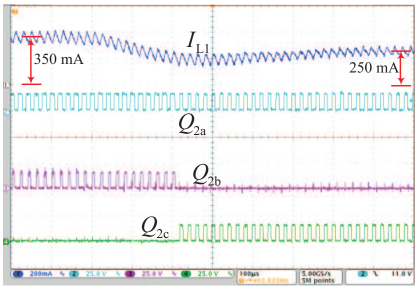

(c)

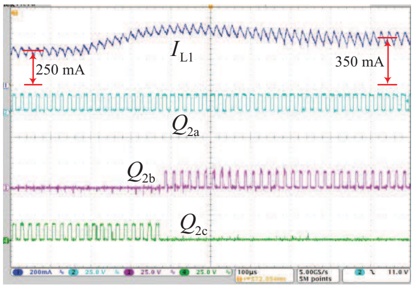

(d)

Figure 5.12: Transient response with adaptive current bus applied to CSM SIMO converter. (a) Largest current changes from 350 mA to 250 mA; (b) from 250 mA to 350 mA; (c) transient response corresponding to (a); and (d) transient response corresponding to (b).

5.5 Summary

In this chapter, we address the practical restrictions of CSM SIMO LED driver. Specifically, novel approaches to improving low efficiency and permitting independent dimming function under low-frequency PWM dimming are studied. We apply the adaptive current bus technique here to reduce the power loss in energy flow paths and hence improve the efficiency. By analyzing the voltage stress of each switch in the CSM SIMO converter, we conclude that the voltage stress of each switch is only dependent on the input voltage or output voltage, and not affected by interactions between different converters. Based on the above analysis, the CSM SIMO dc-dc converter with adaptive current bus fits well with driving LEDs.

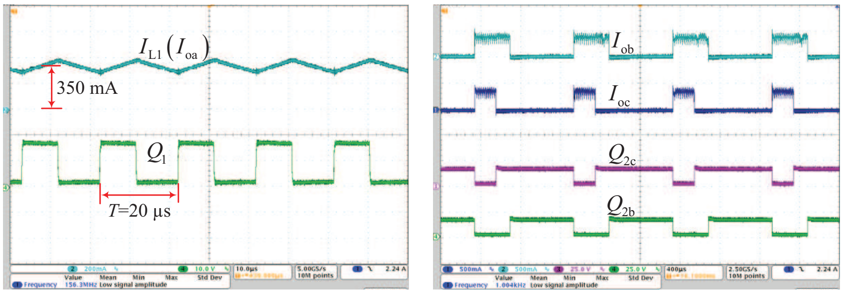

(a) (b)

Figure 5.13: Low-frequency independent dimming function. (a) The largest output current; (b) other output currents.

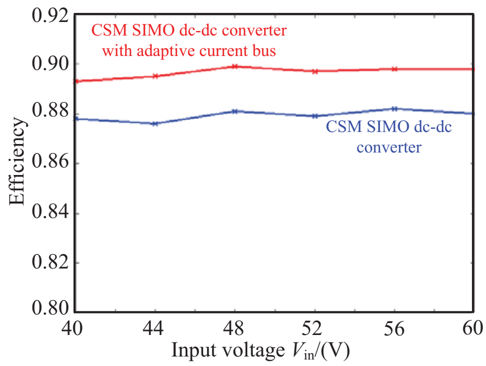

Figure 5.14: Comparison of efficiency of CSM SIMO converter with and without adaptive current bus.

Chapter 6

Conclusions and Suggestions for Future Work

In this chapter, we re-iterate the main contributions of the thesis and discuss some potential topics for future research.

6.1 Main Contributions of the Thesis

Solid-state loads have become increasingly popular in residential, commercial and business environment, e.g., LED lighting systems. According to the statistics, about 19% of global electricity is consumed by lighting. The LED has become a promising new generation light source because of the advantages of environmental safety, long life expectancy and high efficiency. Replacing traditional lightings by LEDs has become a global trend. The specific *v*-*i* characteristics of LEDs have created new challenges in power management system design, especially in the design of power conversion systems which have traditionally been dominated by input voltage sources and resistive loads.

In this thesis, CSM converters have been investigated for driving LEDs. The comparison of VSM and CSM converters, the derivation of CSM SIMO LED driver and the efficiency enhancement of the proposed converter have been studied in Chapters 3, 4 and 5, respectively. CSM drivers are less known but are theoretically more versatile compared to their conventional VSM counterparts. Specifically, the contributions of the thesis are stated as follows.

Chapter 3 examines the driving circuit requirement for LED loads. The starting point is the LED characteristic, and the problem-solving method is basis on basic circuit theory. We investigate VSM and CSM drivers in terms of the main circuit components, the range of duty cycle variation, the sensitivity of the output current to the change of duty cycle, the nonlinearity of the control function and the control complexity. The comparison of the key performance areas in relation to LED lighting applications indicates the importance of consideration of the termination type and the corresponding choice of converter type. Since CSM drivers inherently contain no inductors, they can be conveniently used in constructing multiple-output driving converters employing a minimum number of inductors. The CSM SIMO converter performs better with less cost compared with existing SIMO converters. In high-voltage-step-down applications, the CSM converter offers fixed low voltage stress, and is well suited for high-voltage-step-down applications. Finally, we emphasize that proper application of circuit concepts would form the basis of design of effective driving circuits for LED applications.

Chapter 4 derives the CSM SIMO LED driver specifically based on the CSM buck converter which converts a current to another current basically using high-frequency switching of a storage capacitor. However, the input source, which is normally voltage source, necessitates the use of a current generator stage for feeding the CSM converters. The inherent absence of inductors makes the design of multiple-output converters much simpler, as demonstrated in this chapter. The series-connected structure can achieve independent dimming function with simple open loop control, and the cross-regulation effect can be reduced. The single-inductor multiple-output converter can be constructed easily. The proposed CSM SIMO converter has better performance than the conventional SIMO converter. The simultaneous voltage step-up and step-down functions for multiple-output applications present a very useful feature. Both the PWM dimming method and the analog dimming method are applied to the proposed converter.

Chapter 5 mainly focuses on the practical restrictions of CSM SIMO LED driver. The efficiency of CSM SIMO LED driver is lower than conventional VSM-based SIMO converter, the reason being that the VSM-based SIMO converter is a one-stage design whereas the CSM SIMO converter has two stages of power processing, including a VSM buck converter and a CSM buck converter. Based on the analysis, we apply the adaptive current bus technique to reduce the power loss in energy flow paths and hence improve the efficiency. The combination of the adaptive current bus technique and the proposed converter permits independent dimming function under low-frequency PWM dimming. By analyzing the voltage stress of each switch in the CSM SIMO converter, we conclude that the voltage stress of each switch is only dependent on the input voltage or output voltage, and not affected by interactions between different converters.

6.2 Suggestions for Future Work

Based on the previous works and experiences gathered in recent related works, and the work done in this project, suggestions for extensions and potential areas for further studies are proposed here.

In Chapter 3, in order to compare VSM converters and CSM converters, we have used a VSM buck converter to construct a constant current source. However, it should be noted that other converters can also serve as a current generator. Other forms of current generator can offer different desirable features, further simplifying the control strategy. In this thesis, we mainly focus on the CSM converters from the output terminal perspective. However, renewable energy sources have been extensively used in modern microgrid power distribution systems. The usage of renewable energy sources has created new challenges in the design of power conversion systems which have traditionally been interfacing voltage sources as input. From the input terminal perspective, there are many issues worthy to be studied and considered.

In Chapter 4, based on the CSM buck converter and duality principle, a CSM SIMO LED driver has been proposed and studied. However, all the analysis is based on the use of a DC input. The CSM converter can also be designed to be power factor correction (PFC) regulator. For traditional PFC regulators, due to the power difference between the input and output terminations, electrolytic capacitors are usually adopted for reducing the double line frequency ripple. In a dual version, inductors are usually adopted for reducing double line frequency ripple for CSM PFC regulators. An inductor is a bulky component. Thus, reducing the double line frequency ripple is the most critical issue.

In Chapter 5, an adaptive current bus technique has been applied to a CSM SIMO LED driver for improving the efficiency. This control method can also be applied to the CSM high-voltage-step-down converter. A detailed analysis can be included in the CSM high-voltage-step-down converter with the adaptive current bus technique. A comprehensive comparison can be further developed in terms of the efficiency, the voltage transfer ratio and the voltage stress. In this thesis, we have selected the maximum output current as the reference current. In the future, we can also try to use the minimal output current as the reference current.

Bibliography

[1] Q. Hu and R. Zane, “Led driver circuit with series-input-connected converter cells operating in continuous conduction mode,” *IEEE Trans. Power Electron.*, vol. 25, no. 3, pp. 574–582, 2010.

[2] Y. K. Cheng and K. Cheng, “General study for using led to replace traditional lighting devices,” in *Proc. IEEE Power Electron. Syst. and Appl. Conf.*, 2006, pp. 173–177.

[3] L. Peretto and A. Emanuel, “A theoretical study of the incandescent filament lamp performance under voltage flicker,” *IEEE Trans. Power Delivery*, vol. 12, no. 1, pp. 279–288, 1997.

[4] H. J. Chiu, T. H. Song, S. J. Cheng, C. H. Li, and Y. K. Lo, “Design and implementation of a single-stage high-frequency hid lamp electronic ballast,” *IEEE Trans. Ind. Electron.*, vol. 55, no. 2, pp. 674–683, 2008.

[5] S. Li, S. C. Tan, C. K. Lee, E. Waffenschmidt, S. Y. R. Hui, and C. K. Tse, “A survey, classification, and critical review of light-emitting diode drivers,” *IEEE Trans. Power Electron.*, vol. 31, no. 2, pp. 1503–1516, 2016.

[6] X. Qu, S. C. Wong, and C. K. Tse, “An improved LCLC current-source-output multistring LED driver with capacitive current balancing,” *IEEE Trans. Power Electron.*, vol. 30, no. 10, pp. 5783–5791, 2015.

[7] M. H. Crawford, “Leds for solid-state lighting: performance challenges and recent advances,” *IEEE J. Sel. Topics in Quan. Electron.*, vol. 15, no. 4, pp. 1028–1040, 2009.

[8] X. Qu, S. C. Wong, and C. K. Tse, “Noncascading structure for electronic ballast design for multiple LED lamps with independent brightness control,” *IEEE Trans. Power Electron.*, vol. 25, no. 2, pp. 331–340, 2010.

[9] W. K. Lun, K. Loo, S. C. Tan, Y. Lai, and C. K. Tse, “Bilevel current driving technique for LEDs,” *IEEE Trans. Power Electron.*, vol. 24, no. 12, pp. 2920–2932, 2009.

[10] H. Valipour, G. Rezazadeh, and M. R. Zolghadri, “Flicker-free electrolytic capacitor-less universal input offline LED driver with pfc,” *IEEE Trans. Power Electron.*, vol. 31, no. 9, pp. 6553–6561, 2016.

[11] S. Y. R. Hui, S. N. Li, X. H. Tao, W. Chen, and W. Ng, “A novel passive offline LED driver with long lifetime,” *IEEE Trans. Power Electron.*, vol. 25, no. 10, pp. 2665–2672, 2010.

[12] G. Zhou, J. Xu, and J. Wang, “Constant-frequency peak-ripple-based control of buck converter in ccm: Review, unification, and duality,” *IEEE Trans. Power Electron.*, vol. 61, no. 3, pp. 1280–1291, 2014.

[13] J. Wang, B. Bao, J. Xu, G. Zhou, and W. Hu, “Dynamical effects of equivalent series resistance of output capacitor in constant on-time controlled buck converter,” *IEEE Trans. Ind. Electron.*, vol. 60, no. 5, pp. 1759–1768, 2013.

[14] Y. Li, K. R. Vannorsdel, A. J. Zirger, M. Norris, and D. Maksimovic, “Current mode control for boost converters with constant power loads,” *IEEE Trans. Circ. Syst. I: Reg. Papers*, vol. 59, no. 1, pp. 198–206, 2012.

[15] P. Yang, J. Xu, G. Zhou, and S. Zhang, “A new quadratic boost converter with high voltage step-up ratio and reduced voltage stress,” in *Proc. IEEE Int. Power Electron. and Motion Control Conf. (IPEMC)*, vol. 2, 2012, pp. 1164–1168.

[16] T. J. Liang, S. M. Chen, L. S. Yang, J. F. Chen, and A. Ioinovici, “A single switch boost-flyback dc-dc converter integrated with switched-capacitor cell,” in *Proc. IEEE Int. Conf. Power Electron. and ECCE Asia*, 2011, pp. 2782–2787.

[17] N. M. Mapula and W. R. Liou, “Integrated multi-channel constant current LED driver with pwm boost converter design in 0.35μm process,” in *IEEE Region Ten Conf. (TENCON)*, 2012, pp. 1–6.

[18] D. Liu, A. Hu, G. Wang, and W. Hu, “Current sharing schemes for multiphase interleaved dc/dc converter with fpga implementation,” in *Proc. Int. Conf. Elect., Cont. Eng. (ICECE)*, 2010, pp. 3512–3515.

[19] C. K. Tse, *Linear Circuit Analysis*. London: Addison-Wesley, 1998.

[20] ——, “Zero-order switching networks and their applications to power factor correction in switching converters,” *IEEE Trans. Circ. Syst. I: Fund. Theor. Appl.*, vol. 44, no. 8, pp. 667–675, 1997.

[21] X. Liu, Q. Yang, Q. Zhou, J. Xu, and G. Zhou, “Single-stage single-switch four-output resonant led driver with high power factor and passive current balancing,” *IEEE Trans. Power Electron.*, vol. 32, no. 6, pp. 4566–4576, 2017.

[22] C. S. Huang, D. Chen, C. J. Chen, and K. H. Liu, “Mix-voltage conversion for single-inductor dual-output buck converters,” *IEEE Trans. Power Electron.*, vol. 25, no. 8, pp. 2106–2114, 2010.

[23] H. T. Chen, S. C. Tan, and S. Y. R. Hui, “Nonlinear dimming and correlated color temperature control of bicolor white led systems,” *IEEE Trans. Power Electron.*, vol. 30, no. 12, pp. 6934–6947, 2015.

[24] A. T. Lee, H. Chen, S. C. Tan, and S. Y. R. Hui, “Precise dimming and color control of led systems based on color mixing,” *IEEE Trans. Power Electron.*, vol. 31, no. 1, pp. 65–80, 2016.

[25] Y. Qin, D. Lin, and S. Y. R. Hui, “A simple method for comparative study on the thermal performance of leds and fluorescent lamps,” *IEEE Trans. Power Electron.*, vol. 24, no. 7, pp. 1811–1818, 2009.

[26] H. J. Chiu and S. J. Cheng, “Led backlight driving system for large-scale lcd panels,” *IEEE Trans. Ind. Electron.*, vol. 54, no. 5, pp. 2751–2760, 2007.

[27] P. S. Almeida, D. Camponogara, M. Dalla Costa, H. Braga, and J. M. Alonso, “Matching led and driver life spans: A review of different techniques,” *IEEE Ind. Electron. Mag.*, vol. 9, no. 2, pp. 36–47, 2015.

[28] D. Camponogara, G. F. Ferreira, A. Campos, M. A. Dalla Costa, and J. Garcia, “Offline led driver for street lighting with an optimized cascade structure,” *IEEE Trans. Ind. Appl.*, vol. 49, no. 6, pp. 2437–2443, 2013.

[29] S. Choi and T. Kim, “Symmetric current-balancing circuit for led backlight with dimming,” *IEEE Trans. Ind. Electron.*, vol. 59, no. 4, pp. 1698–1707, 2012.

[30] M. Nishikawa, Y. Ishizuka, H. Matsuo, and K. Shigematsu, “An led drive circuit with constant-output-current control and constant-luminance control,” in *Proc. Telecom. Energy Conf.* IEEE, 2006, pp. 1–6.

[31] H. J. Chiu, L. Y. K, and S. J. Cheng, “A high-efficiency dimmable led driver for low-power lighting applications,” *IEEE Trans. Ind. Electron.*, vol. 57, no. 2, pp. 735–743, 2010.

[32] T. S. Perry, “Red hot light emitting diodes,” *IEEE Spectrum*, vol. 40, no. 6, pp. 26–29, 2003.

[33] M. Craford, R. W. Shaw, A. Herzog, and W. Groves, “Radiative recombination mechanisms in gaasp diodes with and without nitrogen doping,” *J. Appl. Physics*, vol. 43, no. 10, pp. 4075–4083, 1972.

[34] S. Nakamura, “Blue/green semiconductor laser,” in *Proc. IEEE Int. Semiconductor Laser Conf.* IEEE, 1996, pp. 3–4.

[35] I. Akasaki, H. Amano, and S. Nakamura, “The nobel prize in physics 2014,” *The Royal Swedish Academy of Science*, 2014.

[36] R. Haitz and J. Y. Tsao, “Solid-state lighting: the case 10 years after and future prospects,” *Physica status solidi (a)*, vol. 208, no. 1, pp. 17–29, 2011.

[37] M. Arias, A. Vázquez, and J. Sebastián, “An overview of the ac-dc and dc-dc converters for led lighting applications,” *Automatika*, vol. 53, no. 2, pp. 156–172, 2012.

[38] H. Kim, B. Lee, and C.-T. Rim, “Passive led driver compatible with rapid-start ballast,” in *Proc. IEEE Int. Power Electron. Conf.* IEEE, 2011, pp. 507–514.

[39] J. M. Alonso, J. Viña, D. G. Vaquero, G. Martínez, and R. Osorio, “Analysis and design of the integrated double buck–boost converter as a high-power-factor driver for power-led lamps,” *IEEE Trans. Ind. Electron.*, vol. 59, no. 4, pp. 1689–1697, 2012.

[40] W. Chen and S. Y. R. Hui, “Elimination of an electrolytic capacitor in ac/dc light-emitting diode (led) driver with high input power factor and constant output current,” *IEEE Trans. Power Electron.*, vol. 27, no. 3, pp. 1598–1607, 2012.

[41] B. Wang, X. Ruan, K. Yao, and M. Xu, “A method of reducing the peak-to-average ratio of led current for electrolytic capacitor-less ac-dc drivers,” *IEEE Trans. Power Electron.*, vol. 25, no. 3, pp. 592–601, 2010.

[42] J. De Britto, A. Demian, L. De Freitas, V. Farias, E. Coelho, and J. Vieira, "A proposal of led lamp driver for universal input using cuk converter," in *Power Electron. Specialists Conf.* IEEE, 2008, pp. 2640–2644.

[43] A. T. Lee, J. K. Sin, and P. C. Chan, "Scalability of quasi-hysteretic fsm-based digitally controlled single-inductor dual-string buck led driver to multiple strings," *IEEE Trans. Power Electron.*, vol. 29, no. 1, pp. 501–513, 2014.

[44] H. C. Kim, C. S. Yoon, D.-K. Jeong, and J. Kim, "A single-inductor, multiple-channel current-balancing led driver for display backlight applications," *IEEE Trans. Ind. Electron.*, vol. 50, no. 6, pp. 4077–4081, 2014.

[45] H. Chen, Y. Zhang, and D. Ma, "A simo parallel-string driver ic for dimmable led backlighting with local bus voltage optimization and single time-shared regulation loop," *IEEE Trans. Power Electron.*, vol. 27, no. 1, pp. 452–462, 2012.

[46] S. Ji, H. Wu, X. Ren, and F. C. Lee, "Multi-channel constant current (mc 3) led driver," in *Proc. IEEE Appl. Power Electron. Conf. Exp. (APEC)*, 2011, pp. 718–722.

[47] X. Wu, C. Hu, J. Zhang, and C. Zhao, "Series–parallel autoregulated charge-balancing rectifier for multioutput light-emitting diode driver," *IEEE Trans. Ind. Electron.*, vol. 61, no. 3, pp. 1262–1268, 2014.

[48] S. Li, Y. Guo, S. C. Tan, and S. Y. R. Hui, "An off-line single-inductor multiple-outputs LED driver with high dimming precision and full dimming range," *IEEE Trans. Power Electron.*, vol. 32, no. 6, pp. 4716–4727, 2016.

[49] B. Lehman and A. J. Wilkins, "Designing to mitigate effects of flicker in LED lighting: Reducing risks to health and safety," *IEEE Power Electron. Mag.*, vol. 1, no. 3, pp. 18–26, 2014.

[50] H. Y and J. M. M, "Led driver with self-adaptive drive voltage," *IEEE Trans. Power Electron.*, vol. 23, no. 6, pp. 3116–3125, 2008.

[51] Z. Ye, F. Greenfeld, and Z. Liang, "Single-stage offline sepic converter with power factor correction to drive high brightness leds," in *Proc. IEEE Appl. Power Electron. Conf. Exp. (APEC)*, 2009, pp. 546–553.

[52] L. Guo, "Design and implementation of digital controllers for buck and boost converters using linear and nonlinear control methods," Ph.D. dissertation, 2006.

[53] S. C. Tan, Y. M. Lai, M. K. Cheung, and C. K. Tse, "On the practical design of a sliding mode voltage controlled buck converter," *IEEE Trans. Power Electron.*, vol. 20, no. 2, pp. 425–437, 2005.

[54] S. Maity, D. Tripathy, T. K. Bhattacharya, and S. Banerjee, "Bifurcation analysis of pwm-1 voltage-mode-controlled buck converter using the exact discrete model," *IEEE Trans. Circ. Syst. I: Reg. Papers*, vol. 54, no. 5, pp. 1120–1130, 2007.

[55] T. Nabeshima, T. Sato, S. Yoshida, S. Chiba, and K. Onda, "Analysis and design considerations of a buck converter with a hysteretic pwm controller," in *Proc. IEEE Power Electron. Specialists Conf.*, vol. 2, 2004, pp. 1711–1716.

[56] D. C. Hamill, J. H. Deane, and D. J. Jefferies, "Modeling of chaotic dc-dc converters by iterated nonlinear mappings," *IEEE Trans. Power Electron.*, vol. 7, no. 1, pp. 25–36, 1992.

[57] S. Sivakumar, K. Natarajan, and R. Gudelewicz, "Control of power factor correcting boost converter without instantaneous measurement of input current," *IEEE Trans. Power Electron.*, vol. 10, no. 4, pp. 435–445, 1995.

[58] S. Hiti and D. Borojevic, "Robust nonlinear control for boost converter," *IEEE Trans. Power Electron.*, vol. 10, no. 6, pp. 651–658, 1995.

[59] R. C. Pilawa-Podgurski, A. D. Sagneri, J. M. Rivas, D. I. Anderson, and D. J. Perreault, “Very-high-frequency resonant boost converters,” *IEEE Trans. Power Electron.*, vol. 24, no. 6, pp. 1654–1665, 2009.

[60] P. Karamanakos, T. Geyer, and S. Manias, “Direct voltage control of dc–dc boost converters using enumeration-based model predictive control,” *IEEE Trans. Power Electron.*, vol. 29, no. 2, pp. 968–978, 2014.

[61] E. Lefeuvre, D. Audigier, C. Richard, and D. Guyomar, “Buck-boost converter for sensorless power optimization of piezoelectric energy harvester,” *IEEE Trans. Power Electron.*, vol. 22, no. 5, pp. 2018–2025, 2007.

[62] D. Maksimovic and S. Cuk, “Switching converters with wide dc conversion range,” *IEEE Trans. Power Electron.*, vol. 6, no. 1, pp. 151–157, 1991.

[63] B. Sahu and G. A. Rincón-Mora, “A low voltage, dynamic, noninverting, synchronous buck-boost converter for portable applications,” *IEEE Trans. Power Electron.*, vol. 19, no. 2, pp. 443–452, 2004.

[64] J. M. Blanes, R. Gutierrez, A. Garrigós, J. L. Lizán, and J. M. Cuadrado, “Electric vehicle battery life extension using ultracapacitors and an fpga controlled interleaved buck–boost converter,” *IEEE Trans. Power Electron.*, vol. 28, no. 12, pp. 5940–5948, 2013.

[65] X. Liu, J. Xu, Z. Chen, and N. Wang, “Single-inductor dual-output buck–boost power factor correction converter,” *IEEE Trans. Ind. Electron.*, vol. 62, no. 2, pp. 943–952, 2015.

[66] X. Liu, J. Xu, Q. Yang, and D. Xu, “High-efficiency multi-string LED driver based on constant current bus with time-multiplexing control,” *IET Electron. Lett.*, vol. 52, no. 9, pp. 746–748, 2016.

[67] K. S. Seol, Y. J. Woo, G. H. Cho, G. H. Gho, and J. W. Lee, "A synchronous multioutput step-up/down dc-dc converter with return current control," *IEEE Trans. Circ. Syst. I: Reg. Papers*, vol. 56, no. 3, pp. 210–214, 2009.

[68] H. P. Le, C. S. Chae, K. C. Lee, S. W. Wang, G. H. Cho, and G. H. Cho, "A single-inductor switching dc-dc converter with five outputs and ordered power-distributive control," *IEEE J. Solid-State Circ.*, vol. 42, no. 12, pp. 2706–2714, 2007.

[69] C. S. Chae, H. P. Le, K. C. Lee, G. H. Cho, and G. H. Cho, "A single-inductor step-up dc-dc switching converter with bipolar outputs for active matrix oled mobile display panels," *IEEE J. Solid-State Circ.*, vol. 44, no. 2, pp. 509–524, 2009.

[70] D. S. Ma, W. H. Ki, C. Y. Tsui, and P. K. Mok, "Single-inductor multiple-output switching converters with time-multiplexing control in discontinuous conduction mode," *IEEE J. Solid-State Circ.*, vol. 38, no. 1, pp. 89–100, 2003.

[71] X. Liu, J. Xu, M. Qin, and J. Yang, "Single-inductor dual-output buck converter with current mode pulse-train control," *Trans. Chin. Electron. Soc.*, vol. 1, no. 27, pp. 155–161, 2012.

[72] Y. J. Woo, H. P. Le, G. H. Cho, G. H. Cho, and S. I. Kim, "Load-independent control of switching dc-dc converters with freewheeling current feedback," *IEEE J. Solid-State Circ.*, vol. 43, no. 12, pp. 2798–2808, 2008.

[73] D. S. Ma, W. H. Ki, and C. Y. Tsui, "A pseudo-ccm/dcm simo switching converter with freewheel switching," *IEEE of Solid-State Circ.*, vol. 38, no. 6, pp. 1007–1014, 2003.

[74] D. Trevisan, P. Mattavelli, and P. Tenti, "Digital control of single-inductor multiple-output step-down dc-dc converters in ccm," *IEEE Trans. Ind. Electron.*, vol. 55, no. 9, pp. 3476–3483, 2008.

[75] A. Pizzutelli and M. Ghioni, "Novel control technique for single inductor multiple output converters operating in ccm with reduced cross-regulation," in *Proc. IEEE Appl. Power Electron. Conf. Exp. (APEC)*, 2008, pp. 1502–1507.

[76] Y. Guo, S. Li, A. T. Lee, S. C. Tan, C. K. Lee, and S. Y. R. Hui, "Single-stage ac/dc single-inductor multiple-output led drivers," *IEEE Trans. Power Electron.*, vol. 31, no. 8, pp. 5837–5850, 2016.

[77] Y. Wang, J. Xu, and G. Zhou, "A cross regulation analysis for single-inductor dual-output ccm buck converters," *J. Power Electron.*, vol. 16, no. 5, pp. 1802–1812, 2016.

[78] X. Liu, J. Xu, J. Wang, and Q. Mu, "A single-inductor dual-output buck converter with pulse-train control," in *Proc. IEEE Power Electron. Dist. Gen. Syst.*, 2010, pp. 449–452.

[79] Z. Shen, X. Chang, W. Wang, X. Tan, N. Yan, and H. Min, "Predictive digital current control of single-inductor multiple-output converters in ccm with low cross regulation," *IEEE Trans. Power Electron.*, vol. 27, no. 4, pp. 1917–1925, 2012.

[80] J. D. Dasika, B. Bahrani, M. Saeedifard, A. Karimi, and A. Rufer, "Multivariable control of single-inductor dual-output buck converters," *IEEE Trans. Power Electron.*, vol. 29, no. 4, pp. 2061–2070, 2014.

[81] R. Rabinovici and B. Kaplan, "Novel dc-dc convertor schemes obtained through duality principle and topological considerations," *IET Electron. Lett.*, vol. 21, no. 27, pp. 1948–1950, 1991.

[82] B. Riar, D. Howey, D. Thrimawithana, D. Rogers, and R. Zane, "Bidirectional current source converter: Design, control and performance evaluation," in *Proc. IEEE Ann. Southern Power Electron. Conf. (SPEC)*, 2016, pp. 1–6.

[83] Y. Qin, H. S. Chung, D. Lin, and S. Y. R. Hui, "Current source ballast for high power lighting emitting diodes without electrolytic capacitor," in *Proc. 34th Ann. Conf. IEEE Ind. Electron. Soc. (IECON)*, 2008, pp. 1968–1973.

[84] I. Galkin, O. Tetervjonok, and I. Milashevski, "Comparative study of steady-state performance of voltage and current fed dimmable LED drivers," in *Proc. IEEE Int. Comp. Power Electro. Conf.*, 2013, pp. 292–297.

[85] H. Martínez-García and A. Saberkari, "Linear-assisted dc/dc regulator-based current source for LED drivers," *IET Electron. Lett.*, vol. 52, no. 6, pp. 437–439, 2016.

[86] Z. Dong, C. K. Tse, and S. Y. R. Hui, "Basic circuit theoretic considerations of LED driving: Voltage-source versus current-source driving," in *Proc. IEEE Ann. Southern Power Electron. Conf. (SPEC)*, 2016, pp. 1–6.

[87] C. K. Tse, Y. M. Lai, R. J. Xie, and M. H. L. Chow, "Application of duality principle to synthesis of single-stage power-factor-correction voltage regulators," *Int. J. Circuit Theor. Appl.*, vol. 31, no. 6, pp. 555–570, 2003.

[88] O. Tetervenoks and I. Galkin, "Assessment of switch mode current sources for current fed led drivers," in *Proc. Springer Doctoral Conf.*, 2014, pp. 551–558.

[89] R. J. Wai and J. J. Liaw, "High-efficiency-isolated single-input multiple-output bidirectional converter," *IEEE Trans. Power Electron.*, vol. 30, no. 9, pp. 4914–4930, 2015.

[90] D. Sha, K. Deng, and X. Liao, "Duty cycle exchanging control for input-series-output-series connected two ps-fb dc-dc converters," *IEEE Trans. Power Electron.*, vol. 27, no. 3, pp. 1490–1501, 2012.

[91] I. Galkin, I. Milashevski, and O. Teteryonok, “Comparative study of steady-state performance of LED drivers at different modulation techniques,” in *Proc. IEEE Int. Conf. Comp. Power Electron. (CPE)*, 2011, pp. 382–387.

[92] J. Choi, H.-S. Han, and K. Lee, “A current-sourced led driver compatible with fluorescent lamp ballasts,” *IEEE Trans. Power Electron.*, vol. 30, no. 8, pp. 4455–4466, 2015.

[93] J. Shao and T. Stamm, “A cost effective high performance led driver powered by electronic ballasts,” in *IEEE Appl. Power Electron. Conf. Exp. (APEC)*, 2016, pp. 3659–3662.

[94] K. Modepalli and L. Parsa, “A scalable n-color led driver using single inductor multiple current output topology,” *IEEE Trans. Power Electron.*, vol. 31, no. 5, pp. 3773–3783, 2016.

[95] X. Zhan, H. Chung, and R. Zhang, “Investigation into the use of single inductor for driving multiple series-connected led channels,” *IEEE Trans. Power Electron.*, vol. 32, no. 4, pp. 3034–3050, 2017.

[96] X. Liu, J. Xu, M. Qin, and J. Yang, “Single-inductor dual-output buck converter with current mode pulse-train control,” *Diangong Jishu Xuebao (Trans. of China Electrotechnical Soc.)*, vol. 27, no. 1, 2012.

[97] Z. Dong, C. K. Tse, and S. R. Hui, “Current-source-mode single-inductor multiple-output led driver with single closed-loop control achieving independent dimming function,” *IEEE J. Emer. Sel. Topics in Power Electron.*, vol. 6, no. 3, 2018.